

**TRIBOCHEMICAL PROPERTIES OF
META-STABLE STATES OF TRANSITION METALS**

A Dissertation

by

PRASENJIT KAR

Submitted to the Office of Graduate Studies of
Texas A&M University
in partial fulfillment of the requirements for the degree of

DOCTOR OF PHILOSOPHY

May 2008

Major Subject: Materials Science and Engineering

**TRIBOCHEMICAL PROPERTIES OF
META-STABLE STATES OF TRANSITION METALS**

A Dissertation

by

PRASENJIT KAR

Submitted to the Office of Graduate Studies of
Texas A&M University
in partial fulfillment of the requirements for the degree of

DOCTOR OF PHILOSOPHY

Approved by:

Chair of Committee,
Committee Members,

Hong Liang
Donald Darensbourg
Richard Griffin
Miladin Radovic

Chair of Materials Science
& Engineering Faculty,

Tahir Cagin

May 2008

Major Subject: Materials Science and Engineering

ABSTRACT

Tribochemical Properties of Meta-Stable States of Transition Metals.

(May 2008)

Prasenjit Kar, B.Sc.; M.Sc., Assam Central University, India

Chair of Advisory Committee: Dr. Hong Liang

Mechanical forces can be used to trigger chemical reactions through activating bonds and to direct the course of such reactions in organic materials, particularly in polymers. In inorganic materials, the small molecules present significant challenges in directing the reaction kinetics. This dissertation studied the dynamics and kinetics of oxidation of transitional metals, particularly on tantalum through mechanical forces. This is a new area of research in surface science.

Experimentally using a combined electrochemical and mechanical manipulation technique, we compared the equilibrium and non-equilibrium oxidation processes and states of tantalum. An experimental setup was developed with an electrochemical system attached to a sliding mechanical configuration capable of friction force measurement. The surface chemistry of a sliding surface, i.e., tantalum, was controlled through the electrolyte. The mechanical force was fixed and the dynamics of the surface was monitored in situ through a force sensor. The formation of non-equilibrium tantalum oxides was found in fluid environments of hydrogen peroxide, acetic acid and deionized

water. We found that the mechanical energy induced the non-stable state reactions leading to metal-stable oxides.

Analytically, we compared the energy dispersion, reaction kinetics, and investigate physical chemical reactions. We proposed a modified Arrhenius equation to predict the effect of mechanical energy on non-spontaneous reaction under non-equilibrium conditions. At the end, we also propose a modified Pourbaix diagram known as the Kar-Liang diagram. The Kar-Liang diagram helps to understand the behavior of tantalum under non-equilibrium conditions. A complete understanding of the tribochemical reaction of tantalum is achieved through this dissertation.

The dissertation contains six chapters. After the introduction and approach, oxidation of tantalum is discussed in Chapter IV, kinetics in Chapter V. The non-equilibrium Kar-Liang diagram is discussed in Chapter VI, followed by conclusion. This research has important impacts on the field of surface science in understanding the basics of mechanochemical reactions. The resulting theory is beneficial to understand chemical-mechanical planarization (CMP) and to optimize the current industrial processes in microelectronics in making integrated circuits.

DEDICATION

The dissertation is dedicated to Dr. Hong Liang and my parents.

ACKNOWLEDGEMENTS

First and foremost, I would like to thank God for being there always in times of success and distress. Next, my sincere gratitude and thanks go to my committee chair, Dr. Hong Liang, for her constant support all along my academic career in Texas A&M University. This dissertation would not have been possible without her help and guidance. I would also like to thank my committee members, Dr. Donald Darensbourg, Dr. Richard Griffin, and Dr. Miladin Radovic for their guidance and support throughout the course of this research.

Thanks also go to my friends and colleagues and the department faculty and staff for making my time at Texas A&M University a great experience. I also want to extend my gratitude to the National Science Foundation which provided the grants (CMMI-0535578) for my research and to Texas Engineering Experiment Station and Trinity Industries for paying my tuition and stipend.

Last but not the least, thanks go to my mother and father for their encouragement. Without their support I wouldn't be where I am today. And also my special thanks to my fiancée and her relatives for their prayers and support.

NOMENCLATURE

AFM	Atomic Force Microscopy
APCVD	Atmosphere Chemical Vapor Deposition
CMP	Chemical Mechanical Polishing/Planarization
CVD	Chemical Vapor Deposition
DI	Deionized
ECMP	Electrochemical Mechanical Polishing/Planarization
ESCA	Electron Spectroscopy for Chemical Analysis
HOMO	Highest Occupied Molecular Orbitals
IUPAC	International Union of Pure and Applied Chemistry
LPCVD	Low Pressure Chemical Vapor Deposition
LUMO	Lowest Unoccupied Molecular Orbitals
MOCVD	Metal-Organic Chemical Vapor Deposition
MOS	Metal Oxide Semiconductor
RT-LPMOCVD	Rapid Thermal Low Pressure Metal-Organic Chemical Vapor Deposition
STM	Scanning Tunneling Microscope
TCP	Tribochemical Polishing
TECP	Triboelectrochemical Polishing
UHV	Ultra High Vacuum
XPS	X-ray Photoelectron Spectroscopy

TABLE OF CONTENTS

	Page
ABSTRACT.....	iii
DEDICATION.....	v
ACKNOWLEDGEMENTS.....	vi
NOMENCLATURE.....	vii
TABLE OF CONTENTS.....	viii
LIST OF FIGURES.....	x
LIST OF TABLES.....	xiv
 CHAPTER	
I INTRODUCTION.....	1
1.1 History of tribology.....	1
1.2 Mechanochemistry.....	4
1.3 Interface science.....	7
1.4 Triboelectrochemistry.....	12
II MOTIVATION AND OBJECTIVES.....	16
2.1 Motivation.....	16
2.2 Objectives.....	18
III EXPERIMENTAL APPROACH.....	20
3.1 Materials.....	20
3.2 Experimental setup.....	24
3.3 Experimental conditions.....	30
3.4 Characterization techniques.....	34

CHAPTER	Page
IV MECHANO-OXIDATION OF TANTALUM.....	42
4.1 Frictional behavior.....	43
4.2 Meta-stable oxidation states of tantalum.....	45
4.3 Sub-oxide film thickness.....	52
4.4 Non-equilibrium oxidation mechanisms.....	55
4.5 Summary.....	61
V MECHANO-KINETICS OF TANTALUM.....	63
5.1 Frictional behavior.....	66
5.2 XPS analysis of tantalum sub-oxides.....	69
5.3 Mechano-kinetics and Kar-Liang equation.....	84
5.4 Summary.....	88
VI NON-EQUILIBRIUM KAR-LIANG DIAGRAMS FOR TANTALUM.....	89
6.1 Analysis of tantalum under electro-chemical mechanical parameters.....	91
6.2 Analysis of tantalum under mechano-chemical parameters....	99
6.3 Summary.....	109
VII CONCLUSIONS AND FUTURE SUGGESTIONS.....	110
7.1 Conclusions.....	110
7.2 Future suggestions.....	111
REFERENCES.....	113
VITA.....	121

LIST OF FIGURES

FIGURE	Page
1.1 Showing lubrication in ancient Egypt	2
1.2 HOMO-LUMO interaction of compounds under influence of strain energy	6
1.3 Schematic of probable interfacial interaction of oxygen containing molecules with transition metals	8
2.1 A mechanical force text-book model shows the impact of this force targeted on specific bond.....	17
3.1 Table showing the elements that will be investigated in the project.....	20
3.2 Schematic showing the tribochemical set-up for bulk tantalum polishing.....	25
3.3 Illustration of the test setup used to apply a controllable mechanical force on a bulk tantalum.....	26
3.4 A schematic of the triboelectrochemical setup for polishing of bulk tantalum	27
3.5 Illustration of the test setup used to apply a controllable mechanical force on a tantalum wafer.....	29
3.6 A commercial AFM (Pacific Nanotechnology Incorporated) from Dr. Liang's surface science and interface laboratory	36
3.7 Atomic Force Microscopy (AFM) a) contact mode and b) non-contact mode	37
3.8 Non-contact AFM image of a polished Al surface. Left image showing topographic features and right image showing phase image.....	37
3.9 A Kratos Imaging X-ray Photoelectron Spectrometer in Materials Characterization Facility.	39
3.10 XPS raw specimen peaks of tantalum pentoxide and tantalum suboxide ..	40

FIGURE	Page
4.1 Friction coefficient of tantalum sample in 5% wt hydrogen peroxide.....	44
4.2 AFM images of tantalum sample surface before (a) and after (b) electro-mechanical experiments.....	45
4.3a XPS spectra of Ta sample surfaces obtained after immersion in 5%wt H ₂ O ₂ solution with friction and electro potential; friction only; and electro potential only.....	47
4.3b Deconvoluted Ta 4f XPS envelope obtained from the Ta surface after immersion in a solution with 5%wt H ₂ O ₂ with both friction and electro potential.....	48
4.3c Deconvoluted Ta 4f XPS envelope obtained from the Ta surface after immersion in a solution with 5%wt H ₂ O ₂ with friction only.....	49
4.3d Deconvoluted Ta 4f XPS envelope obtained from the Ta surface after immersion in a solution with 5%wt H ₂ O ₂ with electro potential only.....	50
4.4a Line analysis of the AFM topography showing tantalum surface original on right side and tantalum surface unmasked and exposed to tribological mechanism on left side.....	53
4.4b Line analysis of the AFM topography showing tantalum surface unmasked and exposed to electrotribological mechanism on right side and original tantalum surface on left side.....	53
4.5 The average film thickness along with the standard deviation in data analysis for different conditions used in film measurement.....	54
4.6 A schematic summary of experimental results showing atomic structures obtained through different experimental conditions.....	56
4.7 The three found tantalum oxides with their stoichiometric ratio and crystal structure.....	57
4.8 The effects on metal-polishing pad interface at molecular level due to mechanical stress.....	58
4.9 The plausible theory put forward for formation of Ta ₂ O involving band-gap reduction due to mechanical stress.....	60

FIGURE	Page
5.1a Friction obtained in water under the condition of 1N and 0.5 cm/sec. The friction starts to increase at +2.4 V.	66
5.1b Friction obtained in the 0.13 M acetic acid under the condition of 1N and 0.5 cm/sec.....	67
5.2 AFM phase image of the surface of a) sample 1 (left) and b) sample 2 (right)	69
5.3a XPS comparison of all tested samples.....	70
5.3b XPS peaks of Ta in acetic acid under different conditions	71
5.3c Shift in XPS peaks of tantalum in DI water under different conditions....	72
5.3d XPS peak analysis of tantalum sample as the reference (sample 1).	73
5.3e XPS peak analysis of tantalum tested in acetic acid (sample 2).....	74
5.3f XPS peak analysis on tantalum tested in DI water (sample 3).	75
5.3g XPS peak fitting of acetic acid electrochemical only (sample 4).	76
5.3h XPS peak fitting of DI water electrochemical only (Sample 5).....	77
5.3i XPS peak fitting of acetic acid mechanical only (Sample 6).....	78
5.3j XPS peak fitting of DI water mechanical only (sample 7).	79
5.4a Oxidation rate verses applied mechanical energy	86
5.4b Energy comparison of tantalum oxides under influence of applied mechanical energy ϵ	87
6.1 Illustration of pH-potential Pourbaix diagram of tantalum	89
6.2 XPS analysis of tantalum sample in pH 1 after ECMP process.....	92
6.3 XPS analysis of tantalum sample in pH 1 after ECMP process after 48 hrs....	93

FIGURE	Page
6.4 XPS analysis of tantalum sample in pH 7 after ECMP process.....	94
6.5 XPS analysis of tantalum sample in pH 7 after ECMP process after 48 hrs.	95
6.6 XPS analysis of tantalum sample in pH 10 after ECMP process.....	96
6.7 XPS analysis of tantalum sample in pH 10 after ECMP process after 48 hrs.	97
6.8 Illustration of pH-potential Kar-Liang diagram of Ta under ECMP	99
6.9 XPS analysis of tantalum sample in pH 1 after CMP process	100
6.10 XPS analysis of tantalum sample in pH 1, 48 hrs after CMP process	101
6.11 XPS analysis of tantalum sample in pH 7 after CMP process	102
6.12 XPS analysis of tantalum sample in pH 7, 48 hrs after CMP process	103
6.13 XPS analysis of tantalum sample in pH 10 after CMP process	104
6.14 XPS analysis of tantalum sample in pH 10, 48 hrs after CMP process	105
6.15 Illustration of pH-potential Kar-Liang diagram of Ta under non-equilibrium conditions showing the sub-oxides formed.....	107
6.16 Illustration of pH-potential Kar-Liang diagram of Ta under non-equilibrium conditions showing the sub-oxides formed.....	108

LIST OF TABLES

TABLE	Page
1.1 Summary of current understanding of metal-oxygen interface.....	11
3.1 The experimental conditions used in 5% wt H ₂ O ₂ solution.....	30
3.2 The experimental conditions used in 0.13 M acetic acid solution	31
3.3 The experimental conditions used in DI water saturated with KCl	32
3.4 The experimental conditions used to generate Kar-Liang diagram in 0 V	33
3.5 The experimental conditions used to generate Kar-Liang diagram in + 2.4 V.....	34
4.1 Samples subjected to mechano-oxidation and products yielded	51
5.1 Summary of samples and corresponding test conditions	65
5.2 Summary of the sub-oxides formed under different conditions.....	80
6.1 XPS analysis of sample 6.1 after subjecting it to ECMP process	92
6.2 XPS analysis of sample 6.1 subjected to ECMP process after 48 hrs.....	93
6.3 XPS analysis of sample 6.2 after subjecting it to ECMP process	94
6.4 XPS analysis of sample 6.2 subjected to ECMP process after 48 hrs.....	95
6.5 XPS analysis of sample 6.3 after subjecting it to ECMP process	96
6.6 XPS analysis of sample 6.3 subjected to ECMP process after 48 hrs.....	97
6.7 XPS analysis of sample 6.4 after subjecting it to CMP process	100
6.8 XPS analysis of sample 6.4 subjected to CMP process after 48 hrs	101

TABLE	Page
6.9 XPS analysis of sample 6.5 after subjecting it to CMP process	102
6.10 XPS analysis of sample 6.5 subjected to CMP process after 48 hrs	103
6.11 XPS analysis of sample 6.6 after subjecting it to CMP process	104
6.12 XPS analysis of sample 6.6 subjected to ECMP process after 48 hrs.....	105

CHAPTER I

INTRODUCTION

In order to understand basics behind the research, this chapter introduces background information in tribology, mechanochemistry, interface, and metal oxidation. The interactions between oxygen-containing molecules and transition metals were reviewed. Needs in understanding are highlighted.

1.1 History of tribology

Friction may be defined as the resistance force experienced when two bodies slide over another. Tribology is the field of science which deals with the study of mechanical and chemical effects on the surface of the two bodies when they slide over another. The first chemical effect of tribology was experienced by primitive men when they rubbed two log pieces over one another to generate enough heat to light fire. Tribology was also found in construction of pyramids where water was used as lubricant to move logs carrying colossal statues. A transportation of an Egyptian coliseum is shown in an ancient painting in the tomb of Tehuti-Hetep, El-Bershed, using the principles of tribology as seen in figure 1.1. [1]

This dissertation follows the style of *Electrochimica Acta*.

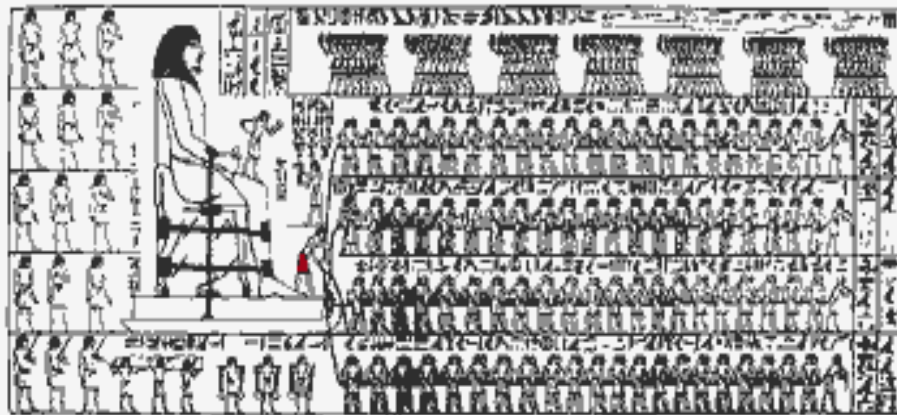


Figure 1.1: Showing Lubrication in Ancient Egypt.[1]

The first scientifically done experiment on tribology was done by Charles Hatchett (1760-1820). [2] He used a simple tribometer which slides back and forth to evaluate wear on gold coins. Hatchett found that gold coins which had grits on it wore fast as compared to self-mated coins. [3]

However the first to put forward the two laws of friction was Leonardo da Vinci (1470s). [4] The two laws of friction as stated by Vinci are:

1. The areas in contact are independent of frictional resistance. Different objects having same weights will experience same resistance irrespective of the area of contact.
2. The force needed to overcome frictional resistance is doubled when weight is doubled. In other words, frictional resistance is directly proportional to weight applied.

Based on these two laws Leonardo da Vinci suggested the law that force applied to move an object is directly proportional to the load applied. [4]

$$\mu = F / N; \text{ where } \mu = \text{coefficient of friction.}$$

Guillaume Amontons (1663-1705) stated that friction was dependent on roughness of surface which was later disproved by scientists believed that friction was due to the roughness on the surfaces. However it was Charles August Coulomb (1736-1806) who added to the da Vinci's second law of friction that the resistance experienced is directly proportional to the compressive force applied when the two bodies slide over another. [5] Coulomb published his work referring to Amontons and hence the second law of friction is known as the "Amontons-Coulomb Law". [6]

F. Philip Bowden and David Tabor in 1950s suggested that in microscopic level friction does indeed depend on contact area and Amontons-Coloumb Law fails in this aspect. [7] They suggested that if we look closely at any surface in microscopic level, even the smoothest surfaces have hills and valleys on them. The true contact area is much smaller than the apparent contact area as seen in macroscopic level. The true contact area in fact contains multiple points of contact called asperities. These contact areas or asperities increase with the increase in compressive force. As a result the true contact area increases with increase in compressive force in microscopic level as opposed to macroscopic level. Thus, at microscopic level the frictional force is dependent on the true contact area.

Effects of friction are far and wide in our daily life. Friction results in increased wear, heating of objects leading to chemical transformation, adhesion and welding

leading to deformation of surface structure. These damaging effects cause huge loss to industry like in railways, machineries used in oil and gas industry and others.[8] The loss involves the replacement of worn out objects. Also the cost of maintenance like usage of lubricants to prolong the life of the materials concerned adds to the financial burden. A whole branch of industrial investigation is devoted to reduce damages done due to friction by lubricant manufacture, surface modification through selection of proper materials, and coating technology. Friction is not always bad. Friction has its uses in breaking technology, in machining, and also in polishing. In our day to day life it is seen that a simple drive on the road needs an appropriate grip that is frictional force between the tires and the road gravel to prevent skidding of cars off the road. Without friction, we can not stand firm on the ground.

As stated that a tribological system is dynamic. It depends not only on the mechanical forces in play but also on the electrochemical and chemical environments. The present dissertation tries to investigate the effects of compressive force on the chemistry of materials. The mechanochemistry is investigated in a tribological environment.

1.2 Mechanochemistry

It is known that shear stress changes the orientation of solids. These drastic changes in the orientation of orbitals facilitate the chemical reactions. Shear stress changes spheres to ellipsoids and cubic symmetry to tetragonal. According to Gillman, the re-orientation of orbitals destabilizes the structure which facilitates reactions which

are not possible in ordinary circumstances. [9] In case of polymer reactions it is mainly strain that plays an important role in driving the mechano-chemical reactions as shown in the figure taken from Gillman's paper published in Science. Figure 1.2 illustrates the effects of strain on orbital structure of molecules. This figure shows that when covalent bonds are subjected to strain energy the gap between highest occupied molecular orbitals (HOMO) and the lowest unoccupied molecular orbitals (LUMO) decreases. As a result the anti-bonding percentage increases leading to destabilization in the structure facilitating chemical reactions. Similarly if a molecule is in the bend state in the ground state and is subjected to straightening by application of strain energy than same destabilization in structure will take place.

Mechano-chemical reactions are found in tribochemical processes involving friction, fretting, wear, etc. apart from other sources such as mechanical alloying. Boldyrev and Bridgman reported a variety of mechano-chemical reactions involving both organic and inorganic compounds. The reactions involve polymerization reactions, substitution reactions, and decomposition reactions.

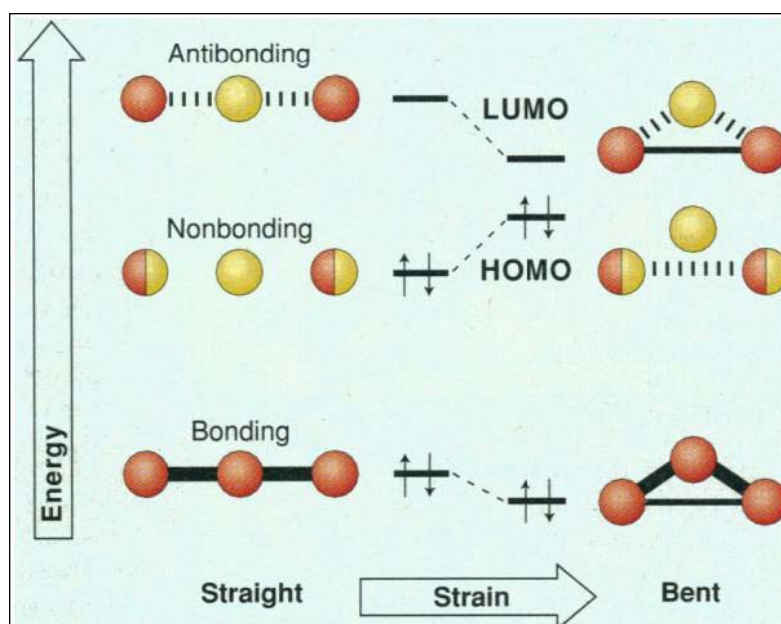


Figure 1.2: HOMO-LUMO interaction of compounds under influence of strain energy. [9]

The mechanism of action in case of solid-state crystal structures is different from covalent structures. [10] In solid state crystal structures the band-gap phenomenon comes into play. It is known that when a strain is applied on a material which is large enough to narrow down the band gaps than the material can be transitioned from an insulator to a metallic state. [11] Isotropic compression does not yield the same result as strain is equal from all directions. However large pressure acting on a material has been found to affect the band gaps resulting in a change of property of the materials. [12]

1.3 Interface science

In interfacial science and engineering, one of the critical issues faced today is to understand the behavior of metals and small molecules under non-equilibrium, particularly mechano-chemical conditions. This understanding becomes important in mitigating the problems faced in real world due to the unique chemistry of elements under extreme environments like high temperature, high stress, etc.

1.3.1 Interfacial interaction of oxygen containing molecules with transition metals

An interface is defined as a transition layer between two or more entities that differ in physical or chemical properties or both. Interface exists in a system which has a sudden change in its equilibrium conditions like density, chemical composition, magnetic property, etc.[13] Oxygen containing molecules (organic or inorganic) are in constant interaction with transition metals in industry under mechanical as well as chemical environments through atmosphere, lubricants, or slurries. Hence a good understanding of the interfacial mechano-chemistry under non-equilibrium conditions is essential to help in increasing the durability of industrial parts made of these types of metals.

The schematic in figure 1.3 summarizes possible pathways of interfacial interactions between oxygen containing molecules and transition metals:

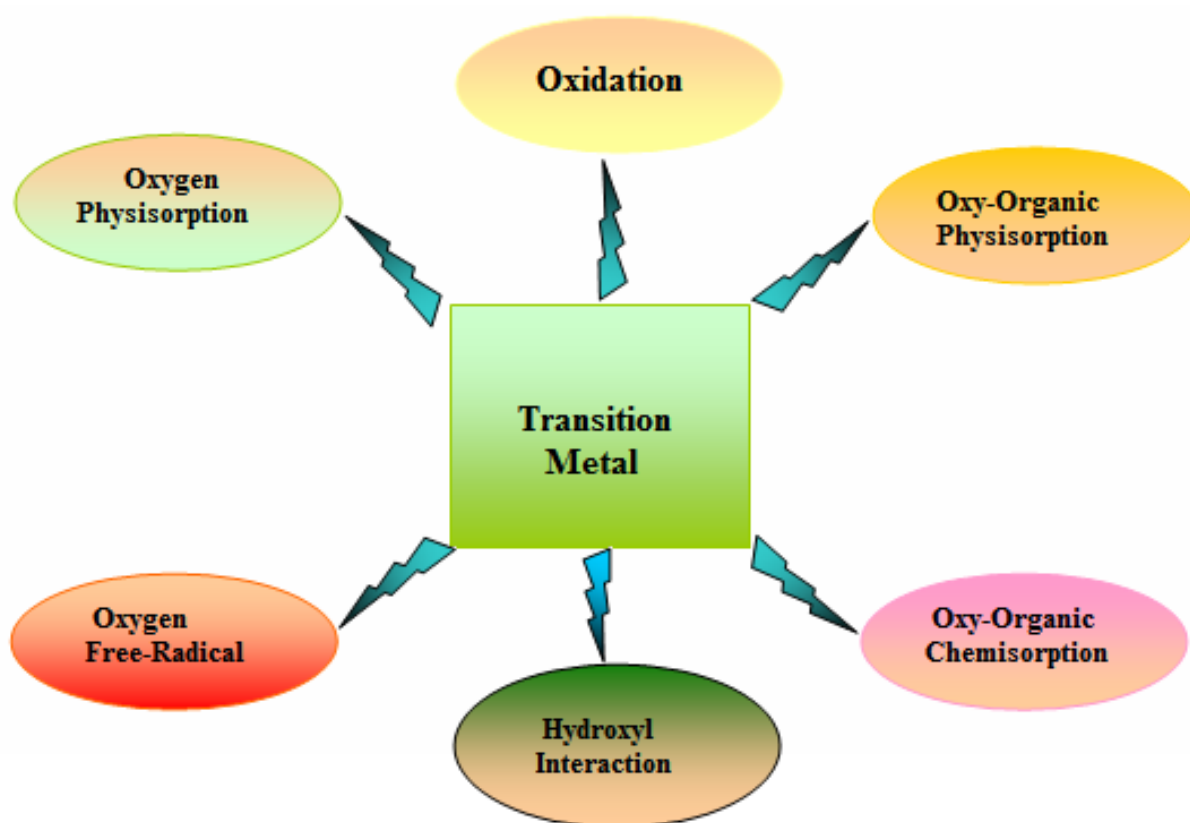


Figure 1.3: Schematic of probable interfacial interaction of oxygen containing molecules with transition metals.

A brief overview is given on these different types of interfacial reactions observed between oxygen containing molecules as follows:

1.3.2 Oxidation mechanism on transition metals

The oxidation of metals on interaction with oxygen is an important industrial phenomenon. The oxidation generally takes place by dissociative chemisorption of oxygen molecules on the transition metal surface. The activation energy barrier for the dissociative chemisorption of molecule decreases as we move towards the left of the periodic table.[14] However it is noted that under certain conditions, especially if the transition metals to the left side of the periodic table are considered like iridium, dioxygen is known to have acted as ligands in reactions termed as oxygenation reactions.[15]

1.3.3 Oxygen physisorption

Physisorption of molecular oxygen is the first step in transition metals before it is chemisorbed. However at low temperatures say 20 K, oxygen is known to have physisorbed on transition metals like Pt.[16]

1.3.4 Free radical interaction

Oxygen interaction in the form of free radical with transition metals is mostly found in biological systems.[17] It has been reported that in presence of H_2O_2 and Fe salt free radical $\cdot\text{OH}$ is generated.[18] Also, in vivo (cellular interface) the generation of H_2O_2 via enzymes and its subsequent interaction with metallo-enzymes also leads to the formation of free radical $\cdot\text{OH}$. [17]

1.3.5 Hydroxyl interaction

The transition metal – OH (Hydroxyl) bond is considered to be a very strong bond of electrostatic nature with charge transfer occurring from the metal to the – OH

group. Water is also known to chemiadsorb on transition metals forming aqua ligands. Under UHV conditions the dissociative adsorption is observed leading to the formation of – OH groups.[19]

1.3.6 Chemisorption interaction of oxygen containing organic molecules

Similar to dioxygen chemisorption, oxygen containing small organic molecules like methanol undergoes dissociative adsorption on the transition metal surfaces.[20] However in case of long chained molecules dissociative adsorption is not seen. Long chained molecules especially polar lubricating oils do form a transfer film on the metal surface under tribological conditions showing chemisorption.[21]

1.3.7 Physisorption interaction of oxygen containing organic molecules

Oxygen containing small organic molecules like methanol can be made to physisorb at fixed potentials under ultra high vacuum conditions.[22] Long chain oxygen containing organic molecules which show wetting of the transition metal surface actually undergo physisorption. Polar oil shows greater physisorption on transition metal surface as compared to non-polar oils due to the preferential orientation of the polar molecules due to dipole interactions. [23]

To summarize the discussion, Table 1.1 lists the current understanding of the metal-oxygen interactions and needs:

Table 1.1: Summary of current understanding of metal-oxygen interface

Category	Mechanisms	References	Need
Oxidation	Dissociative absorption	[14], [15]	New mechanisms with new surface chemistry.
Oxygen physisorption	Van der Waal's interaction at low temperature	[16]	
Oxygen free-radical	Free-radical OH generation	[17], [18]	
Hydroxyl interaction	Dissociative absorption, Chemical interaction	[19]	
Organic chemisorption	Chemical interaction, Dissociative absorption (Small molecules)	[20], [21]	
Organic physisorption	Van-der Waal's interaction at low temperatures	[22], [23]	

1.4 Triboelectrochemistry

Since last century numerous studies have been involved studying the effects of potential on the wear and friction. This has led to the development of a new field of study known as triboelectrochemistry.[24],[25] Till 1980s the main work has been done on aqueous solutions due to their high reactivity.[26] Recently works on conventional hydrocarbon based lubricants have also been reported.[27]

The importance of the study of triboelectrochemistry is due to its interdisciplinary nature. It covers the areas of materials science, electrochemistry, mechanics, thermodynamics and surface science. Generally speaking triboelectrochemistry is a new developing field within tribology.[28] It primarily involves the study of the physical and chemical changes that occurs between two rubbing surfaces in an electrochemical setup. As stated above the research on triboelectrochemistry started with aqueous solutions and today involves effects of non-aqueous media and also the effects of electrochemical control on the friction and wear of two rubbing bodies.

The dissertation concentrates on two areas of triboelectrochemistry. One is the tribochemical investigation in aqueous media and other is tribochemical polishing. A brief description of research done on tribochemical investigation in non-aqueous media shall also be given. However this investigation is not in the scope of the dissertation.

1.4.1. Triboelectrochemistry in aqueous media

When two surfaces rub on each other in presence of an electrolytic solution then significant modifications occur on the physico-chemical nature of the surface. These

changes depend on the pH of the solution, the applied potential and contact pressure. [29],[30],[31],[32],[33] The triboelectrochemical setup in aqueous media usually employs three electrode systems, such as in corrosive wear studies of stainless steel [34], [35]. The mechanism is complex and involves basically three steps as follows [36]:

1. The contact load applied on the working electrode decreases due to the effects of electrostatic repulsion of the electrical double layer.
2. The formation of oxide layers depends on the electric field generated by the double layer.
3. The rate of the electrochemical reaction on the rubbing surfaces is controlled by the applied electric field.

Due to the complicated mechanisms involved electrochemists prefer to use other surface characterization techniques like X-ray photoelectron spectroscopy (XPS) and atomic force microscopy (AFM) to understand better the chemical changes taking place on the surface.

1.4.2 Triboelectrochemistry in non-aqueous media

The conventional electrochemical methods fail in the case of triboelectrochemistry in non-aqueous media due to low conductivity of lubricants. As such two-electrode method is applied to facilitate direct voltage application.[37] The wear and friction behavior depends on the polarity of the molecules under investigation.[38],[39]

1.4.3. Triboelectrochemistry in electrochemical mechanical polishing

Polishing in layman terms means to shine a surface to perfection. This is achieved due to surface planarization which results in a perfect smooth surface. In case of electronic chips this has added importance due to layer by layer deposition engaged in chip fabrication. [40],[41] Chemical mechanical polishing has long been used to polish electronic chips. The mechanism of action is two folds. The mechanical forces as well as the abrasives undergo a synergic process to wear out the rough edges and give an atomic level planarization precision.[42] The electrochemical mechanical polishing (ECMP) that this dissertation deals with basically combines the electrochemical set-up with the conventional chemical mechanical polishing (CMP). Usually a two electrode or a three electrode system is used for the polishing process with the working electrode acting as the anode. Metal oxide layer is formed and simultaneously polished giving a more effective polishing technique. [43] There is another form of electrochemical mechanical polishing known as tribological electrochemical polishing (TECP). TECP is based on tribochemical polishing (TCP) in which the working surface is rubbed on a hard surface like ceramics and stainless steel as proposed by Dr. Fischer et al. [44],[45] In TECP the polishing pad also acts as one of the electrode and is metallic in nature. TECP due to its firm surface is said to have high polishing efficiency. The post-CMP cleaning which is a problem faced in CMP industry is considerably removed due to non usage of abrasive materials in this procedure. [28]

The dissertation deals with the triboelectrochemical investigation of the polishing of tantalum. The mechano-chemical effects on the oxidation states of tantalum are

studied. The procedure applied is electrochemical mechanical polishing (ECMP) and chemical mechanical polishing (CMP).

CHAPTER II

MOTIVATION AND OBJECTIVES

2.1. Motivation

As discussed previously, there are needs to advance current understanding of metal-oxygen interactions under non-equilibrium conditions. Specifically, the interfacial interactions of the oxygen based molecules, both organic and inorganic, under tribological conditions are yet to be understood. The non-equilibrium conditions often are associated with the tribological process, where synergy of physical or chemical interactions is concerted in a system having dynamic contact such as sliding. The area of contact between the two surfaces undergoes chemical changes under such non-equilibrium conditions. The present research generates and characterizes the tribochemical interactions that occur due to the interaction of oxygen containing molecules with an industrially important transition metal used extensively in semiconductor industry. Tantalum is selected as the material to be investigated.

The non-equilibrium processes result in the formation of unique metastable products which are hitherto unknown. Mechanical parameters like shear, pressure, and velocity induce breaking of the weak bonds forming a non-equilibrium product.[46] Non-equilibrium oxides like Wustite have been known to form by aid of high energy mechanical activation.[47] Rare-earth oxides are also known to have been formed by mechano-activation.[48] These non-equilibrium oxides have found multiple uses in batteries,[49],[50] ferro-electrics,[51] and catalysis[52],[53],[54],[55].

It is known theoretically that under these mechano-chemical parameters the surface and near surface atoms react corresponding to the stress and at certain moments, the inter-atomic bonds are stretched and others compressed. Under applied forces, the inter-atomic distance of solids decreases, this leads to greater overlap of wave functions[9]. Similarly, shear force leads to the change of bond angles and hence facilitating decrease in band gap bringing about a chemical transformation of the moieties.[56],[57].This research aims to generate and investigate these meta-stable transformations and understand the theory behind their formation. Also the effects of additional energy such as electrical energy in the generation of metastable products are investigated. The effects of mechanical energy on chemical properties will be studied. Figure 2.1 illustrates the simple relationship between mechanical and chemical interactions.

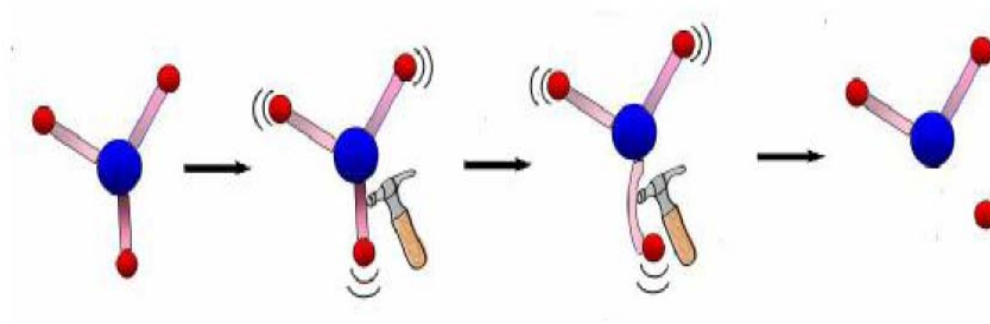


Figure.2.1: A mechanical force text-book model shows the impact of this force targeted on specific bond. When the impact of mechanical force generated is higher than the bonding strength of the molecule alternative chemical reactions take place under such conditions.

Further more, this research will develop mechano-chemical techniques to generate meta-stable reaction products. High resolution and in situ techniques will be developed or used to help understanding the mechanisms of such. The research generates a unique non-equilibrium diagram that would be benefit for industry to understand the effects of electrochemical-mechanical force on the oxidation of tantalum during polishing, such as chemical-mechanical polishing (CMP) in microelectronics. The development of *in situ* monitoring technique will be benefiting the detection of any surface changes as a result of tribochemical reaction.

2.2. Objectives

There are three major scientific objectives to be achieved in this research.

2.2.1. Understanding of non-equilibrium reactions and interfacial properties

Investigation of non-equilibrium reactions and resulting meta-stable phases is to be carried out. Understanding of dynamics and kinetics of the reaction process will be obtained. In addition, a non-equilibrium diagram will be proposed in comparison with the current equilibrium Pourbaix diagrams.

2.2.2. Development of methodology to study tribochemical surface properties

A unique approach is applied to develop a test methodology that can be used to in situ monitor, evaluate, and optimize tribochemical and triboelectrochemical processes and generate desired (meta-stable) phases. The methodology is expected to understand the behavior of corrosive as well as oxidizing fluids on the tantalum metal surface.

2.2.3. Obtaining knowledge of mechanisms of meta-stable phase formation

The major challenges in this aspect are the limited amount, their sensitivity, and stability of materials to be analyzed. A series of high resolution techniques will be tested out and a methodology will be developed at the end. Techniques include AFM, and XPS, among others. The purpose is to understand principles of formation of meta-stable phases and learn properties of the same. Knowing the relationships of process-property of meta-stable phases has signification scientific and technological importance.

In the next chapter a detailed analysis will be provided on the experimental conditions for the proposed research.

CHAPTER III

EXPERIMENTAL APPROACH

3.1 Materials

3.1.1 Tantalum

The metal that has been primarily investigated in this project is tantalum (Ta). Figure 3.1 shows the position of tantalum in periodic table.

The figure shows a schematic periodic table. The d-block elements are shaded in grey. The element Tantalum (Ta) is highlighted in yellow. A yellow arrow labeled "d - block" points to the grey-shaded region. The element Oxygen (O) is highlighted in light green in the second row from the top right. The f-block elements are shown as two rows of grey boxes below the main table.

Figure 3.1: Table showing the elements that will be investigated in the project.

According to International Union of Pure and Applied Chemistry (IUPAC) a transition metal is defined as "*an element whose atom has an incomplete d sub-shell, or which can give rise to cations with an incomplete d sub-shell.*"[58] This excludes zinc

(Zn), cadmium (Cd) and mercury (Hg) from the group. Traditionally however they have been included in the d-group elements.

The reasons for including the transition element tantalum of the transition metal series are enumerated as follows:

Tantalum (Ta) belongs to the third transition metal Series and has an electronic configuration of $5d^34s^2$ [59]. Tantalum is a non-reactive metal under air, water, strong acids or alkaline solutions. This unique property of being unaffected in non-equilibrium conditions is derived from the fact that it forms a passive, impervious layer of Ta_2O_5 . [60] The thin layer of Ta_2O_5 has found applications in dielectric for storage capacitors, gate insulators in metal-oxide-semiconductor (MOS) devices, optical coatings, anti-reflection coatings and coatings for hot mirrors. [61] Investigation of meta-stable products of Ta during chemical mechanical polishing (CMP) is essential to better understand the effects of tantalum oxide coating in devices. The CMP industry will benefit a lot in proper understanding of the tribochemical changes that occur during polishing of the tantalum surface. Electro-tribochemical polishing is investigated as major Ta_2O_5 passive layer is formed in CMP through anodization procedure. [62] Moreover the Pourbaix diagram of tantalum shows a uniform +5 oxidation state in all anodization potentials in all pH solutions. [63] A new Kar-Liang diagram is to be devised which takes into account the effects of mechanical force on the chemistry and electrochemistry of tantalum. This will help to better understand the non-equilibrium processes of tantalum thus helping in industrial applications.

For experimental purposes both tantalum bulk and tantalum wafers were used. Tantalum disk was obtained from Goodfellow with a purity of 99.99% wt. The sample disk was firstly cleaned using acetone, isopropanol, and deionized water after polishing on a 800-1200 grit sand paper. Tantalum wafers have been also used in experiments related to generation of Kar-Liang diagram. The tantalum wafers were provided by Intel.

3.1.2 Solvents

As stated in Chapter I the dissertation involves the study of chemical-mechanical and electrochemical-mechanical polishing of tantalum. Hence different solvents are used to facilitate the polishing process. The solvents and their concentration have been chosen based on the standards used in CMP industry.[60] The properties on the basis of which the three different solvents have been chosen in order to better understand the mechano-chemical reactions of tantalum are enumerated in this section as follows:

3.1.2.1 Hydrogen peroxide (H₂O₂)

Hydrogen peroxide has been chosen as one of the solvents due to it being an oxidizing agent. It has a high oxidizing potential of 1.8 V which is higher than that of potassium permanganate at 1.7 V and chlorine at 1.4 V. [64] Hydrogen peroxide also easily decomposes in water to form water and oxygen.[60] This property is particular useful in oxidation reaction of the tantalum surface.

Hydrogen peroxide 35%wt was obtained from Sigma Aldrich. In experiments the stock solution was diluted to 5% wt and had a pH of 4. The 5% wt was chosen as it is the standard used in preparation of commercial slurries for CMP industry.[65]

3.1.2.2 Acetic acid (CH₃COOH)

Acetic acid was chosen as one of the solvent as it is used in post-CMP cleaning process. Acetic acid is a good corrosive agent and effectively removes the surfactant molecules in post-CMP cleaning. [66] Moreover acetic acid is also a good reducing agent. It is also used as a complexing agent in the slurry used in post-CMP cleaning.

Acetic acid stock solution was obtained from EMD Chemicals. The stock solution was diluted to 0.13 M as it was the standard used in preparation of commercial slurries for CMP industry.

3.1.2.3 Deionized water (H₂O)

Deionized water was used as a control in the experiment. Also deionized water has been used in CMP and ECMP processes for two decades to make atomically flat surfaces. [66] Moreover for Pourbaix diagram studies deionized water is essential as the +5 oxidation state in anodization potential is stable at a wide range of pH in water.

Deionized water was obtained from deionized water filter in Department of Physics, Texas A&M University, College Station.

3.1.2.4 Potassium chloride (KCl)

Potassium chloride is used as a conducting salt in the electrolytic solution. Deionized water is saturated with KCl making it more conductive in ECMP experiments. KCl was obtained from EMD Chemicals of GR grade for the experiments.

3. 2 Experimental setup

As stated earlier the nature of the work of this research can be classified into two fields – A) triboelectrochemistry and B) tribochemistry. But both works are unified in the theme of investigation of interaction of oxygen containing molecules with transition metal in this case tantalum under mechano-chemical conditions.

3.2.1 Tribochemistry set-up

The tribochemical setup facilitates the chemical mechanical polishing of tantalum. As schematic is shown in figure 3.2 in which the CSM tribometer is modified to mimic a polishing apparatus. A polymer shaft holds the working surface which is the tantalum piece. A polyethylene pad is used as the polishing pad. The whole setup is immersed in the desired electrolytic solution. The resulting friction is measured in the computer console. A rotating motion is applied. The tantalum piece remains static whereas the polishing pad rotates. In the next section we shall discuss the triboelectrochemical set-up.

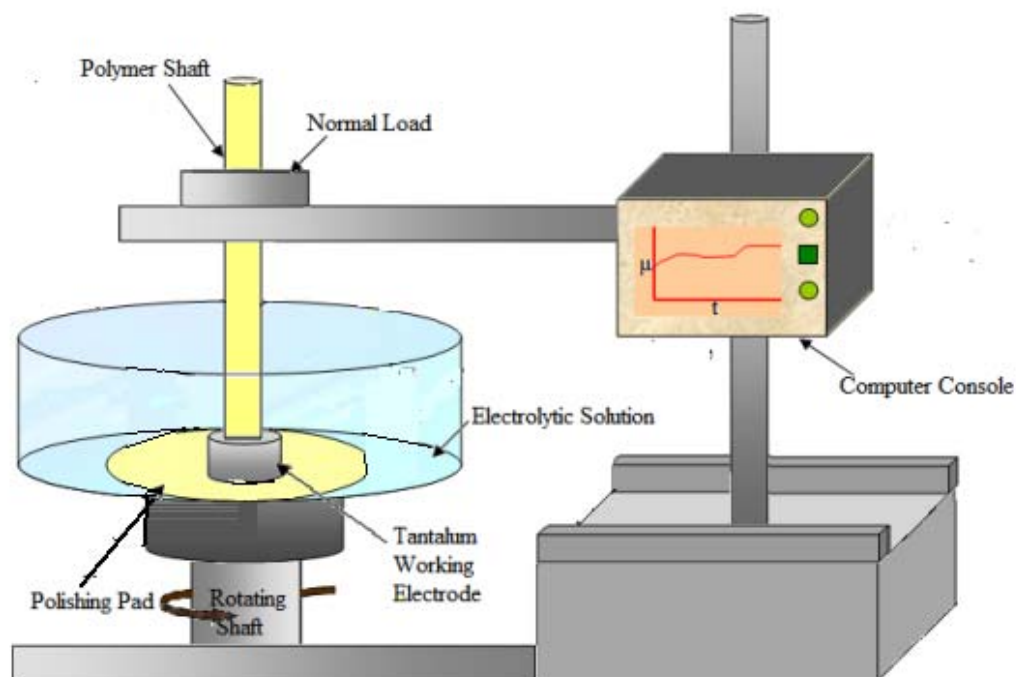


Figure 3.2: Schematic showing the tribochemical set-up for bulk tantalum polishing.

3.2.2 Triboelectrochemistry set-up

The system setup is shown in figure 3.3 consisting samples and electrodes. The insert on the right of figure 3.3 illustrates the interface of the test sample and its rubbing partner, a polymeric polishing pad. Sliding direction is shown with arrows. The sliding speed, down force, and electrolyte can be varied with as desired. This technique enables us to quantify the amount of input mechanical energy with controlled electrical potential and pH values.

Figure 3.3 shows a three-electrode system that is employed to perform the potentiostatic 3-electrode electrochemical reactions. There is a potentiostat, a polymer shaft (1), test sample (2), reference electrode (3), counter electrode (4), and a polymer

pad (5). The workpiece is tantalum. The shaft connected to the tantalum that slides against the polymer pad at a desired speed under a fixed applied load. The tangential force is generated and recorded. The tantalum (2) is the working electrode and is attached to a polymer shaft (1). The tantalum sample is wired and connected to the reference calomel electrode (3). The counter electrode is made of a platinum wire (4). The wire around the tantalum sample is protected with epoxy resin. The mechanical polishing of the tantalum sample was done on a SepharidimTM fluorescent yellow polishing pad (5), made of fiber reinforced polyethylene. The polymer pad has been chosen due to its stability.

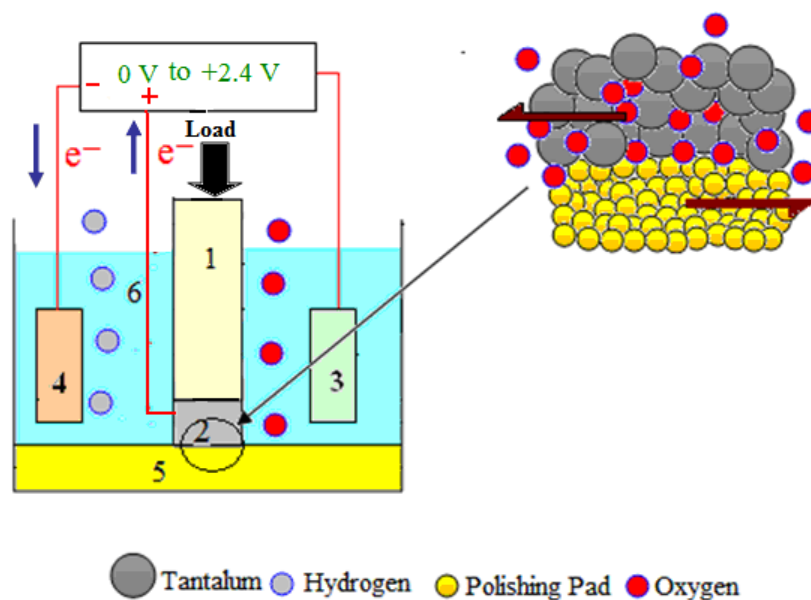


Figure 3.3: Illustration of the test setup used to apply a controllable mechanical force on a bulk tantalum.

The tantalum is pressed and slide against a polymeric polishing pad. The applied force is controlled and the sliding force (frictional force) is measured through a force sensor. A potentiostat used as a power supply is attached to the mechanical system. Alternation of chemical solutions (electrolyte) and application of electrical potential will allow variety chemical and electrochemical reactions of tantalum and its environments. A schematic of the actual set-up is shown in figure 3.4.

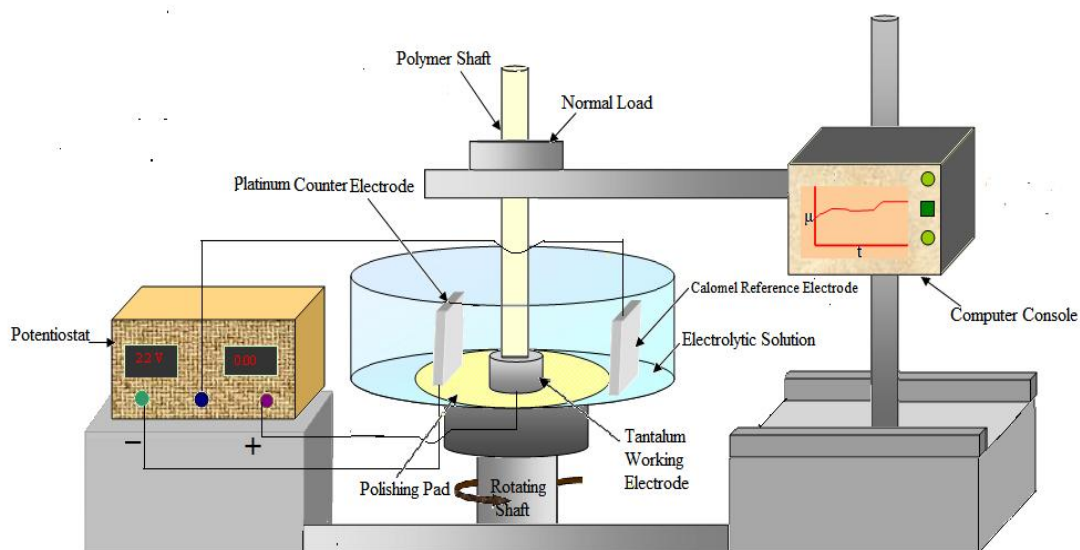


Figure 3.4: A schematic of the triboelectrochemical setup for polishing of bulk tantalum.

The frictional behavior was *in situ* monitored reflecting any surface changes. As soon as there is phase change on the application of potential it is immediately detected as co-efficient of friction change on the monitor. The kinetics of the phase change can also be roughly predicted through this system.

3.2.3 Triboelectrochemistry set-up for experiments on tantalum wafers

The schematics in sections 3.2.1 and 3.2.2 show the experimental set up devised for the polishing of bulk tantalum. However tantalum wafers are flat rectangular pieces and in order to perform any electrochemical-mechanical polishing on them changes have to be made in the design of the experiment.

The wafers were wired up first using a conductive resin and then putting a water proof resin on the top of the conductive resin. Instead of the polishing pad in this set up the wafer was used as the base. The polymer pad was cut in 2cm^2 in length and attached to the polymer shaft. A reciprocal sliding motion was employed in order to conduct the electrochemical measurement. This setup enables study in electrochemical-mechanical/mechanical experiments of tantalum in different solutions. A schematic of the setup is shown in figure 3.5.

Figure 3.5 shows a three-electrode system that is employed to perform the potentiostatic 3-electrode electrochemical reactions. There is a potentiostat, a polymer pad (2), reference electrode (3), counter electrode (4), test sample (5), and a polymer shaft (5). The work piece is tantalum. The shaft connected to the polymer pad that slides against the tantalum wafer at a desired speed under a fixed applied load. The tangential force is generated and recorded. The tantalum (5) is the working electrode and is attached to a polymer shaft (5). The tantalum sample is wired as mentioned earlier and connected to the reference calomel electrode (3). The counter electrode is made of a platinum wire (4). The mechanical polishing of the tantalum sample was done on a

Sepharidim™ fluorescent yellow polishing pad (2), made of fiber reinforced polyethylene. The polymer pad has been chosen due to its stability. Time was also kept as a factor. Once experiment was performed the samples were analyzed. The same samples were again analyzed after a period of 2 days i.e. 48 hours.

There are two main differences in the setup for polishing a tantalum wafer and a setup for polishing a bulk tantalum. First in case of polishing of bulk tantalum circular sliding motion is employed whereas in case of polishing of tantalum wafer a sliding reciprocal motion is employed. Secondly in case of polishing of bulk tantalum, the working electrode i.e. the tantalum is the static partner but in case of polishing a tantalum wafer it is the polishing pad which is the static partner.

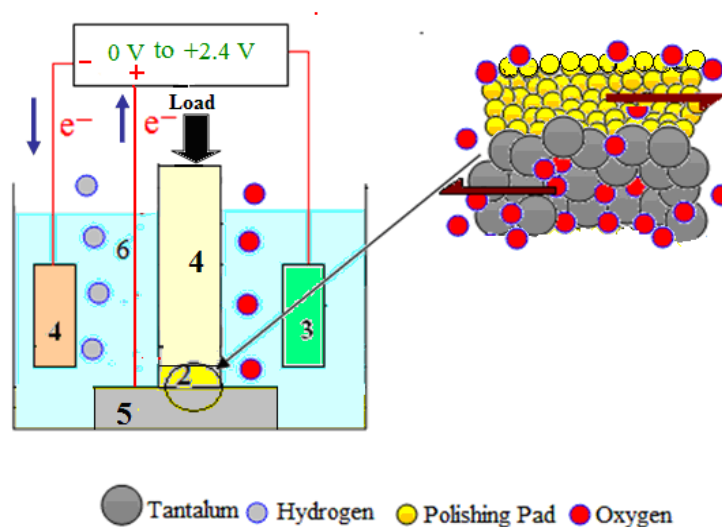


Figure 3.5: Illustration of the test setup used to apply a controllable mechanical force on a tantalum wafer.

3.3 Experimental conditions

The section highlights the experimental conditions employed to study the mechano-chemistry of tantalum. The experimental parameters and the reason for their selection are discussed. The reason for the selection of three solvent systems for investigation of the mechano-chemistry of tantalum has already been discussed in section 3.1.2. In this section each of the experiments performed based on the solvent used is enumerated. Tables are generated to explain the conditions investigated in a clear manner. Reference samples were bulk tantalum as received from Good Fellow and tantalum wafer as received from Intel.

3.3.1 Experimental conditions under 5% wt hydrogen peroxide solution

A set of two experiments were formed in an electrolytic solution of 5% wt hydrogen peroxide solution. Table 3.1 shows the experimental conditions employed.

Table 3.1: The experimental conditions used in 5% wt H₂O₂ solution

Solvent used	Potential applied	Speed	Load
5% wt Hydrogen Peroxide (pH 4)	n/a	0.5 cm/sec	1 N
	+ 2.4 V	0.5 cm/sec	1 N

3.3.2 Experimental conditions under 0.13 M acetic acid solution

A set of two experiments were formed in an electrolytic solution of 0.13 M acetic acid solution. Table 3.2 shows the experimental conditions employed.

Table 3.2: The experimental conditions used in 0.13 M acetic acid solution

Solvent used	Potential applied	Speed	Load
0.13 M Acetic acid (pH 3)	n/a	0.5 cm/sec	1 N
	+ 2.4 V	0.5 cm/sec	1 N

3.3.3 Experimental conditions under deionized (DI) water

A set of two experiments were formed in an electrolytic solution of DI water saturated with potassium chloride (KCl). Table 3.3 shows the experimental conditions employed.

Table 3.3: The experimental conditions used in DI water saturated with KCl

Solvent used	Potential applied	Speed	Load
DI water saturated with KCl (pH 6)	n/a	0.5 cm/sec	1 N
	+ 2.4 V	0.5 cm/sec	1 N

In tables 3.1, 3.2 and 3.3 it is observed that primarily two types of experiments have been performed. One is the mechano-chemical experiment in which no potential is applied and the other is the electrochemical-mechanical experiment in which a potential of +2.4 V is applied. The potential of +2.4 V is chosen as it was at this point that a dramatic increase in the co-efficient of friction data was observed in case of 5% wt hydrogen peroxide solution. The electrical potential of +2.4 V was chosen according to the equilibrium Pourbaix diagram where the Ta +5 state existed otherwise. It was kept constant in case of all other solvents for a uniform comparative study. The speed is kept at 0.5cm/sec and the load is kept at 1 N. This is because too high a speed or heavy a load has the probability to wear off the oxide film formed on the tantalum surface. The pH of the solutions is measured after preparation as shown in the tables.

The frictional behavior was *in situ* monitored reflecting surface changes. Electric potential was applied on the tantalum after a stabilized friction coefficient was achieved.

The friction experiments were carried out with the Ta disk sliding against a rotating polishing pad or the polishing pad sliding against the wafer.

3.3.4 Experimental conditions for studies on Pourbaix diagram

As a part of the process to understand the stability of +5 oxidation state in non-equilibrium conditions under mechanical force, a series of experiments were performed under various pH conditions. The pH solutions were adjusted with sulfuric acid and potassium hydroxide of different molarities. Time was also kept as one of the parameters in the experiment to understand the stability of the sub oxide states generated in tantalum. Table 3.4 represents the experimental conditions under mechanochemical parameters. No potential is applied.

Table 3.4: The experimental conditions used to generate Kar-Liang diagram in 0 V

Solvent used	Time (hrs)	pH	Load	Speed
DI water saturated in KCl (0 V)	0	1	1 N	0.5 cm/sec
	0	7	1 N	0.5 cm/sec
	0	10	1 N	0.5 cm/sec
	48	1	1 N	0.5 cm/sec
	48	7	1 N	0.5 cm/sec
	48	10	1 N	0.5 cm/sec

Table 3.5 represents the experimental conditions under electrochemical-mechanical parameters. Potential is applied is +2.4 V. The reason for the choice of the particular potential has been explained in section 3.3

Table 3.5: The experimental conditions used to generate Kar-Liang diagram in +2.4 V

Solvent used	Time (hrs)	pH	Load	Speed
DI water saturated in KCl (+ 2.4 V)	0	1	1 N	0.5 cm/sec
	0	7	1 N	0.5 cm/sec
	0	10	1 N	0.5 cm/sec
	48	1	1 N	0.5 cm/sec
	48	7	1 N	0.5 cm/sec
	48	10	1 N	0.5 cm/sec

The pH 1, 7 and 10 were chosen to test the highly acidic, neutral and highly basic conditions and their effects on tantalum under mechanical and electrochemical-mechanical parameters.

3.4 Characterization techniques

Two main characterization techniques are used to understand the chemical changes on the tantalum surface as a result of the application of mechano-chemical and electro-chemical-mechanical energy. One is the atomic force microscopy (AFM) to

understand and detect the phase changes. The other is the X-ray photoelectron spectroscopy (XPS) to understand and detect the change in oxidation states on the tantalum surface due to the effects electrochemical-mechanical energy.

3.4.1 Atomic Force Microscopy (AFM)

Atomic Force Microscope (AFM) was invented by G. Benning and C.F. Quate in 1986. [67] It completely changed the way scientists studied surface science and brought micro level analysis to nano-level. The instrument design was based on Scanning Tunneling Microscope (STM) and the stylus profilometer. The advantage of AFM is that it can create three dimensional images of high precision of the surface topography of a given specimen. With the help of AFM surface features with dimensions of a few nanometers can be measured. A magnification of 1,000,000X [68] can be achieved because of AFM hitherto not possible.

The AFM images the surface topography by raster scan. The probe generally used is a single crystal silicon. A laser beam is incident on the cantilever on which the probe is mounted. As the probe scans the incident laser beam is deflected to the photo detector and image is observed. With the help of AFM surface phenomena such as adhesion, friction, phase distribution, wear, hardness, etc. can be studied.

There are two modes of operation in AFM. One is the contact mode and the other is the non-contact mode. In contact mode the AFM tip scans on the surface thus giving a topographic feature of the specimen. Friction (lateral force) can be measured with the help of contact mode. In case of non contact mode the probe feels the change in electrostatic forces of attraction or repulsion as it rasters across the topography of the

specimen and registers the image. For our experiments we used the non-contact mode in order to detect phase changes due to application of mechano-chemical or electro-chemical-mechanical forces. Figure 3.6 shows a commercial AFM whereas figure 3.7 shows the differences between a non-contact mode AFM and a contact mode AFM. An example of a non-contact mode AFM image is also shown in figure 3.8



Figure 3.6: A commercial AFM (Pacific Nanotechnology Incorporated) from Dr. Liang's surface science and interface laboratory. [69]

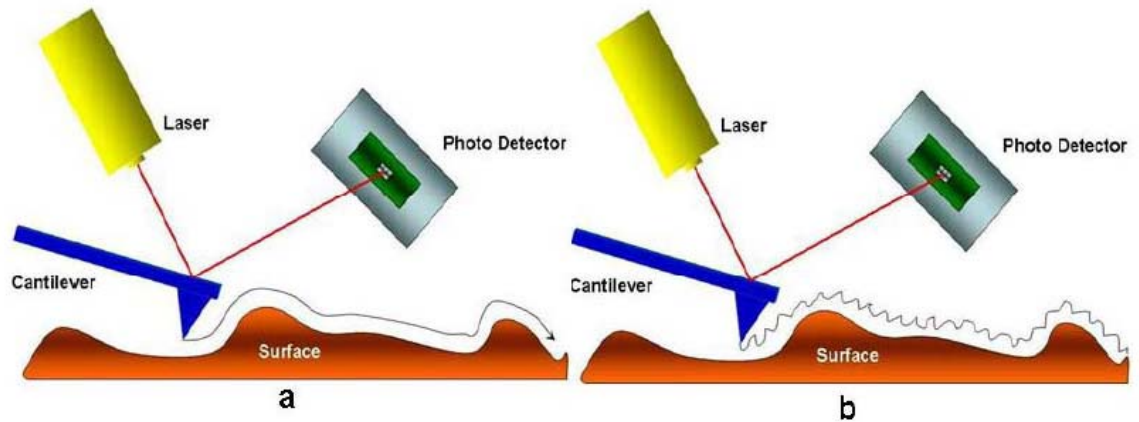


Figure 3.7: Atomic Force Microscopy (AFM) a) contact mode and b) non-contact mode. [69]

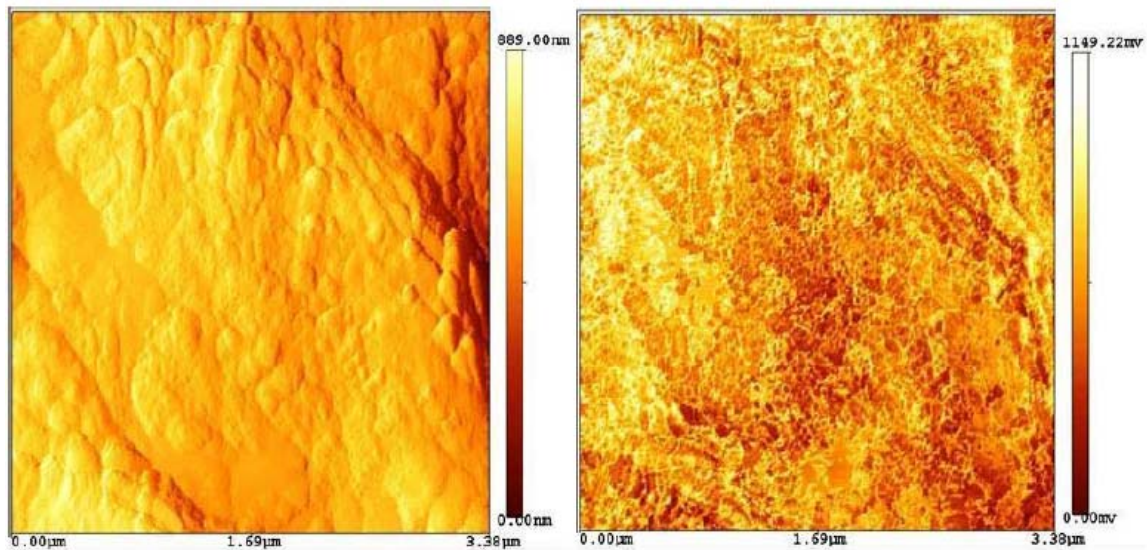


Figure 3.8: Non-contact AFM image of a polished Al surface. Left image showing topographic features and right image showing phase image. [69]

3.4.2 X-ray Photoelectron Spectroscopy (XPS)

X-ray photoelectron spectroscopy (XPS) is used for oxidation state detection as well as elemental percentage detection in a wide variety of samples which includes

metals, polymers, ceramics, semi-conductors and biological materials. The specimen can either be solid, liquid or gaseous. [8] R.G. Steinhardt et al reported the first work on XPS on the detection of physical and chemical properties of a surface specimen. [70] K. Seigbahn made significant contributions in the development of XPS and was awarded the Nobel Prize for Physics in 1981 for this invention of his. XPS is also known as Electron Spectroscopy for Chemical Analysis (ESCA). [71][72]

The specimen surface is irradiated with monochromatic soft X-rays under high vacuum. The electrons emitted by the surface atoms are then detected. The output signal is plotted as a function of number of emitted electrons with either binding energy or kinetic energy. Due to electrons being emitted from specific orbital every element has a fingerprint spectrum. Through standardized handbook it is possible to identify the elements and their oxidation states by studying the peak shifts. Quantitative analysis of elements is also possible by measuring peak areas [73], [74]. A commercial XPS instrument is shown in figure 3.9 and a specimen XPS raw peak of tantalum is shown in figure 3.10.



Figure 3.9: A Kratos Imaging X-ray Photoelectron Spectrometer in Materials Characterization Facility. [69]

The following figure 3.10 shows the raw peaks of tantalum pentoxide and tantalum suboxide. The shift in peak indicates a change in the stoichiometric ration of tantalum and oxygen.

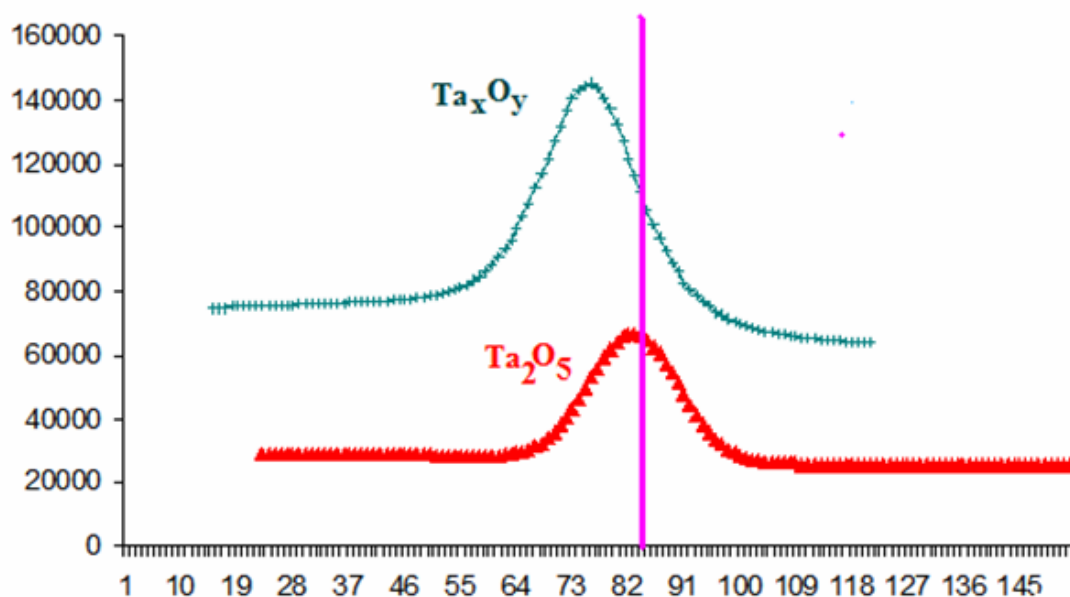


Figure 3.10: XPS raw specimen peaks of tantalum pentoxide and tantalum suboxide.

A Kratos Axis Ultra Imaging X-ray photoelectron spectrometer (XPS) with the spherical mirror analyzer was operated at a base pressure of 10^{-10} Torr for all the experiments performed. Mg $K\alpha$ X-ray radiation (1253.6 eV) at a power of 350 W was used. The number of cycles per experiment was 3. All binding energies have been recalibrated for sample charging effect with reference to the C 1s line at 284.0 eV. The XPS peak areas and peak decomposition were determined by using the software XPSPEAK4.1. The line shapes of Ta 4f provide information about the chemical bonding environment. Fitting the peak to suitable functions allows the bonding information to be extracted. The curve fitting was done using XPSPEAK 4.1 software, with Newton's iteration method and 200 iterations.

In the following chapters we will look into detail the results of the various experiments performed. A new theory will be put forward for mechano-chemical equations and a non-equilibrium Kar-Liang diagram will be generated based on the findings.

CHAPTER IV

MECHANO-OXIDATION OF TANTALUM*

Industrial processes such as polishing and planarization utilize mechanical forces to make smooth surfaces.[7] In different chemical environments, mechanical forces can result unique chemical reactions.[9],[44],[75],[76],[77],[78],[79],[80] Among those reactions, mechanical-force-related metal oxidation is not found in chemistry textbook. Understanding fundamental issues of metal-oxides, such as metal-insulator transition, would enable us to design photovoltaic devices, gas sensors, microelectronics, and corrosion protection devices. [81], [82]

As discussed in the experimental section of Chapter III, we assembled a system that is able to generate, monitor, and evaluate oxidation states of metals *in situ*, through an electrochemical-mechanical approach. The system is similar to what has been used for tribocorrosion study [83], [84]. The observation of controlled oxidation enables us to study the kinetics of the process and monitor any phase changes. The system setup is described in details in chapter III in test-setup section (3.2).

The objective of investigation described in this chapter is to study a different type of oxidation, mechanical-force assisted passivation. Experimental approaches used here is to use electrotribochemistry to monitor the mechano-chemical effects of oxidation of tantalum surface. Results are discussed in the following.

*Oxidation of Tantalum by Mechanical Force, P. Kar, K. Wang, H. Liang (Electrochemical and Solid-State Letters, 2008, Volume 11, Number 2, **in print**).

4.1 Frictional behavior

Friction experiments were performed in a 5%wt H₂O₂ electrolyte. There are total 2 types of experiments that were conducted. The first experiment was conducted without applying an electrical potential between tantalum and platinum electrodes. A load was applied to the Ta. The sliding motion generates a tangential force, i.e., friction. A constant friction coefficient is shown in figure 4.1. The test duration was 15 minutes when friction was stabilized.

The friction coefficient μ , is defined as the ratio of the tangential force F_t divided by the applied normal force F_N , i.e., $\mu = F_t/F_N$. In the second experiment, a potential of 2.4 V was applied after 9 minutes at which time the friction coefficient jumped as shown in figure 4.1. The increase in friction stabilized after about 5 minutes. The load and velocity remained the same in both experiments. The experiment was repeated 3 times and found to give repeatable results with increase in friction with the increase in potential. In order to generate a reference sample, the third experiment was conducted with a potential of +2.4 applied without any mechanical force. The sample surface generates the thermodynamically stable state of oxide, Ta₂O₅. It is used as the reference.

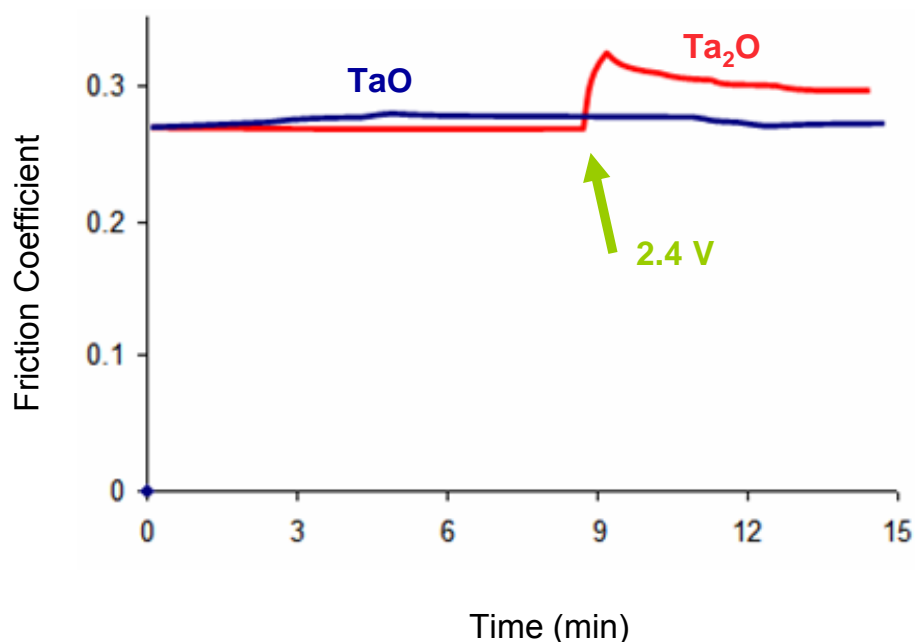


Figure 4.1: Friction coefficient of tantalum sample in 5% wt hydrogen peroxide. When an electrical potential was applied at 9 minutes, there was a jump in friction.

Sample surfaces were afterwards analyzed with an atomic force microscope (AFM). The phase images are shown in figures 4.2a and 4.2b. The left figure (4.2a) is the surface image taken before and the right (4.2b) being after electrochemical-mechanical experiment. The color intensity presents the distribution of different phases through phase imaging. After test the phases shown are uniformly distributed in the area scanned. As shown in figure 4.1, the initial friction of both samples was the same. With an applied +2.4 volt, the friction increased and then stabilized at around 0.3. Correlating friction with the AFM phase images in figures 4.2a and 4.2b, the fact of having a high friction with uniformed phase distribution indicates the dominating factor being surface chemistry.

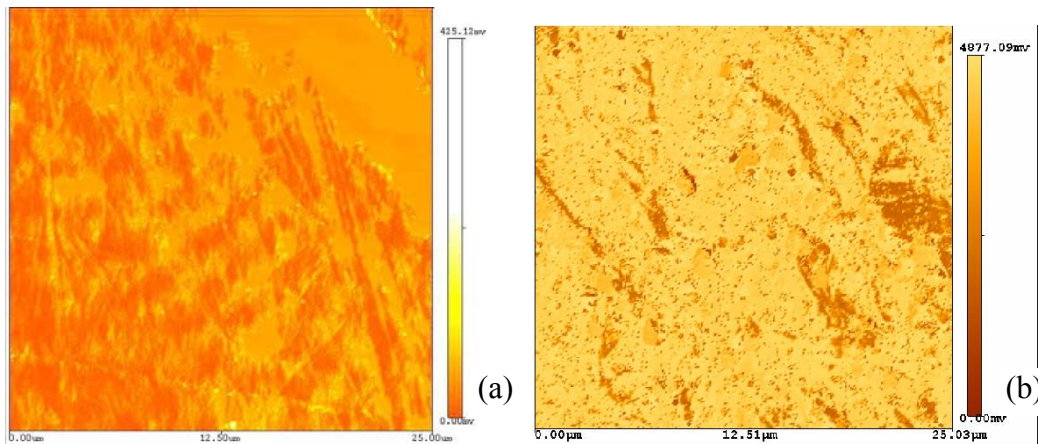


Figure 4.2: AFM images of tantalum sample surface before (a) and after (b) electro-mechanical experiments. Comparing with pre-surface (a), the Ta surface after test was smooth with uniform phases distributed in the sample. The phases are Ta and its oxides.

The X-ray photoelectron spectroscopy (XPS) identified the oxides on the sample surfaces. Dr. Liang's Surface Science Laboratory has in the past reported effects of friction on oxidation of Cu during polishing [85],[66],[86],[87] and on phase transformation of ice.[88],[89] The present work reports the friction-induced unique oxidation of tantalum that widens our understanding in the non-equilibrium state of substances.

4.2 Meta-stable oxides of tantalum

The X-ray photoelectron spectroscopic peaks are shown in figure 4.3. Figure 4.3a shows three samples having different peaks. Samples are labeled by their test conditions. The oxide state will be discussed later. The arbitrary unit (y-axis) is used here in order to compare the binding energy (x-axis). The arbitrary unit (y-axis) is used here in order to

compare the binding energy (x-axis). Figures 4.3b-4.3d are deconvolution of those three original peaks. Figures 4.3b is for the sample being tested with friction and electrical potential. Four large and four small peaks exist. Within the binding energy of 26 and 28 eV, $4f_{5/2}$ and $4f_{7/2}$ +5 oxidation state Ta peaks were found that have been reported as pentoxide.[61] Comparing other oxide peaks with published data,[90] the peaks around 25 and 27 eV are + 4 and + 3 $f_{5/2}$ and $f_{7/2}$ peaks respectively. These peaks are strong ones. At lower binding energy area (20 – 23 eV), the + 2 and + 1 peaks exist. According to published data, the binding energy of metallic Ta is in the range of 20 eV to 23eV.[90] Among all peaks, there was no metallic Ta shown. Figures 4.3d is for the reference sample (as cleaned). Results showed two characteristic peaks Ta_2O_5 . For $4f_{5/2}$ and $4f_{7/2}$ peaks, the binding energy is in the published data. It is known that the fully oxidized stoichiometric Ta_2O_5 has two associated peaks at around 26 and 29 eV.[90] This was seen in the reference sample in Fig. 4.3d. As noted that the reference sample was processed without mechanical force. Comparing with other two samples where friction was applied, it is clear that friction induces a peak shift. The shift direction depends on the chemical environments.

Figure 4.3a as mentioned earlier shows the raw XPS data of the three conditions.

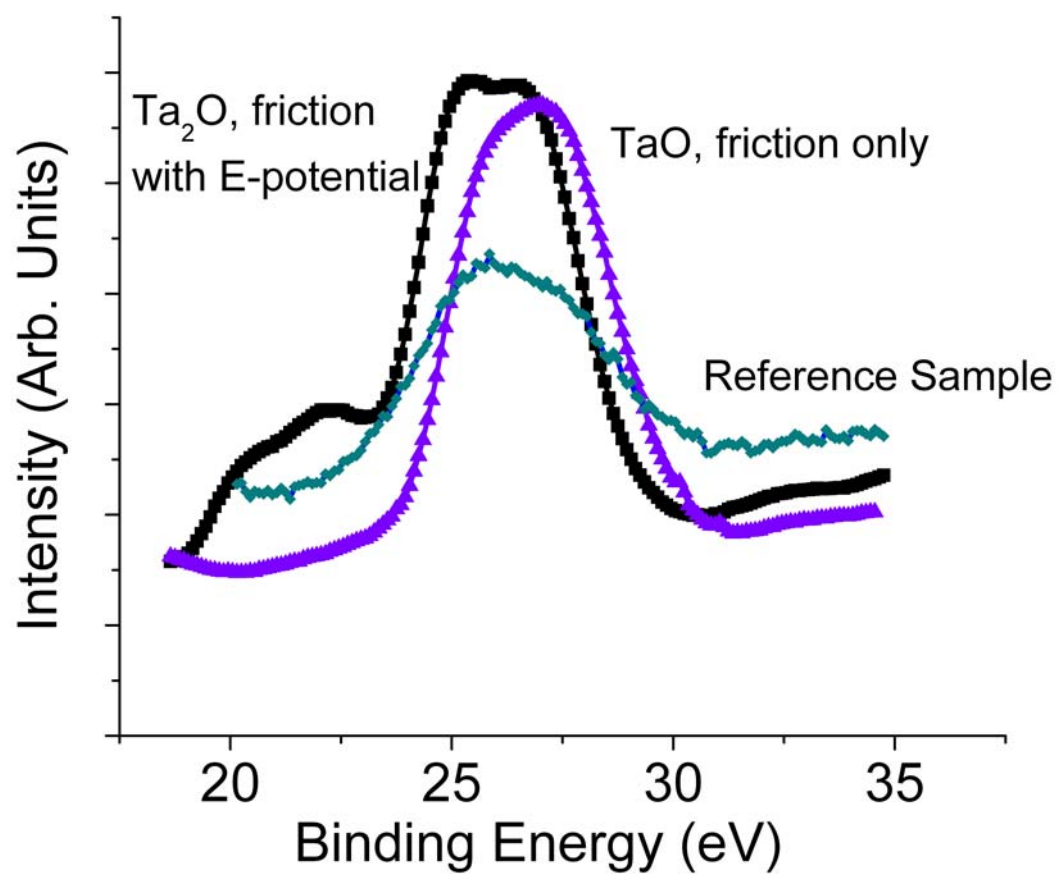


Figure 4.3a: XPS spectra of Ta sample surfaces obtained after immersion in 5%wt H₂O₂ solution with friction and electro potential; friction only; and electro potential only.

Figure 4.3 b shows friction and electrochemical conditions combined.

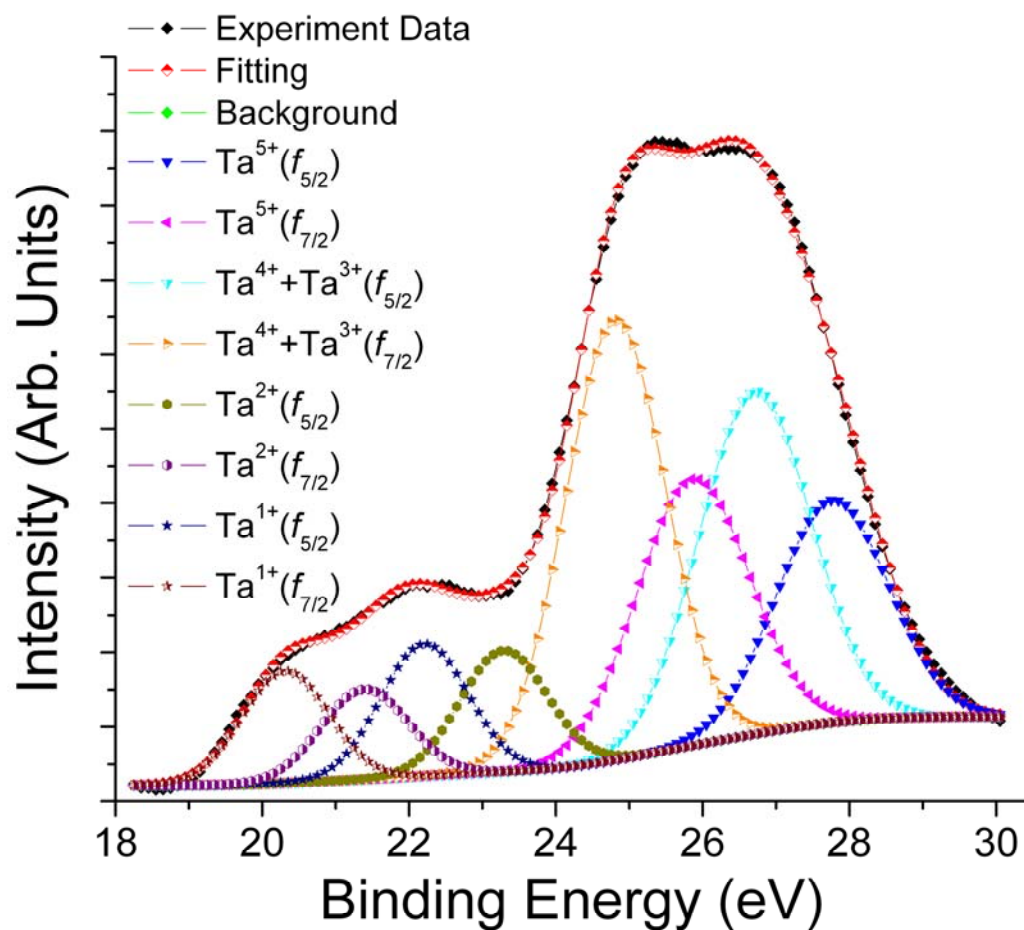


Figure 4.3b: Deconvoluted Ta 4f XPS envelope obtained from the Ta surface after immersion in a solution with 5%wt H₂O₂ with both friction and electro potential.

Figure 4.3c shows friction only conditions.

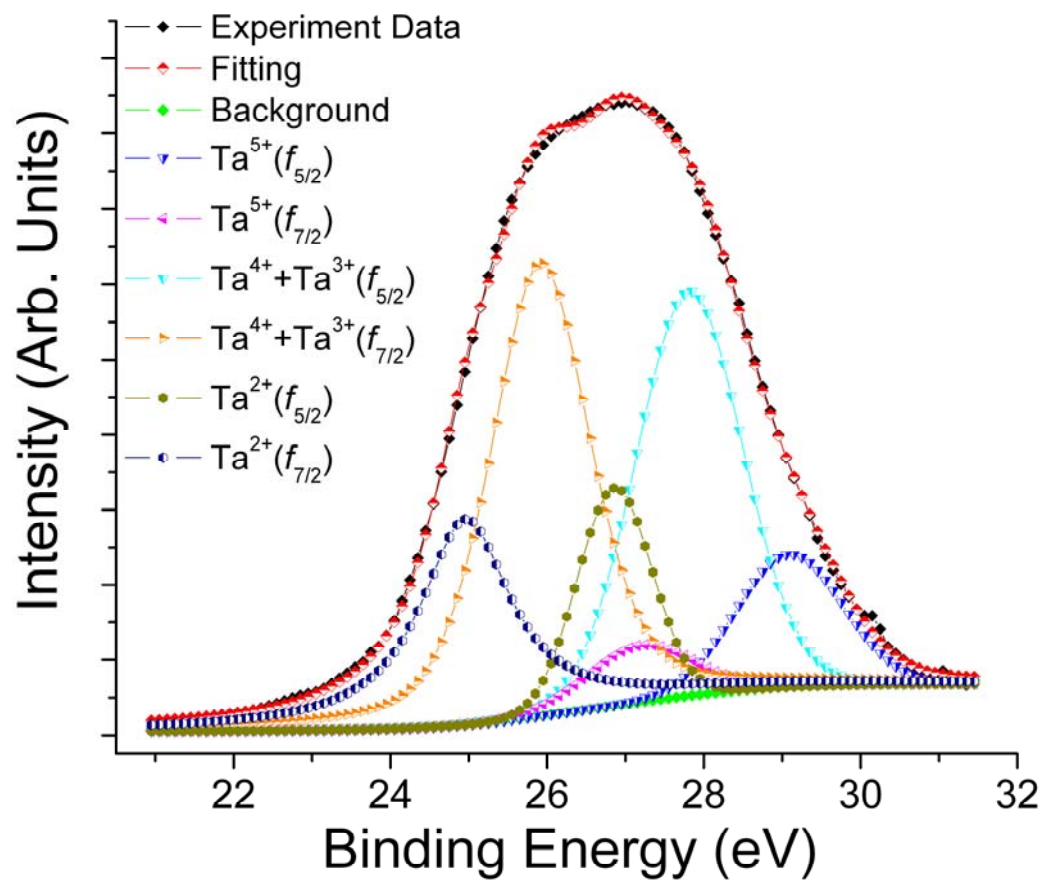


Figure 4.3c: Deconvoluted Ta 4f XPS envelope obtained from the Ta surface after immersion in a solution with 5%wt H₂O₂ with friction only.

Figure 4.3d shows the reference sample subjected to only electrochemistry.

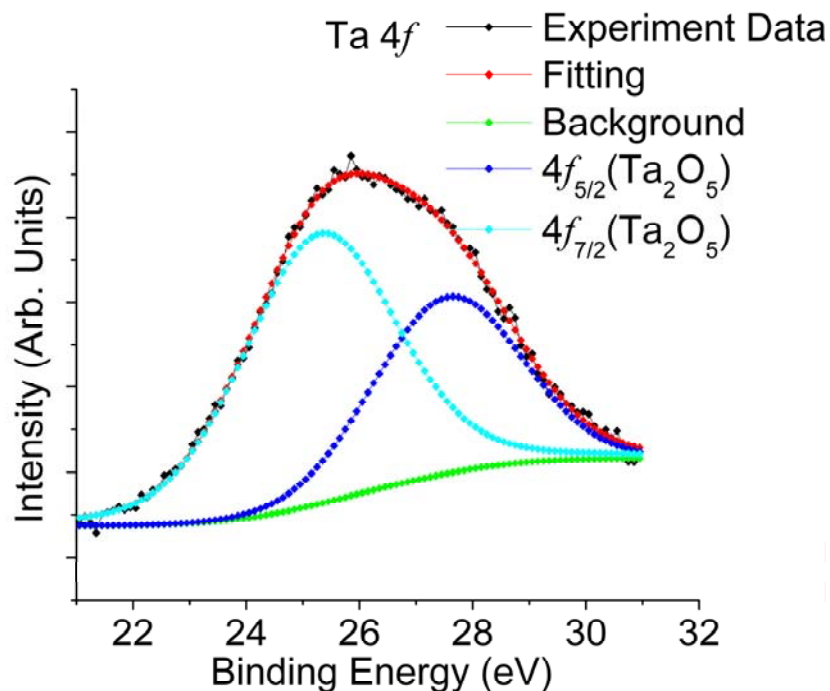


Fig.4.3d: Deconvoluted Ta 4f XPS envelope obtained from the Ta surface after immersion in a solution with 5%wt H₂O₂ with electro potential only.

In the case of suboxides, they were found to coexist with Ta₂O₅. Comparing the tantalum XPS peaks representing the three samples obtained under different process conditions, it is evident that different tantalum oxides appeared from different conditions. Primarily it is observed that Ta⁺¹ state is present during the application of electro-chemical mechanical energy whereas it was not observed when only mechanical energy is applied or when the sample is subjected to electrochemical energy only. With friction force, Ta⁺², Ta⁺³, Ta⁺⁴ were formed. With friction and electrical potential, Ta⁺¹, Ta⁺², Ta⁺³, Ta⁺⁴ were found. With electrical potential only, the equilibrium Ta⁺⁵ was

found, as for the reference sample. These results prove that frictional force, i.e., surface tangential force, induces non-equilibrium tantalum oxides.

It is noted that the hydroxyl peak was not found in our experiments. Comparing with oxide peaks, they were too weak to be detected. The table 4.1 below summarizes the findings of the XPS data.

Table 4.1: Samples subjected to mechano-oxidation and products yielded

Sample	Potential	Speed	Load	Product
Tantalum in 5% wt hydrogen peroxide	+2.4	0.5 cm/sec	1 N	Ta+1, Ta+2, Ta+3, Ta+4, Ta+5 (Sample 3b)
	n/a	0.5 cm/sec	1N	Ta+2, Ta+3, Ta+4, Ta+5 (Sample 3c)
	+2.4	n/a	n/a	Ta+5 (Sample 3d)

4.3 Sub-oxide film thickness

The thickness of sub-oxides was measured using the AFM. An interface of reference sample and the tested surface was generated using a mask technique. Details about this technique have been reported by Dr. Liang's group.[89] A brief description of the procedure is described here. The oxide thickness information is necessary for reliable surface analysis. The film needs to be thick enough so that the XPS analysis detects sufficient information.

In the experiment, a portion of the sample surface was masked so that this part surface is not exposed to the chemical environments. The unmasked surface was then subjected to both tribochemical and electrotribochemical reactions. After experiments, the mask was taken off so that the original surface appears. AFM scanning was then conducted across the interface of the original and unmasked areas. Figure 4.4a shows the interface region where tribological experiment was performed in conjunction with reference surface. Figure 4.4b shows the interface region where electrotribochemical experiment was performed in conjunction with the reference surface. The bright region is the oxidized layer whereas the relatively darker region is the masked area. Both in figures 4.4a and 4.4b the line scan is diagonal. The difference of the height across the interface is the height reduction or addition, as shown in figure 4.4. A line normal to the two parallel diagonal lines is then drawn to measure the average peak to valley depth. It is then compared with the reference sample to compare the thickness of the film.

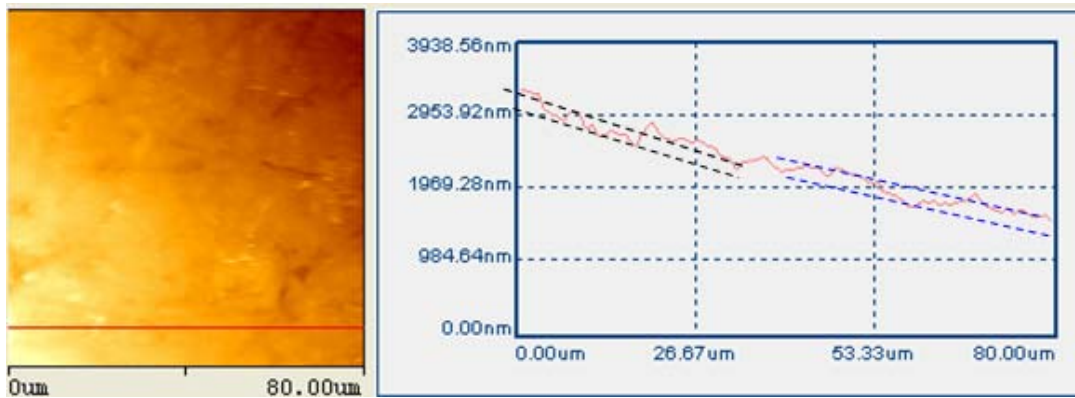


Figure 4.4a: Line analysis of the AFM topography showing tantalum surface original on right side and tantalum surface unmasked and exposed to tribological mechanism on left side.

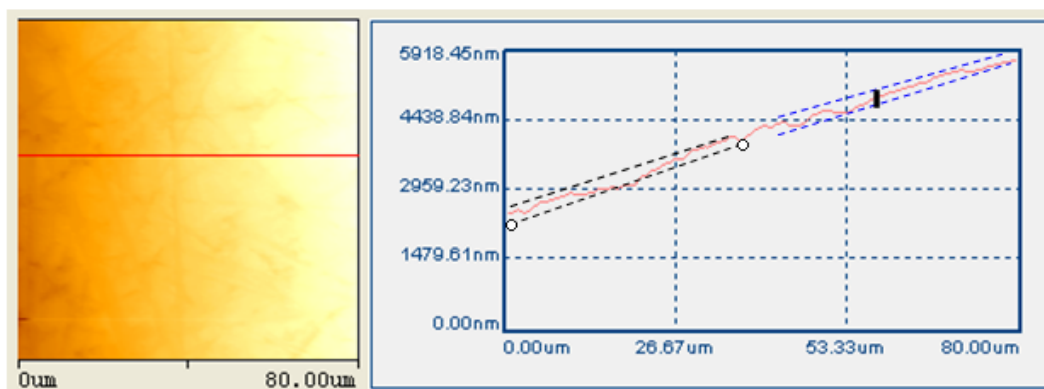


Figure 4.4b: Line analysis of the AFM topography showing tantalum surface unmasked and exposed to electro-tribological mechanism on right side and original tantalum surface on left side.

The oxide thickness of the sample prepared through pure mechanical polishing was about 250 nm while for that of electrochemical-mechanical was around 215 nm. It has been reported that the thickness of the native oxide of tantalum is around 2-3 nm [91],[92],[93],[94] As mentioned earlier, the test duration for both samples was not the same in order to compare the change of friction due to applied potential. This would not affect the thickness measurement as the initial mechanical force duration was same. On

anodization due to release of oxygen molecules, greater friction leads to thinning of the film. The graphical representation figure 4.5 below gives a visual comparison of the thickness of the different films formed along with their standard deviations.

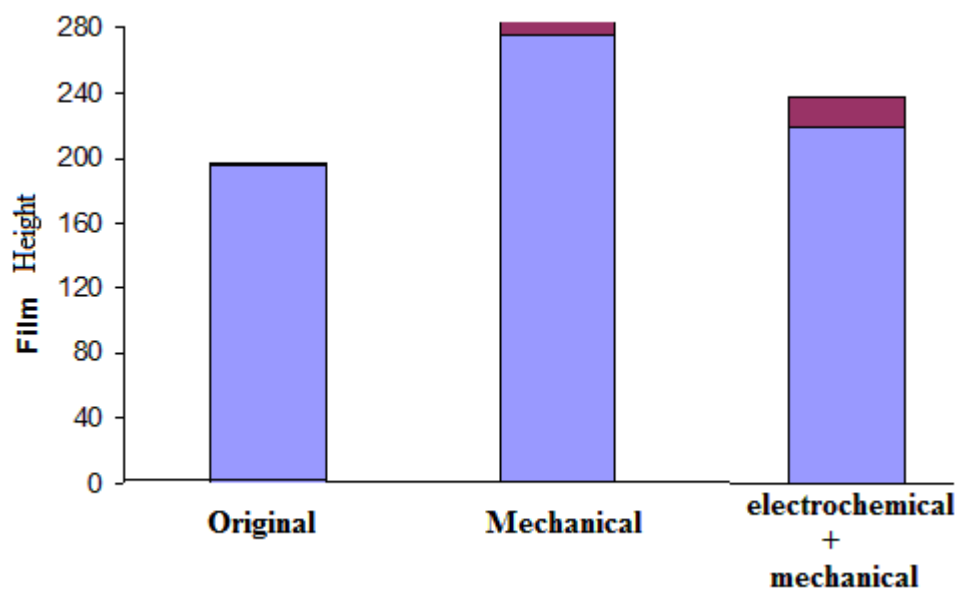


Figure 4.5: The average film thickness along with the standard deviation in data analysis for different conditions used in film measurement.

The difference of thicknesses is thus apparently due to the kinetics of oxidation that will be discussed in the following chapter. The friction-induced oxidation is proven in this work.

4.4 Non-equilibrium oxidation mechanisms

There are two possible mechanisms of the formation of non-equilibrium tantalum oxides. One is oxidation of the Ta surface due to friction; the second is the conversion of the Ta₂O₅ to its sub-oxides. As noted that the Ta⁺¹ has the least binding energy comparing with other oxides. It is the least stable oxide. The energy needed to decompose the equilibrium state tantalum pentoxide to Ta⁺¹ is larger than the Gibbs energy to oxidize Ta. Detailed discussion is given later. Therefore, it is energetically favorable for Ta to be oxidized to form Ta₂O rather than get decomposed from the stable Ta⁺⁵ state. This was further proved by our experiments. The formation of Ta⁺¹ only occurred when an electrical potential applied (along with friction). The Ta⁺¹ was developed from the Ta metallic surface. The possible electrochemical reactions can be written as follows:



Reaction (1) occurs under non-equilibrium conditions due to mechanical forces.

They can be summarized in the following form:

$$\Delta H_{NE} = \Delta H_{\text{Ta}_n\text{O}} - n\Delta H_{\text{Ta}} \quad (2)$$

The ΔH_{NE} is the total energy needed to form tantalum oxides in this non-equilibrium process, while $\Delta H_{\text{Ta}_n\text{O}}$ and ΔH_{Ta} are Gibbs energy for Ta_nO and Ta. This formula indicates that there was an extra energy needed for the formation of sub-oxides. The extra energy can be calculated. The energy difference is induced by applying mechanical forces and electrical potential. It can be expressed by:

$$\Delta H_{NE} - \Delta H_E = \Delta H_{\mu} \pm \Delta H_{e^-} \quad (3)$$

The ΔH_E is the total energy to form Ta_2O_5 through the equilibrium process, ΔH_u is the energy induced by mechanical force, and ΔH_e is that of electrical potential. The positive and negative signs indicate the direction of current through the working electrode, tantalum. The change in energy on the left of equation (3) is attributed to the mechanical energy and electrical potential applied. The mechanical energy is affected by the bonding strength of Ta-O. Figure 4.6 summarizes the effects of friction and electrical potential on tantalum oxides highlighting the major difference between the two conditions – with Ta^{+1} state absent in the mechanical force only condition and present in the electrochemical-mechanical condition.

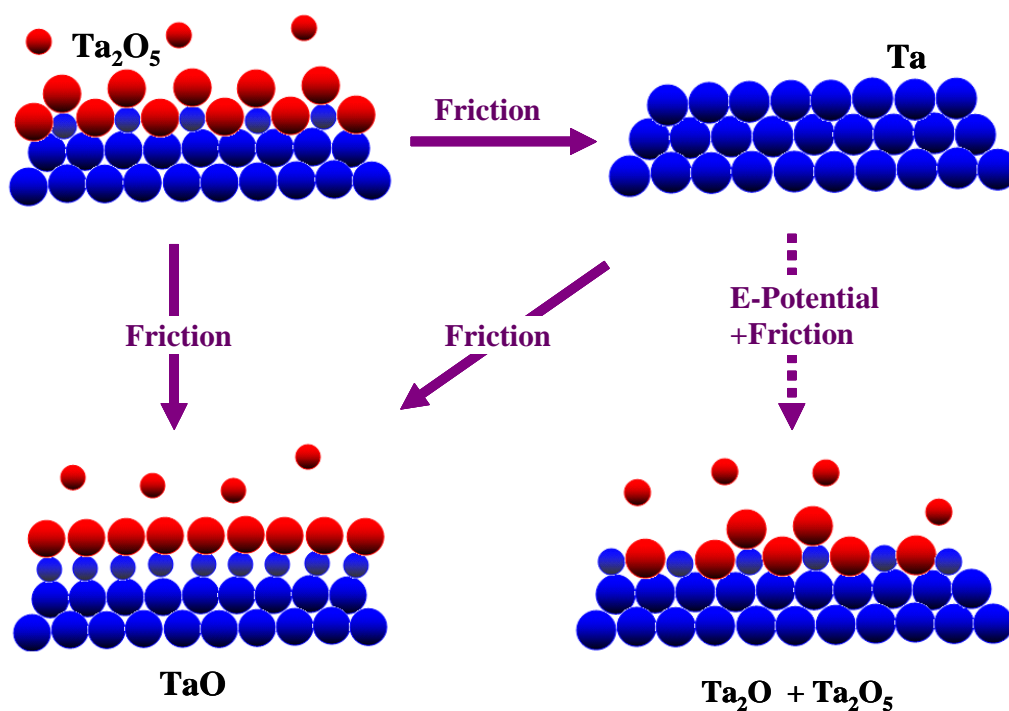


Figure 4.6: A schematic summary of experimental results showing atomic structures obtained through different experimental conditions.

Figure 4.7 exhibits the relationship between the binding energy (from Figure 4.3) and the stoichiometric ratio of tantalum oxides. Three oxides with distinguished crystal units are shown. The lower the stoichiometric ratio between tantalum and oxygen, the lower is the binding energy. The transition between Ta_2O_5 and TaO or Ta_2O requires sufficient external energy to activate change, as indicated by down arrows in Figure 4.6.

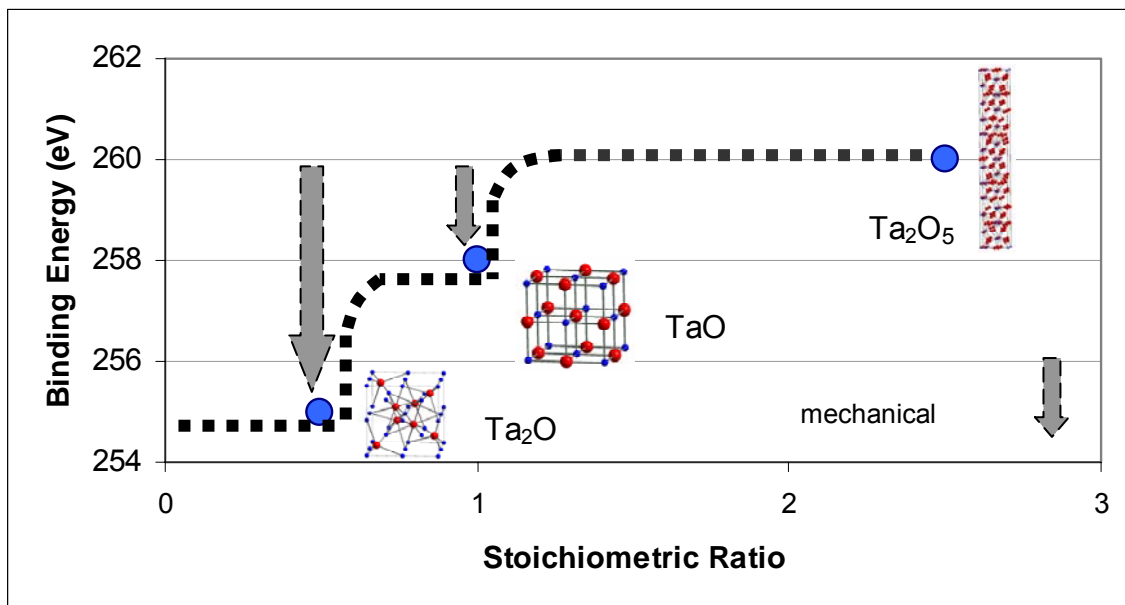


Figure 4.7: The three found tantalum oxides with their stoichiometric ratio and crystal structure. The associated mechanical energy is shown by arrows.

A question that arises is how much was the mechanical energy that was supplied to the process and was it sufficient enough to cause rearrangement of atoms to give metastable states of tantalum. The sliding speed was 0.5 cm/sec and the applied load was 1 N. The frictional energy rate (energy per unit time) is calculated as $\dot{E}_f = \mu \cdot N \cdot v$, where

μ is the friction coefficient, N is the applied load, and v is the sliding speed. According to our experimental condition, there was $1.5 \cdot 10^{-3} \text{ Nm}$ ($6.24 \cdot 10^{18} \text{ eV}$) amount energy was introduced to the system through friction per second. Considering the number of tantalum and oxide atoms on the sample surface, the amount of mechanical energy is overwhelming compared the binding energy of tantalum oxides. It means that there is more than enough mechanical energy to trigger the change of tantalum oxides. The mechanical contact stress can be estimated using the basic contact theory (non-sliding) [95] and the representation of a plastic deformation zone (sliding).[96] During sliding, the contact stress is compressive at the front of a slider and tensile at the end of it. The surface and near surface atoms react corresponding to the stress and at certain moments, the inter-atomic bonds are stretched and others compressed. Figure 4.8 gives a molecular level schematic of the process that takes place to yield the sub-oxides on application of mechanical force.

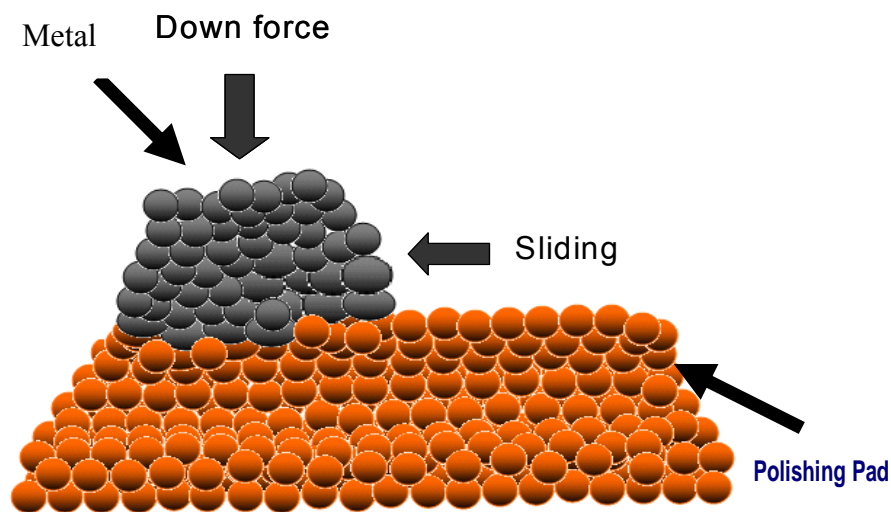


Figure 4.8: The effects on metal-polishing pad interface at molecular level due to mechanical stress.

A simple calculation (pages 55-56) of frictional energy introduced during sliding has shown that the mechanical energy is much higher than the energy for chemical reactions. With types of oxides detected, we are able to compare binding energy and crystal structures, as shown in figure 4.7. The equilibrium Ta_2O_5 is thermodynamically stable. The sub-oxides such as Ta^{+1} and Ta^{+2} were formed due to mechanical swiping, as shown by the grey arrows.

In our first test where mechanical force was applied alone, the resulting oxides were Ta^{+2} , Ta^{+3} , and Ta^{+4} . In the chemical environment, Ta_2O_5 was formed. This apparent contradiction can be explained from the fact that due to mechanical force, the reaction equilibrium of Ta shifts towards the meta-stable states instead of Ta_2O_5 . In case of electro-mechanical condition, the Ta^{+1} was formed apart from Ta^{+2} , Ta^{+3} , Ta^{+4} . Due to electrochemical potential application in addition to mechanical force a still lower oxidation state of Ta was obtained.

There is another possible mechanism for the observed phenomenon. It has been reported that under compressive applied forces, the inter-atomic distance of solids decreases, this leads to greater overlap of wave functions resulting decreased band gap. [9] Similarly, a tensile force increases the band gap.[12],[57] As noted earlier that the band gap can be changed due to stress as seen in change in electrical properties of carbon nanotubes on stress, [97], and in semi-conductors [98], [99]. It is possible that the mechanical force compresses the band gap in Ta_2O_5 in order to form Ta_2O . The investigation of this plausible mechanism can be done in future studies. A schematic of

the possible mechanism as proposed above is shown in figure 4.9. This hypodissertation will be studied in future.

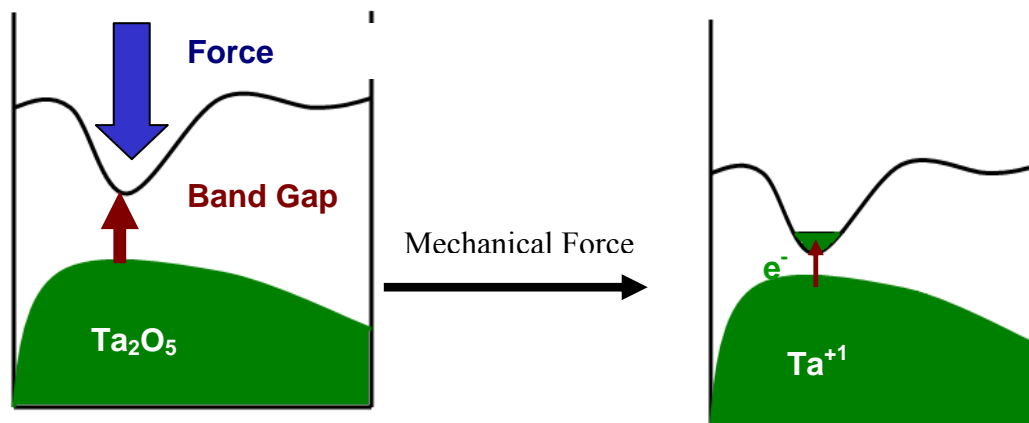


Figure 4.9: The plausible theory put forward for formation of Ta₂O involving band-gap reduction due to mechanical stress.

In addition, an interesting finding of our results is the existence of all forms of suboxides, Ta⁺¹, Ta⁺², Ta⁺³, Ta⁺⁴ and Ta⁺⁵ in the case of electrochemical-mechanical interaction; while only Ta⁺², Ta⁺³, Ta⁺⁴ and Ta⁺⁵ were found in the case of mechanical rubbing only. The Ta⁺³, Ta⁺⁴ have higher intensity as seen in XPS as compared to Ta⁺⁵. These oxidation states were proven to be the intermediates formed during the mechano-oxidation process. The high intensity of the Ta⁺³ and Ta⁺⁴ suboxide peaks shows the dynamic equilibrium process. Also among all the metastable forms the Ta⁺³ and Ta⁺⁴ are energetically more favourable to form under non-equilibrium conditions. This is another reason for the high intensity of the Ta⁺³ and Ta⁺⁴ peaks. The main distinguishing

feature between electrochemical-mechanical reaction and mechanical reaction is the absence of Ta^{+1} in the latter. The reason thereof has been described earlier.

The reactions can be summarized as follows:



The least stable Ta_2O could revert back to be more stable. The existence of intermediate sub-oxide products Ta^{+2} , Ta^{+3} , and Ta^{+4} is an indication. This means that the mechanical-oxidation is a continuous dynamic and non-equilibrium reaction process which reverts back and forth between the equilibrium and non-equilibrium states.

Overall, the interactions between mechanical forces, electrical potential, and sample surfaces resulted into different types of tantalum oxides. The mechanical force, that was applied to the tantalum surface in the present study was frictional force.

4.5 Summary

We used an *in situ* technique to generate non-equilibrium tantalum oxides with assistance of mechanical forces. Using this technique, controlled mechanical forces and electrical potential were applied to a tantalum surface. The mechanical force was applied as the surface tangential force, i.e., friction, promotes the formation of tantalum suboxides, Ta_2O , TaO , among others. Those two oxides were the least stable ones under their unique experimental conditions. Our investigation advanced previous reported electrochemical and corrosion study using a simpler setup. The alteration of oxidation

was in addition achieved with an applied electrical potential in 5% H₂O₂ solution. Analysis indicates that the formation of suboxides were from Ta surface. There is another plausible mechanism of some of the Ta⁺⁵ reverting to lower oxide forms by band gap compression. It however needs further investigation as mentioned earlier. The native tantalum oxide was cleaned through mechanical sweeping. The setup we used is useful for discovering new chemical reactions activated by a controlled external force. Results obtained here are beneficial for understanding electrical-chemical-mechanical polishing (ECMP), an important process step in microelectronics industry today. This study of oxidation of tantalum under mechanical parameters is first of its kind.

CHAPTER V

MECHANO-KINETICS OF TANTALUM*

Non-equilibrium processes result in the formation of unique meta-stable products that are not found under equilibrium conditions. In the previous chapter we have discussed about the mechano-oxidation of tantalum. We found that in 5% wt hydrogen peroxide in both mechanical and electro-chemical-mechanical conditions, tantalum forms sub-oxides. The next goal is to understand the kinetics of the mechano-chemical reactions of tantalum. This is achieved by using a series of electrolytes of different pH and comparing their friction coefficients. Also comparison of the products formed also gives an idea on the synergic effects of mechanical and chemical energy in driving the kinetics of the equation.

Towards the end of this chapter we propose a modified Arrhenius-Eyring equation which we termed as Kar-Liang equation in which the mechanical factor was considered. We found that the mechanical energy induced the non-stable state reactions leading to metal-stable oxides. This equation can be used to predict mechano-chemical reactions that are important in many industrial applications.

As mentioned in chapter II and chapter V, mechanochemical reactions have been reported in literature [9],[44],[75],[76],[77],[78],[79],[80]. However there is a lack of understanding of the dynamic and reaction kinetics in the field of mechanochemistry.

* *Force Dominated Non-equilibrium Oxidation Kinetics of Tantalum*, P. Kar, K. Wang, H. Liang (**accepted** *Electrochimica acta*, 2008).

The present study investigates the oxidation behavior of tantalum under mechanically-activated non-equilibrium conditions. This study is helpful in understanding the reaction kinetics of transition metal surfaces under working conditions.

As stated earlier tantalum exists in +5 state under all pH in equilibrium conditions. [63] Tantalum also exists in the energetically favorable oxidation states of +1, and +3 [100]. The formation of stable tantalum oxide has been reported using different methods – primarily CVD (Chemical Vapor Deposition)[101], APCVD (Atmosphere CVD)[102], LPCVD (Low Pressure)[103], RT-LPMOCVD (Rapid Thermal Low Pressure Metal-Organic CVD)[104], MOCVD (Metal-Organic CVD)[105], Liquid Source CVD[106], Sputtering[107], Pulse Laser Ablation[108] and Anodization[62]. A standard method for producing meta-stable oxides of tantalum has not been reported. In mechano-chemical processes the reactants are subjected to physical parameters such as friction and pressure. This mechano-activation of bonds yields metastable products as illustrated in chapter IV and published by Kar et al in *Electrochemistry Solid State Letters*. [109]

This research focuses on understanding mechano-oxidation mechanisms. We apply a synergetic approach combining electrochemical and mechanical impacts to manipulate, observe *in situ*, and characterize connecting interfaces. Fundamentally, we focus on the mechanisms of mechano-activated oxidation process. Doing so, we will firstly develop process to generate such oxides; and secondly, we will study the mechanisms of the formation process. Specifically, this chapter concentrates on the anodization procedure for the formation of oxide films of tantalum using potentiostatic

conditions. The oxidative environment under deionized water with KCl will be compared with a corrosive environment of acetic acid solution. Potentially, the anodic films formed have good insulating properties.[110] This helps to understand the oxidative and corrosive process in tantalum under electro-mechanical parameters. The understanding is beneficial to the process of chemical-mechanical polishing, a standard step for making integrated circuits. The table 5.1 shows the samples used for the study of mechano-oxidation kinetics.

Table 5.1: Summary of samples and corresponding test conditions

Samples	Potential	Load	Speed
1) Reference Ta sample	n/a	n/a	n/a
2) Ta in acetic acid (0.13 M)	+2.4 V	1 N	0.5 cm/sec
3) Ta in deionized water with KCl	+2.4 V ,	1 N	0.5 cm/sec
4) Ta in acetic acid (0.13 M)	+ 2.4 V	n/a	n/a
5) Ta in deionized water with KCl	+ 2.4 V	n/a	n/a
6) Ta in acetic acid (0.13 M)	n/a	1 N	0.5 cm/sec
7) Ta in deionized water with KCl	n/a	1 N	0.5 cm/sec

As mentioned in chapter III water was used as a control medium. The KCl was added to increase the conductivity of the solution. Acetic acid was used to test the effect of an agent to limit oxidation.

5.1 Frictional behavior

The coefficient of friction was measured and is plotted in figure 5.1. Figure 5.1a is the friction coefficient against time obtained from deionized water with KCl. The friction coefficient is around 0.75. At around 3rd second, when an electrical potential (+2.4 V) was applied to the system, there is a gradual increase in friction to 0.86.

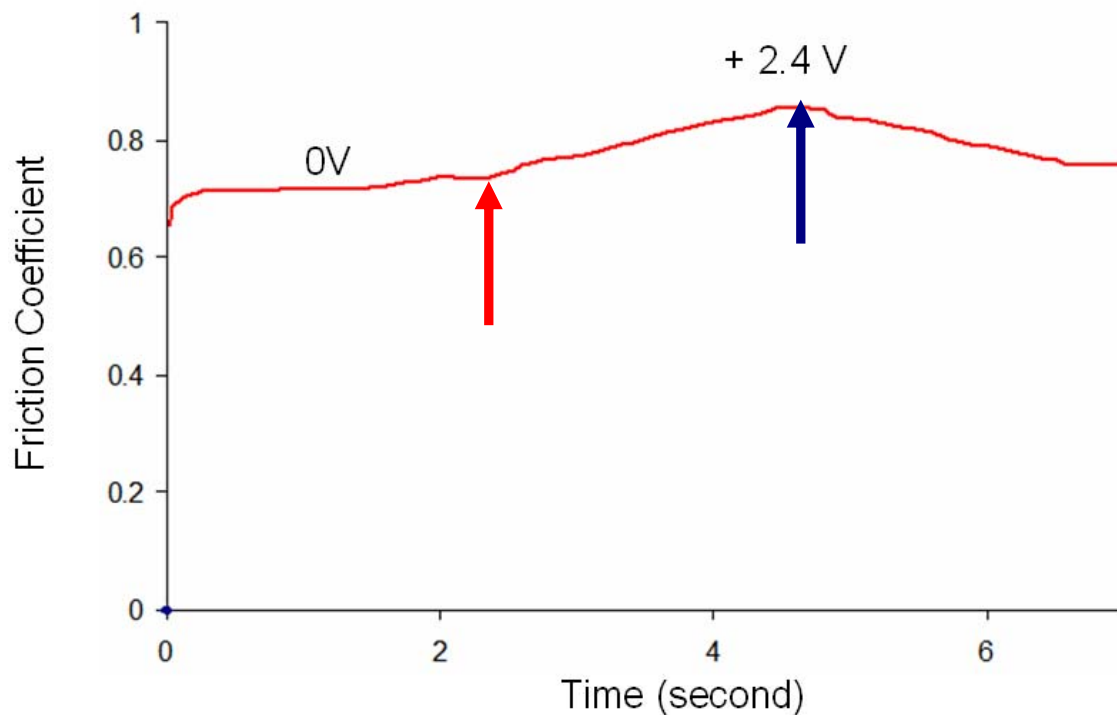


Figure 5.1a: Friction obtained in water under the condition of 1N and 0.5 cm/sec. The friction starts to increase at +2.4 V. The red arrow points to the exact time when the potential was applied and blue arrow when the potential was removed.

This is not so in the acetic acid case. Figure 5.1b is that obtained from acetic acid. The friction coefficient is around 0.3 at the beginning, much lower than that in water. It is seen that at the 16th second, the friction coefficient jumps to 0.38 almost immediately when a potential of +2.4 V was applied. After the potential was taken off, the friction goes back to 0.3. When a higher voltage +4.4 V was applied, the friction coefficient jumped higher to 0.46.

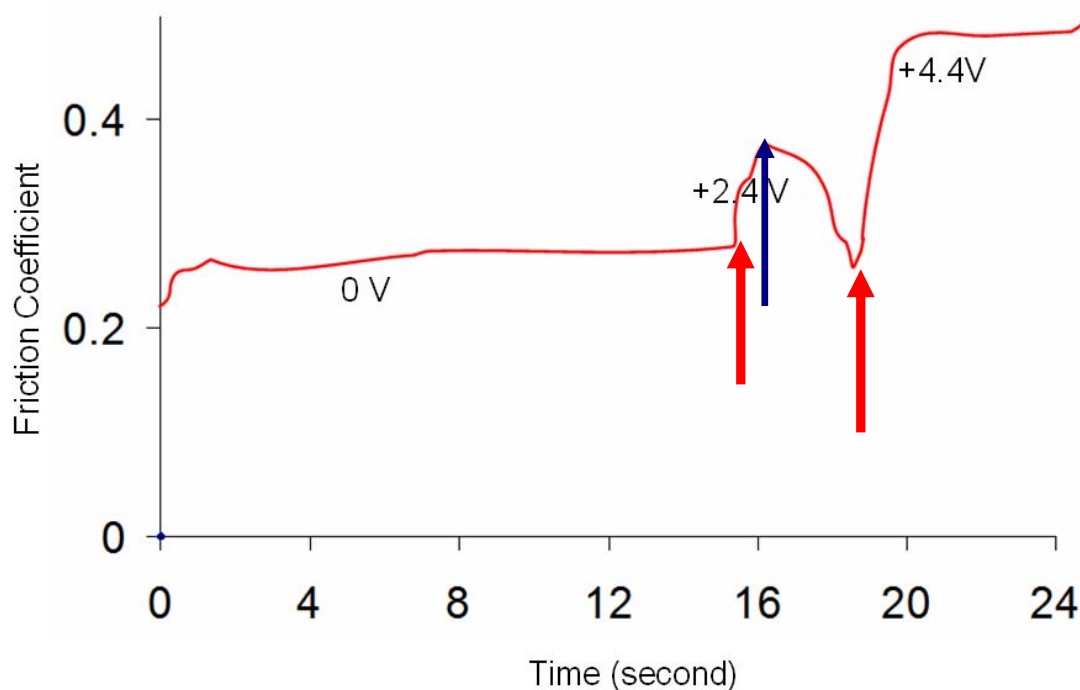


Figure 5.1b: Friction obtained in the 0.13 M acetic acid under the condition of 1N and 0.5 cm/sec. The first increase of friction is seen at +2.4 V and then the potential is switched off. The second increase is seen at the same condition with the potential of +4.4 V. The red arrow points to the exact time when the potential was applied and blue arrow when the potential was removed.

Experimental results showed interesting friction results, as seen in figure 5.1. Figure 5.1a displays polishing behavior of tantalum in distilled water. The friction coefficient was stable at the beginning at around 0.75. After a voltage of +2.4V applied, it gradually increased to 0.86. Since the only change is associated with tantalum oxidation, the curve indicates a slow rate of oxidation. Figure 5.1b is a similar curve of friction coefficient. At the initial stage, the friction was stable at around 0.25. When a voltage of +2.4V was added, the friction immediately increased to around 0.38 and it dropped back immediately once the voltage was turned off. More over, when the voltage was applied at +4.4V, the friction was immediately increased to around 0.47. There are two different behaviors found here: a lower friction coefficient of Ta in acetic acid than that in water; and an immediate increase of friction with applied potential for Ta in acetic acid while a slow increase for that in water. The initial surface conditions were the same for both samples. The deionized water with KCl was not expected to change the oxidation state of tantalum while the acetic acid etches the native oxide. Thus the surface change is mainly associated with the nature of surface oxides or surface roughness. In order to verify this, AFM analysis was conducted using a close-contact mode for phase image (an indication of microstructure), as shown in figure 5.2. The left hand side picture was taken of sample with reference surface (sample 1), and right hand side of the tantalum sample in acetic acid (sample 2). The sample 1 has a mosaic structure. The sample 2 on the contrary displays large grain-like structure. Comparing two figures, it is seen that on electro-mechanical polishing the native oxide surface (sample 1) of Ta has a totally different surface microstructure in sample 2.

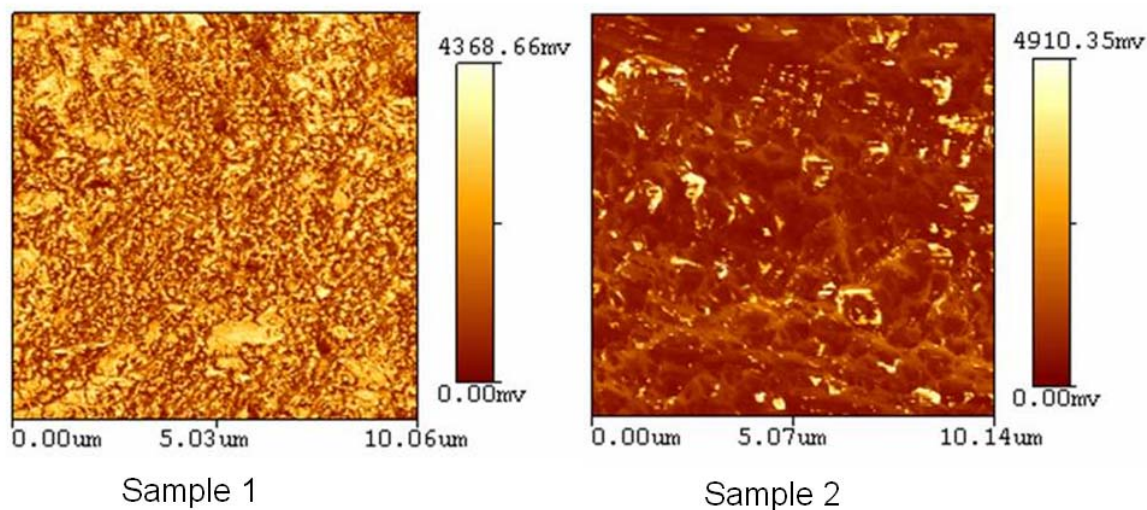


Figure 5.2: AFM phase image of the surface of a) sample 1 (left) and b) sample 2 (right).

To identify those microstructures, XPS analysis is discussed in the next section. The different microstructures do conclusively prove the existence of different compounds when tantalum is subjected to electro-mechanical energy.

5.2 XPS analysis of tantalum sub-oxides

XPS analysis was conducted after experiments and the spectroscopic peaks are plotted as shown in figure 5.3. Figure 5.3a shows the comparison of the XPS peaks of sample surfaces obtained under all test conditions. Dashed lines were added for comparison purpose. This figure shows that samples do not exhibit the same peaks indicating the change of surface chemistry due to different experimental conditions.

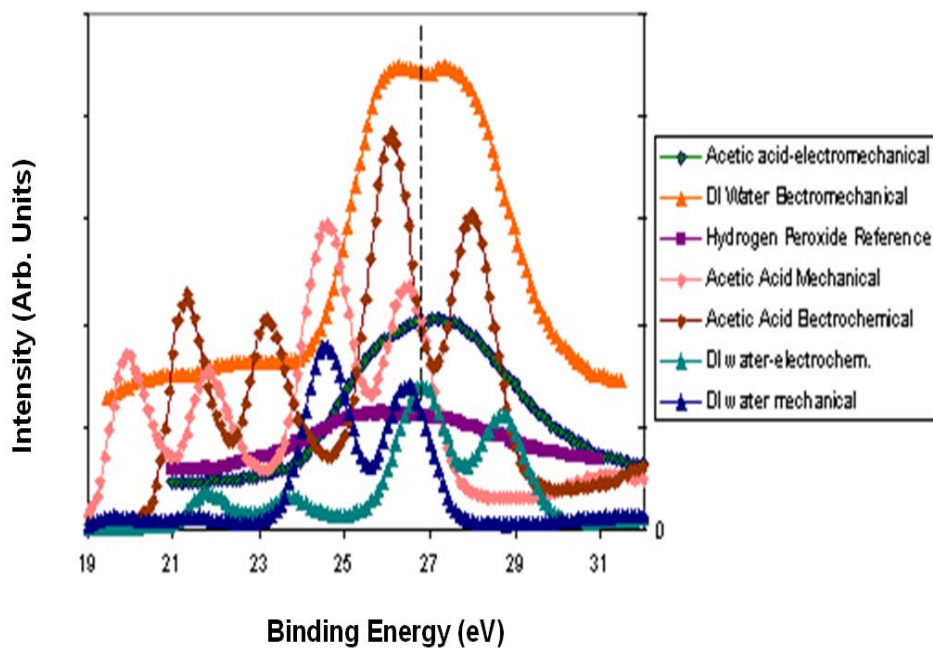


Figure 5.3a: XPS comparison of all tested samples.

The figure 5.3b is the comparison of Ta in acetic acid under different experimental parameters (samples 2, 4, 6 in Table 1). There is a marked shift in peaks towards lower binding energy especially when the mechanical condition is compared to the pure electrochemical condition, suggesting the formation of sub-oxides. When comparing two samples tested in acetic acid, it is seen that the mechanical manipulation (red) actually shifted the peak (maroon, electrochemical) towards the lower binding energy direction.

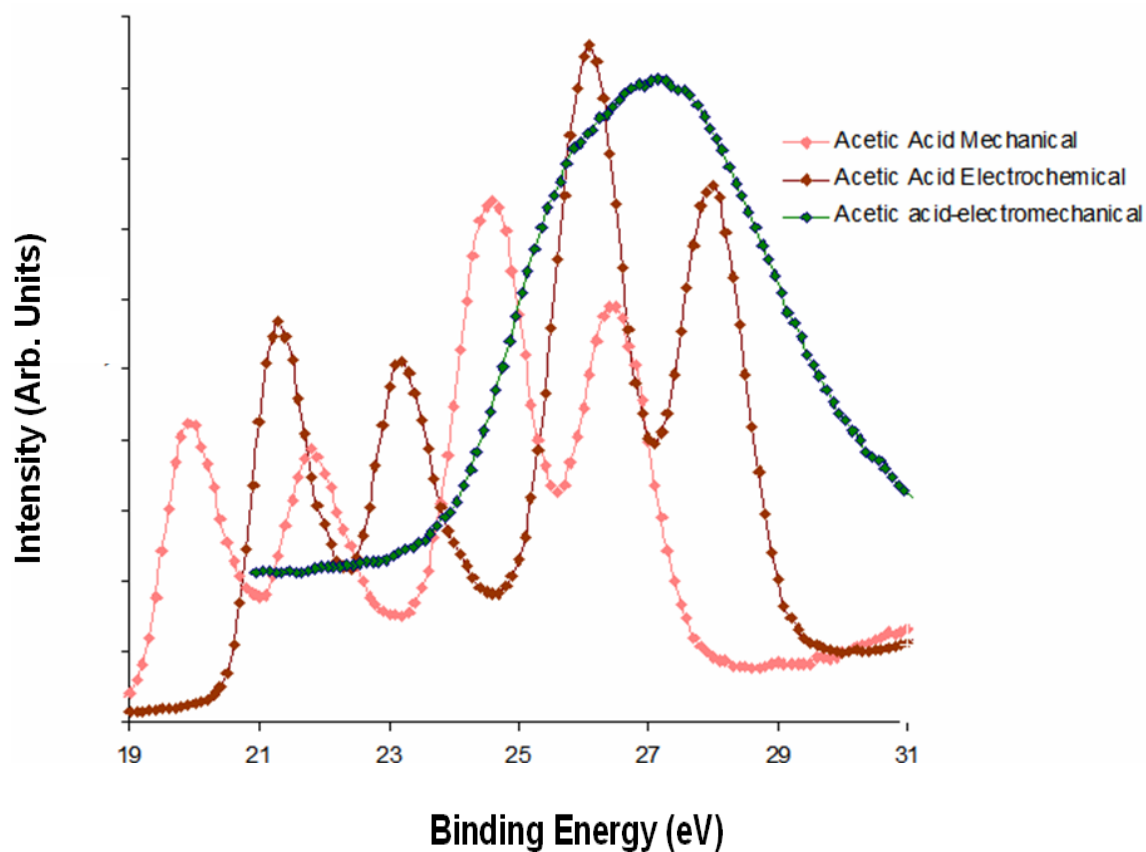


Figure 5.3b: XPS peaks of Ta in acetic acid under different conditions.

Figure 5.3c is the comparison of peaks of tantalum in deionized water with KCl under three test conditions (samples 3, 5, 7 in Table 1). In this figure, peak shifts were again observed due to test conditions. The arbitrary unit in y-axis is used here in order to bring the curves close together so that the comparison of the binding energy (x-axis) is convenient.

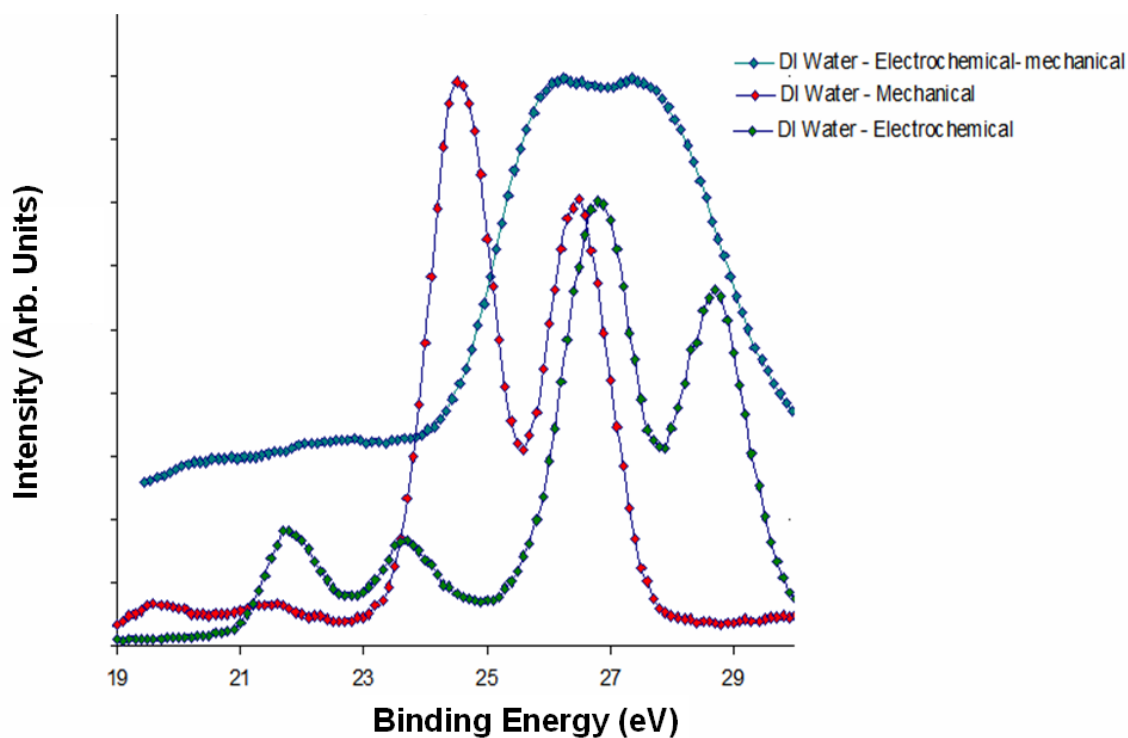


Figure 5.3c: Shift in XPS peaks of tantalum in DI water under different conditions.

When comparing two samples tested in water, it is seen that the mechanical manipulation (red) actually shifted the peak (green, electrochemical) towards the lower binding energy direction.

Figures 5.3d-5.3j are decomposition of the original peaks as seen in figure 5.3a. The test conditions represented in figure 5.3a were listed in table 5.1. Figure 5.3d represents tantalum metal surface in its native state (sample 1). The +5 oxidation state XPS peaks of $4f_{5/2}$ and $4f_{7/2}$ are found at 27.4 eV and 25.6 eV and concurs with the published data.[90]

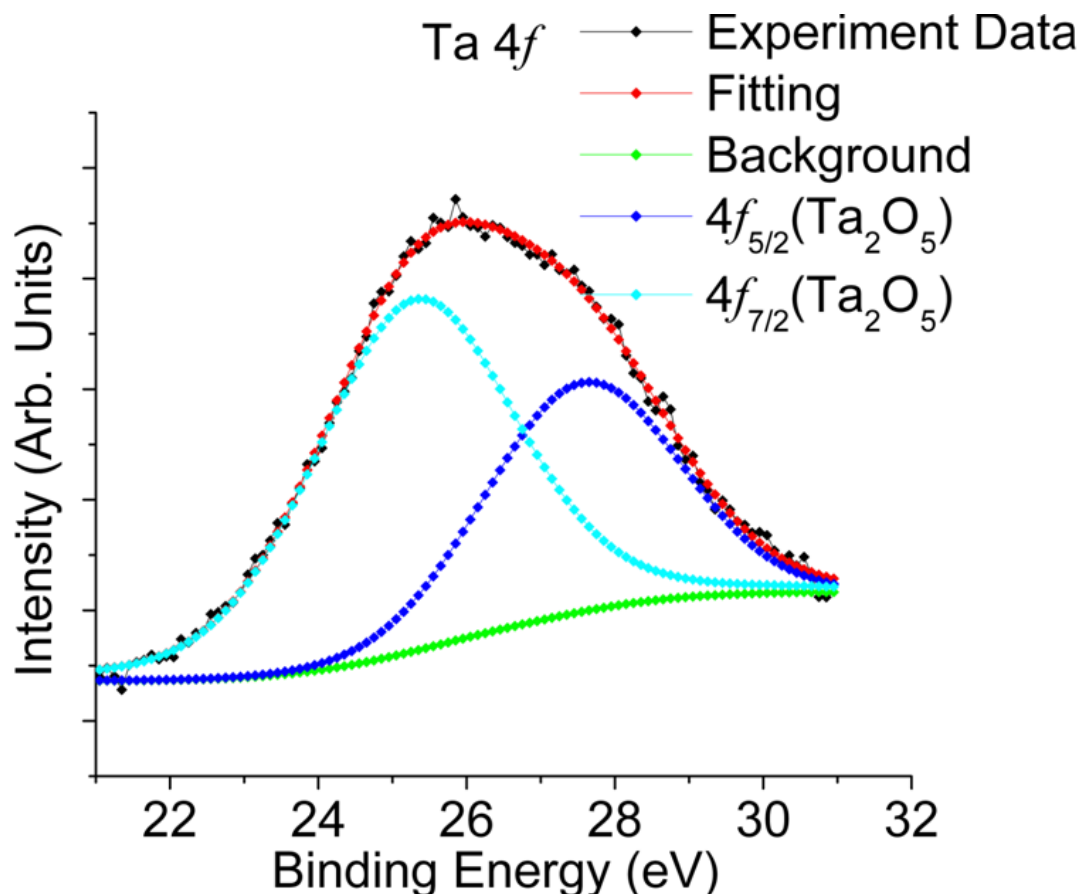


Figure 5.3d: XPS peak analysis of tantalum sample as the reference (sample 1).

Apparently, the shift observed in figures 5.3b and 5.3c did not show the same peaks. Figure 5.3e is tantalum in acetic acid under electrochemical-mechanical conditions (sample 2) and figure 5.3f is that of obtained in water (sample 3). Comparing with published data [90] in figure 5.3f, the $f_{5/2}$ and $f_{7/2}$ peaks at 25.8 and 28.5 eV correspond to +4/+3 overlap peaks respectively. These peaks are strong ones. It is noted that one state of oxide generally represents two peaks. During fitting, paired peaks were analyzed together so that the state of oxide was correct. At lower binding energy area the

+2 oxidation state of tantalum does not exist in figure 5.3f. However, we find that $f_{5/2}$ and $f_{7/2}$ peaks for +1 oxidation state of tantalum exist at 24.3 eV and 23.2 eV respectively [90]. The metallic tantalum XPS $f_{5/2}$ and $f_{7/2}$ peaks are observed for figure 5.3f at 22 eV and 20.5 eV in accordance with published data.[90] Compared to figure 5.3f, the sub-oxide Ta+1 and also the metallic Ta XPS peaks are absent in figure 5.3 e. The $f_{5/2}$ and $f_{7/2}$ peaks for Ta+2 oxidation state are observed at 26.4 eV and 22.3 eV respectively.[90] These are well within the published range. Apart from that high intense peaks for Ta+3/Ta+4 were observed at 25.3 eV and 27.6 eV, the medium intensity Ta +5 $f_{5/2}$ and $f_{7/2}$ peaks are observed at 29.7 eV and 27.3 eV.

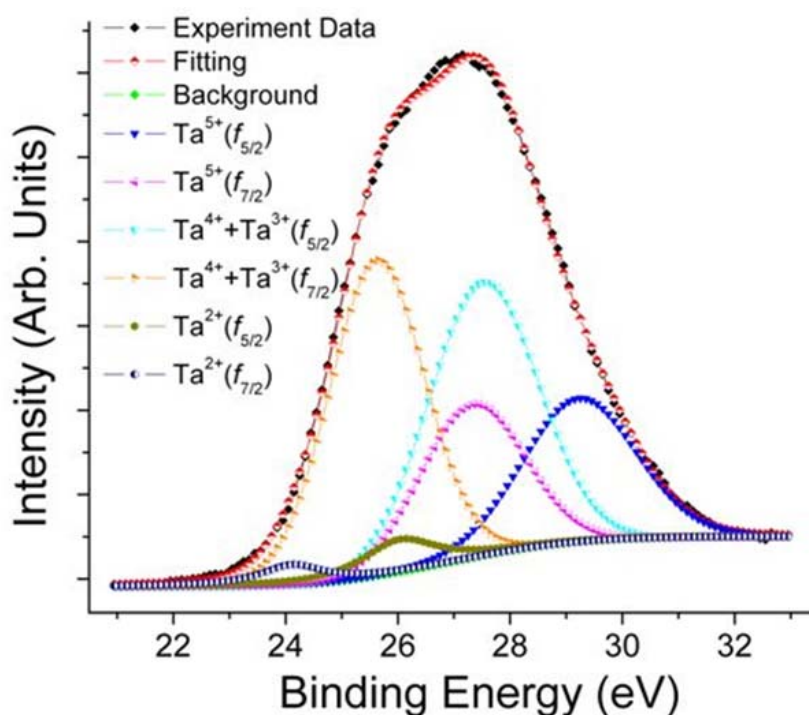


Figure 5.3e: XPS peak analysis of tantalum tested in acetic acid (sample 2).

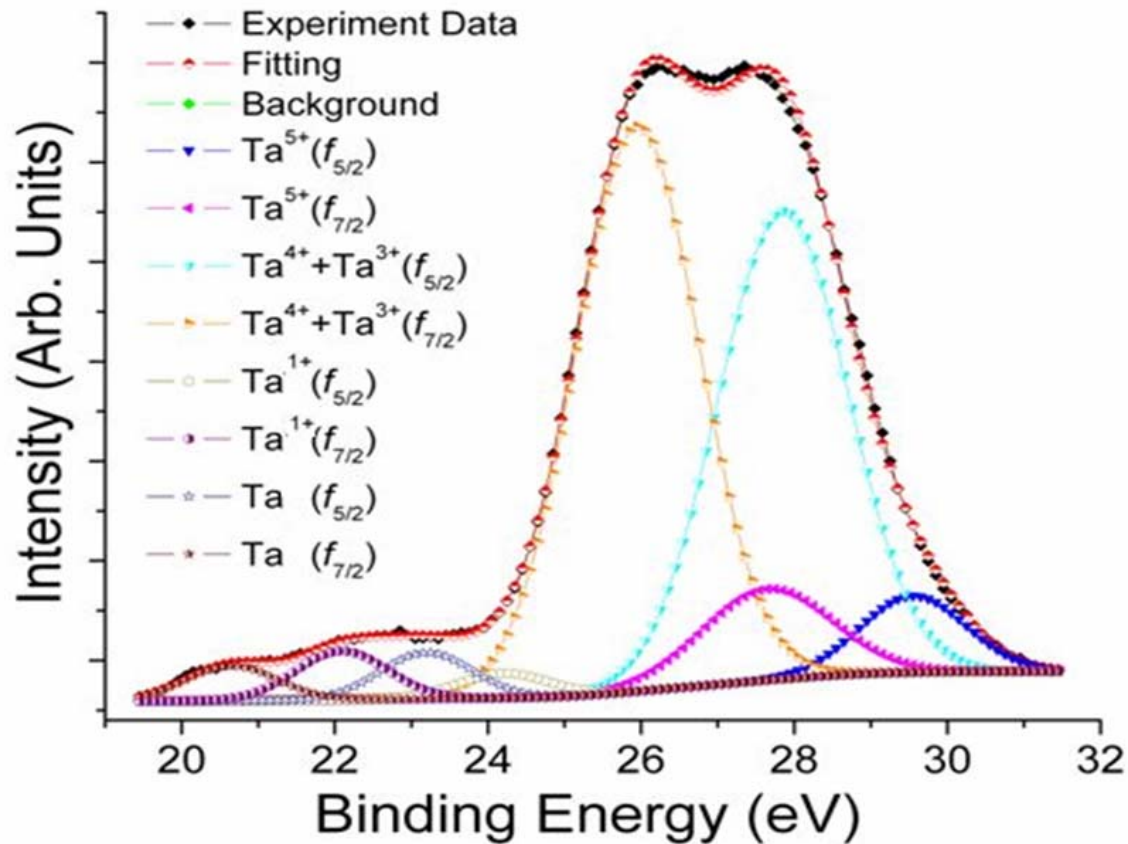


Figure 5.3f: XPS peak analysis on tantalum tested in DI water (sample 3).

For Ta in acetic acid under simple electrochemical experiment as shown in figure 5.3g, Ta +5 are seen of $4f_{5/2}$ and $4f_{7/2}$ at 28.9 eV and 27.1 eV respectively. Ta +4 is seen at the peaks at 28.4 eV and 26.5 eV and Ta metallic is confirmed by the 23.6 eV and 21.8 eV peaks.

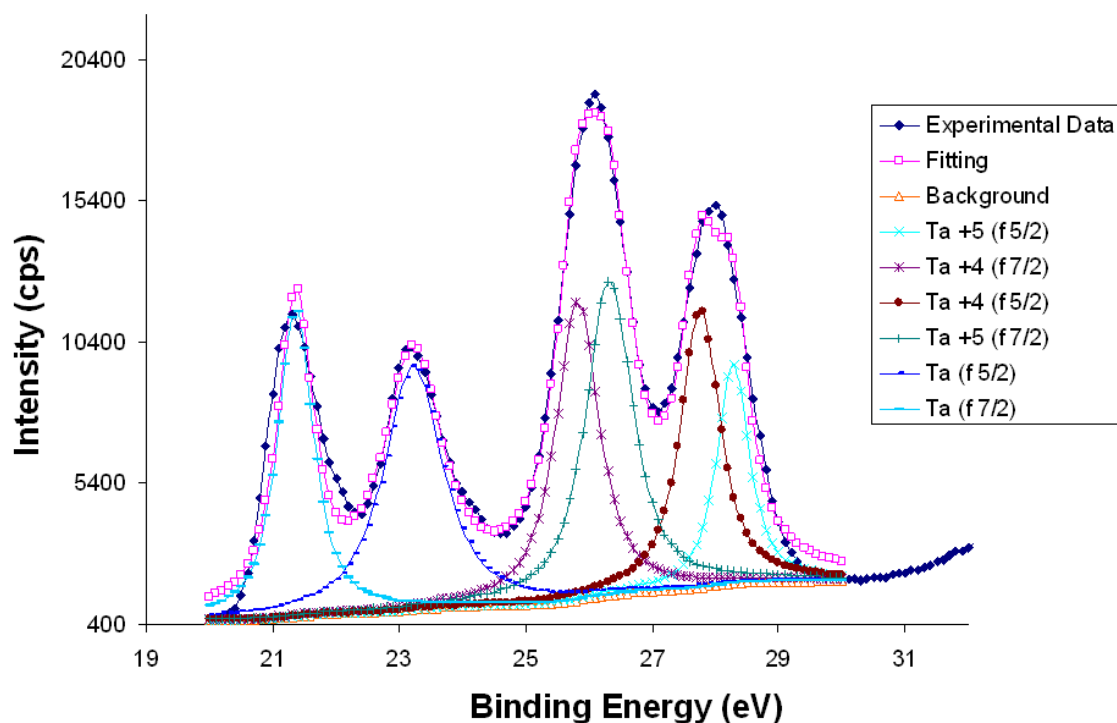


Figure 5.3g: XPS peak fitting of acetic acid electrochemical only (sample 4).

Tantalum in DI water with KCl under simple electrochemical experiment as shown in figure 5.3h confirms the presence of Ta+5 due to observation of $4f_{5/2}$ 28.9 eV and $4f_{7/2}$ 27.1 eV peaks. Similarly Ta + 4 peaks are detected due to the peaks at 28.4eV and 26.5 eV and Ta metallic is observed due to presence of $4f_{5/2}$ 23.6 eV and $4f_{7/2}$ 21.8 eV.

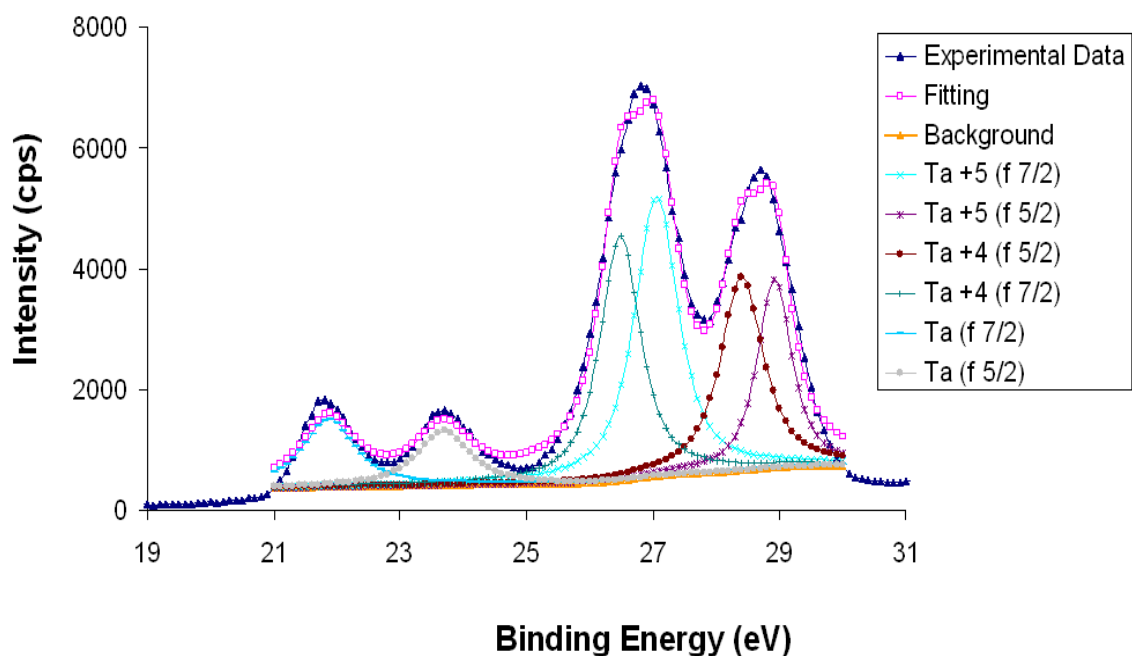


Figure 5.3h: XPS peak fitting of DI water electrochemical only (Sample 5).

It is seen that the sub-oxides exist on Ta surface in both acetic acid and DI water in KCl environments under mechanical forces. With mechanical forces, the Ta in acetic acid XPS peaks are analyzed in Fig 5.3i. The sub-oxide of Ta+3 is detected at $4f_{5/2}$ 26.7 eV and $4f_{7/2}$ 24.8 eV which matches with the literature values.[90] Similarly the sub-oxide of Ta+2 is also detected due to the presence of $4f_{5/2}$ 26.7 eV and $4f_{7/2}$ 24.8 eV peaks. Metallic Ta peaks are observed at $4f_{5/2}$ 21.8 eV and $4f_{7/2}$ 20 eV.

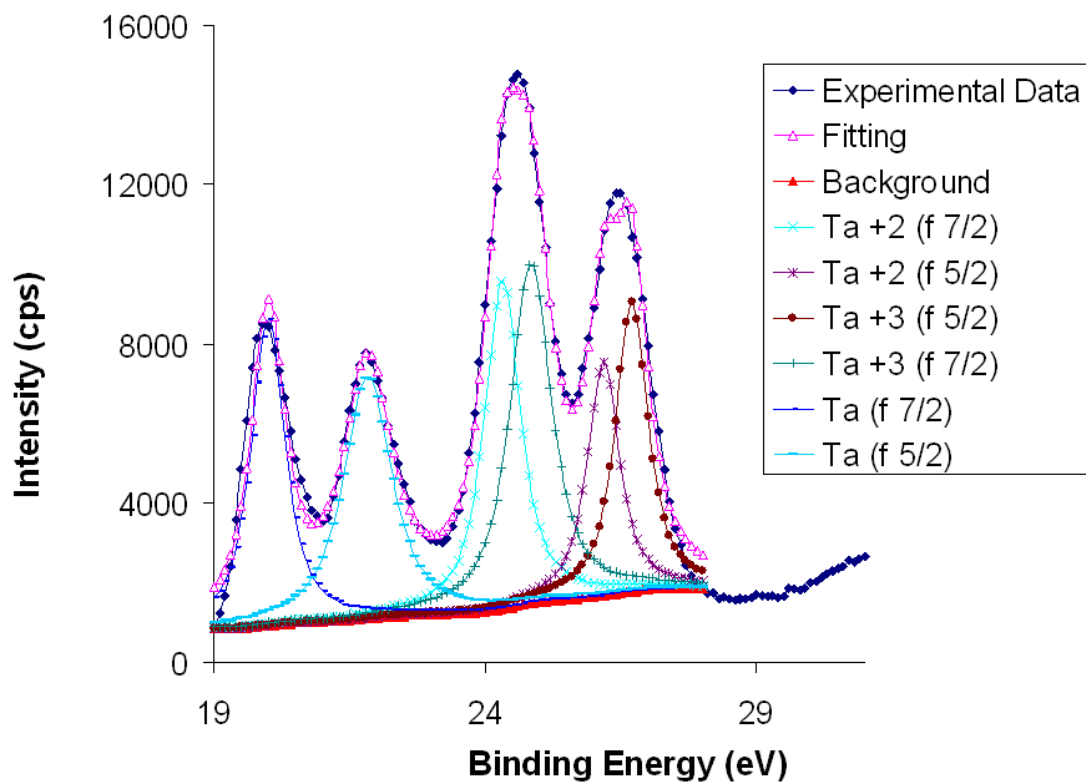


Figure 5.3i: XPS peak fitting of acetic acid mechanical only (Sample 6).

Similar results are obtained when XPS peaks for Ta in water under mechanical forces are analyzed as shown in figure 5.3j. We found that Ta +3 and Ta +2 co-exist on Ta in water under mechanical conditions similar to what appeared on Ta in acetic acid. Ta+3 peaks are seen of $4f_{5/2}$ and $4f_{7/2}$ in figures 5.3j at 26.7 eV and 24.8 eV respectively. Ta+2 peaks are seen of $4f_{5/2}$ and $4f_{7/2}$ at 26.2 eV and 24.3 eV respectively. Finally, Ta peaks are seen of $4f_{5/2}$ and $4f_{7/2}$ at 21.3 eV and 21.8 eV respectively.

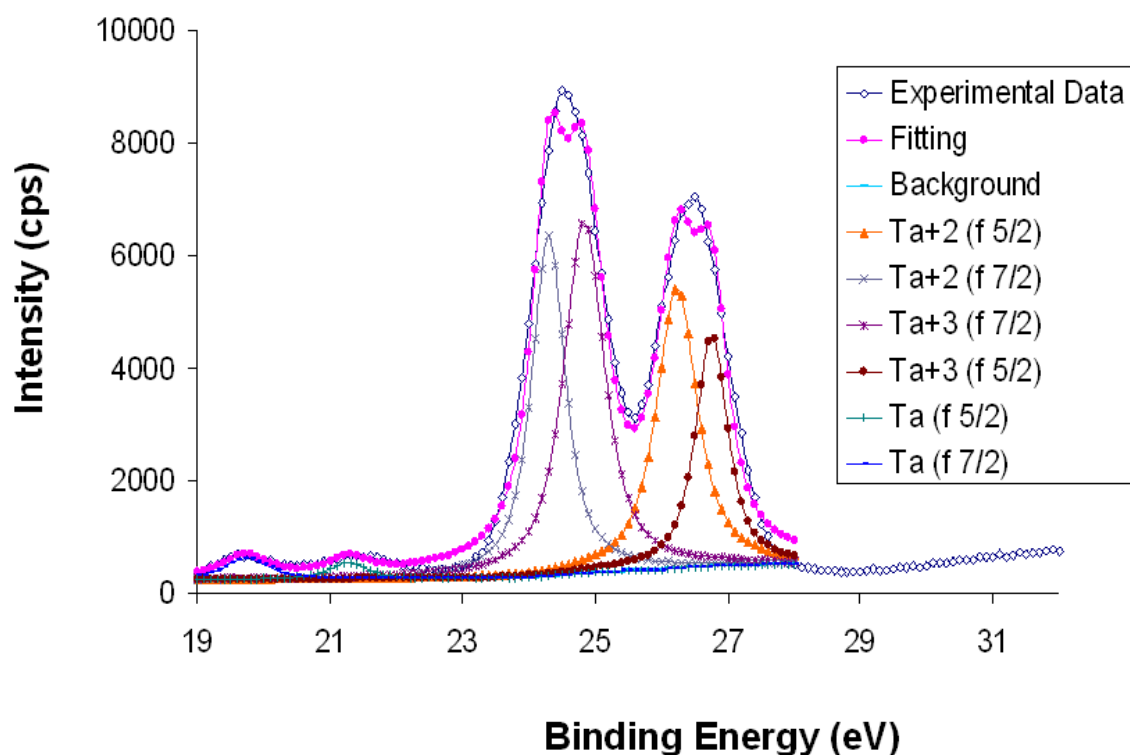


Figure 5.3j: XPS peak fitting of DI water mechanical only (sample 7).

When we compare the results of the mechanical energy experiments with simple electrochemistry of Ta in acetic acid and water we find the absence of the lower sub-oxides from the XPS peaks. Instead in both the cases we find metallic Ta peaks and Ta+5 peaks. Ta+4 peaks are also observed but its presence can be attributed to a non-equilibrium action during the application of electrochemical energy. The presence of lower sub-oxides (Ta+2, Ta+3) in both chemical environments when subjected to mechanical energy confirms that the existence of the mechanical energy did indeed shift

the peaks toward the lower binding energy direction. The table 5.2 gives a summary of the oxides formed corresponding to the experimental conditions.

Table 5.2: Summary of the sub-oxides formed under different conditions

Samples	Oxidation states of Ta observed
1) Reference Ta sample – as received	+5
2) Tantalum in acetic acid (0.13 M) (electro-chemical-mechanical)	+5 , +4, +3, +2
3) Tantalum in deionized water with KCl (electro-chemical-mechanical)	+5, +4, +3, +1, 0
4) Tantalum in acetic acid (0.13 M) (electrochemical)	+5, +4, 0
5) Ta in deionized water with KCl (electrochemical)	+5, +4, 0
6) Ta in acetic acid (0.13 M) (mechanical)	+3, +2, 0
7) Ta in deionized water with KCl (mechanical)	+3, +2, 0

Analysis of XPS results showed that both samples 3 and 2 had $4f_{7/2}$ and $4f_{5/2}$ peaks for Ta in +5 oxidation state. The main difference of the reference sample 1 with sample 2 and sample 3 is that later two have tantalum sub-oxides presented. Sample 2 that is tantalum in acetic acid showed absence of lower sub-oxide peaks of Ta +1 and also metallic tantalum as observed in sample 3 which is tantalum in deionized water with KCl. When we compare the AFM results with the XPS analysis we find that both results complement each other. As shown in the AFM phase images, a distinct difference in phases was observed in case of tantalum in acetic acid (sample 2) as opposed to the reference sample (sample 1).

The absence of Ta+1 and Ta metallic XPS peaks from sample 2 as compared to sample 3 can be understood when we read the friction coefficient data for both samples. The friction coefficient of sample 3 was as high as 0.86 as compared to the friction coefficient of sample 2 which was 0.47 at its highest value. Given the load and velocity parameters being constant, it can be concluded that chemical environment has a role to play in friction coefficient. The acetic acid acted as a lubricant since it was more viscous than the deionized water with KCl. This was observed with a low friction coefficient value (0.25 – 0.47) in figure 5.2b as compared to tantalum in deionized water with KCl (0.75 – 0.86, figure 5.2a). The reduction of friction coefficient leads to lowering of mechanical energy being experienced by the sample 2. The absence of sub-oxide Ta+1 and metallic Ta peaks and weak Ta+2 oxidation state peak corroborated the observation.

With a high mechanical energy through high friction (figure 5.2a), as tested in the deionized water with KCl, we found sub-oxides as well as metallic Ta as expected on XPS. As for the sample with a low friction, this resulted in the absence of sub-oxide peaks due to low mechanical energy experienced at the interface.

The comparison of tantalum peaks can be seen in figure 5.3a. The peak shifted towards lower binding energy with greater application of mechanical energy. Sample 3 which experienced highest frictional energy shifted the most. This is corroborated by XPS analysis as discussed earlier. The presence of Ta⁺³/Ta⁺⁴ peaks at higher intensity as compared to expected Ta⁺⁵ oxidation state also indicated the effects of mechanical force on the oxidation state of Ta. As Ta⁺³/Ta⁺⁴ states are more stable and have lower energy of formation than the Ta⁺¹/Ta⁺² states they are found in greater intensity as compared to the lower sub-oxides.[90]

The comparison of the experiments of Ta only mechanical and Ta only electrochemistry under the two different chemical environments assists to understand the combined electrochemical-mechanical experiments. The results in electrochemical only shows the presence of only stable oxide states of Ta⁺⁵/Ta⁺⁴ and the metallic Ta. However when the mechanical force was applied, observation of Ta⁺²/Ta⁺³ was made. This proves that mechanical energy assists to form the sub-oxides. When “mechanical” results are compared with “electrochemical–mechanical” ones, it is found that Ta in acetic acid shows similar compounds for electrochemical-mechanical as observed in mechanical with the exception of absence of Ta⁺⁴/Ta⁺⁵ in “pure mechanical” results. This in fact proves mutually competing reactions in which the products of both purely

mechanical and purely electrochemical are present in case of electro-chemical mechanical experiment.

The same observation found in sample from water with KCl shows the absence of Ta⁺² (sample 3) and Ta⁺¹ (sample 7). The lower shift in case of electrochemical-mechanical experiments in case of water as opposed to acetic acid can be explained due to the nature of the bonds in acetic acid and water. Acetic acid due to its corrosive nature removes the oxide film during the anodization process resulting in gas. The low frictional is related to this phenomenon. In case of water molecules, direct oxidation with Ta does not take place. This results in a high friction force being subjected to the Ta in water during electromechanical-chemical reaction.

It is possible that apart from oxides of tantalum, other types of compounds exist. Due to the presence of KCl in the electrolytic solution it is likely that Ta might exist in TaOCl₃ or TaO₂Cl or TaCl₅ form. Also, Ta(CH₃COO)₅ form might also exist. In all the possible compounds mentioned, the Ta +5 is the stable state. The presence of those compounds does not affect our observation significantly. Since our focus is to investigate non-equilibrium oxidation state of Ta, those other types do not affect our study. The XPS results proved the existence of metastable oxides of Ta under the influence of mechanical force. Metastable oxides are defined as the sub-oxides of Ta which are not predicted in the Pourbaix diagram. These oxides were detected in our XPS studies under non-equilibrium conditions involving electrochemical-mechanical and mechanical interactions. We will discuss the kinetics in next section.

5.3 Mechano-Kinetics and Kar-Liang equation

It was proven from the XPS and friction results that mechanical energy played an important role in sub-oxide formation. We take the modified Arrhenius-Eyring equation for transition state theory of chemical reactions:

$$k = (k_b T / h) e^{-\Delta G^\ddagger / RT} \quad (1)$$

where k is the oxidation time, k_b is the Boltzmann's constant, T is absolute temperature, h is the Plank's constant, and the ΔG^\ddagger is the Gibbs energy of activation. This equation indicates that a substance with high Gibbs energy of activation would lead to a low reaction rate of formation. For a reaction to proceed from a stable to an unstable sub-oxide state, we require the stable oxide to overcome the activation energy barrier in Eq (1).

Now for a spontaneous reaction, ΔG^\ddagger is negative, and hence the reaction proceeds at a high rate. However, for a non-spontaneous reaction that is the conversion of a stable oxide state to a non-stable oxide state, ΔG^\ddagger is positive making the overall rate of oxidation a slow process. The formation of the unstable sub-oxide is almost negligible under such conditions. If we add a mechanical energy term, ε , to the equation (1), the ΔG^\ddagger and ε , will be competing with each other to dominate the overall reaction. The equation becomes, as called the Kar-Liang equation:

$$k = (k_b T / h) e^{(-\Delta G^\ddagger + \varepsilon) / RT} \quad (2)$$

Now, for a non-spontaneous reaction, when $\Delta G^\ddagger > \varepsilon$, the effect of ε is negligible and mechano-chemical reaction does not take place. When $\Delta G^\ddagger \leq \varepsilon$, the mechano-chemical reaction takes place as the contribution of ε becomes significant. This means that the mechanical energy reaches a critical level to trigger the mechano-chemical reaction. In this case, the reaction became spontaneous. A higher ε will lead to the formation of energetically-unfavorable products, i.e., suboxides. This has been seen in our XPS and AFM analysis. Our results showed that applying mechanical energy could induce low valent sub-oxides formation of tantalum. The greater the mechanical energy, the more sub-oxides were formed. The effect of mechanical energy ε is further evaluated. We take $k_b = 8.617 \times 10^{-5}$ eV/k; $h = 4.136 \times 10^{-15}$ eV.s; $R = 8.63 \times 10^{-5}$ eV.k⁻¹.atom⁻¹; and $T = 273$ k. The oxidation rate k is thus plotted against mechanical energy in eV, as shown in figure 5.4a. At room temperature, with the increased ε , the reaction rate increases exponentially. The slope of this plot is 3.33, leading to an increase of $10^{3.33}$ /sec.eV. This means that an addition of mechanical energy 1 eV leads to an increase of reaction rate of at least 1000 1/sec. This increase is significant comparing with the equilibrium reaction rate without mechanical energy. This effect makes the sub-oxide formation possible (spontaneously).

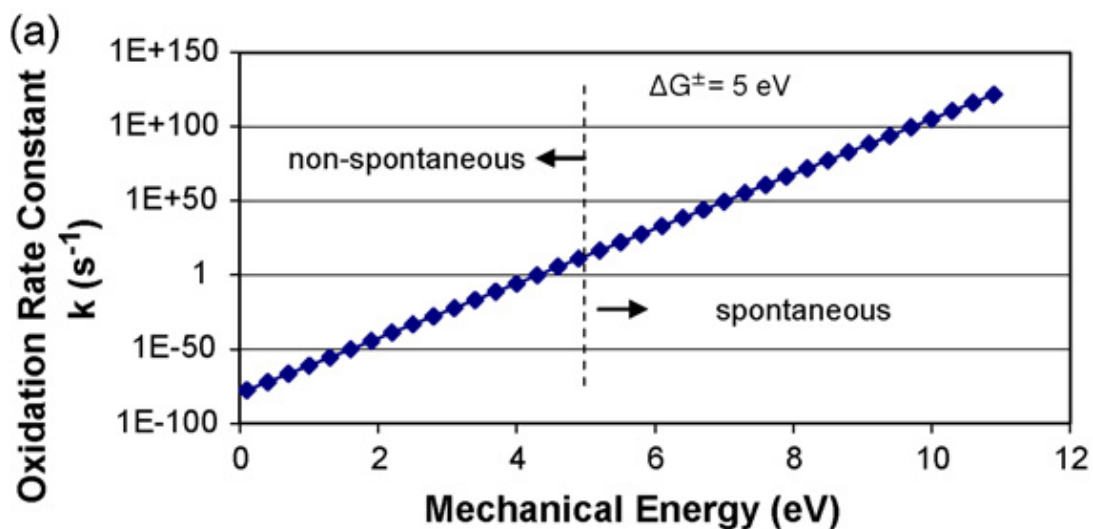


Figure 5.4a: Oxidation rate verses applied mechanical energy.

The effects of mechanical energy on oxidation can be illustrated in a proposed physical model, as shown in Figure 5.4b. The amount of applied mechanical energy is illustrated with dashed arrows. The y-axis is the potential energy of tantalum oxides and x-axis the reaction coordination number.

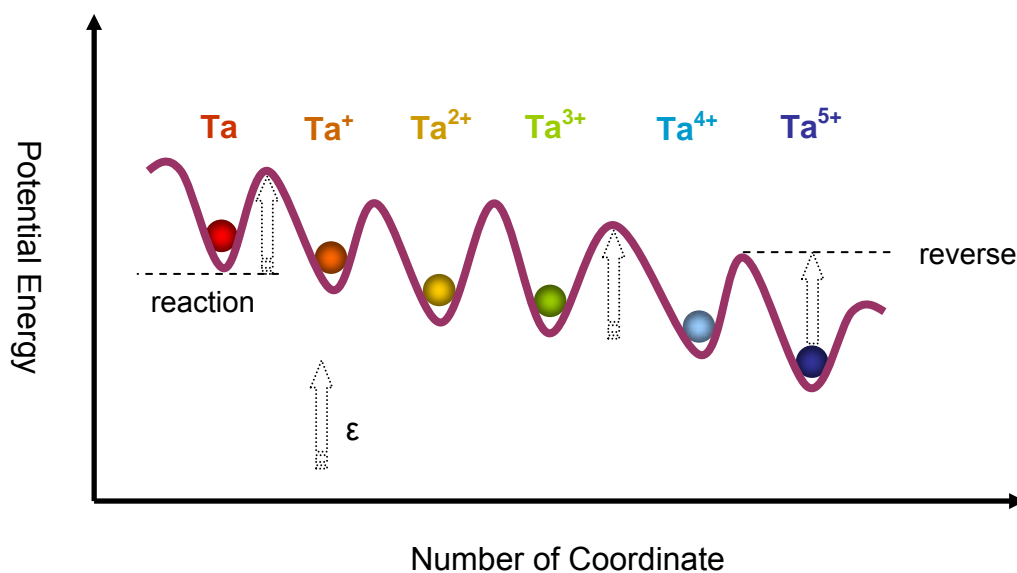


Figure 5.4b: Energy comparison of tantalum oxides under influence of applied mechanical energy ϵ .

For better comparison, the potential energy is not in scale. Here the different oxides have different level of potential energy indicating different stability. With friction, extra energy is introduced (ϵ) that overcomes the activation energy to become the next state of oxide. The thermal factor in the mechano-chemical kinetics is neglected as a causative agent for the formation of tantalum sub oxides. This is because tantalum +5 oxide state is known to be highly stable at high temperatures of upto 1450 degrees Celsius. [111] The temperature of the electrolytic media did not reach even 100 degree Celsius. So the possibility of thermal energy having a major contribution in sub-oxide formation can be effectively neglected.

5.4 Summary

We used a mechanical plus electrochemical approach to carefully study surface properties and sliding performance of tantalum in acidic solutions. During electrochemical reactions under mechanical stress, the sub-oxides of tantalum were generated. Thermal and kinetic analysis of the processes correlated mechanical energy with sub-oxide formation of tantalum. We proposed a modified Arrhenius-Eyring equation in which the mechanical energy parameter was considered. The overall activation energy of reaction includes two competing terms: Gibbs free energy and the mechanical energy. We found that the addition of the mechanical energy increased the oxidation rate exponentially with non-stable state reactions leading to the formation of metal-stable oxides. The mechanical energy made the kinetics favorable for formation of oxides that were originally-thermodynamically unfavorable. The amount of mechanical energy dominates the formation kinetics of the non-equilibrium state of oxides. The Kar-Liang equation can predict mechano-chemical reactions. The present approach is not only a new branch of chemical science, but also has important industrial applications, such as chemical-mechanical polishing.

CHAPTER VI

NON-EQUILIBRIUM KAR-LIANG DIAGRAMS FOR TANTALUM

This chapter will show a series of non-equilibrium Kar-Liang diagrams under different conditions for tantalum. The experimental conditions for generating the non-equilibrium diagrams has been described in chapter III in tables 3.4 and 3.5 (see page 33). The conditions have been chosen to mimic the equilibrium pH-potential Pourbaix diagram of tantalum. It is seen from the Pourbaix diagram that tantalum is stable in +5 conditions in a wide range of pH and potentials. [63]

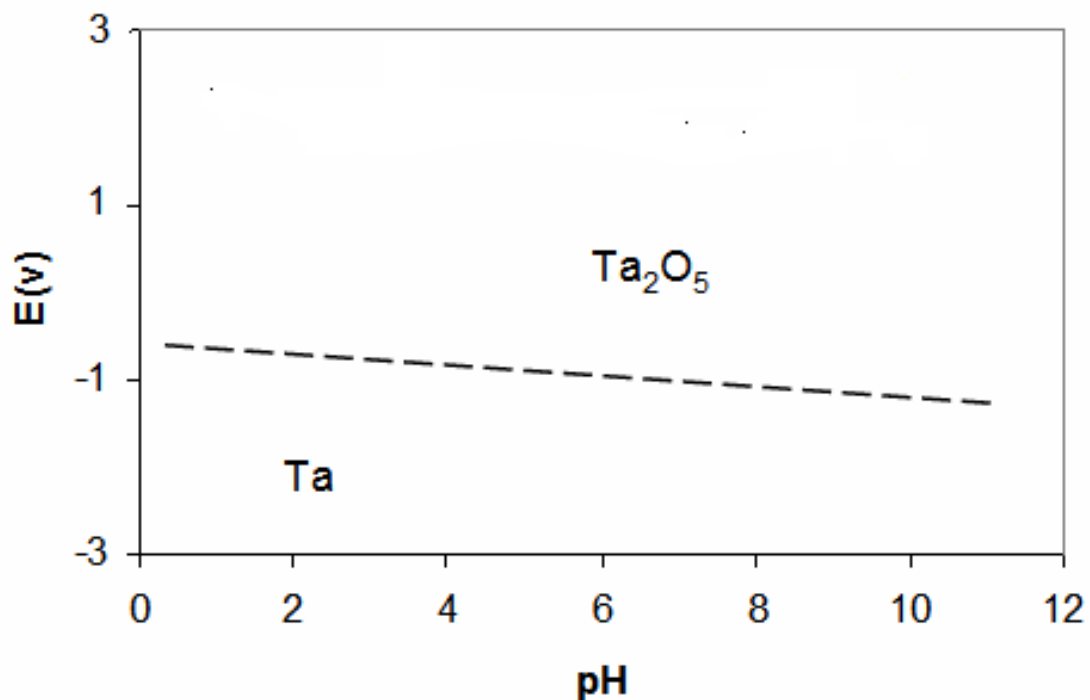
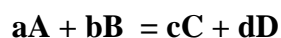


Figure 6.1: Illustration of pH-potential Pourbaix diagram of tantalum. [63]

The Pourbaix diagram maps the equilibrium phases of an aqueous electrochemical system. In case of tantalum as seen in figure 6.1 +5 is the stable oxidation state. However as mentioned earlier and seen from our mechano-oxidation experiments that tantalum exists in other oxidation states like +3, +2, and +1 also. (See chapters IV and V). As such a new set of diagrams are proposed based on the non-equilibrium conditions of tantalum. Such diagrams will be especially useful for semiconductor industry to understand the changes in oxidation state of tantalum under mechanical energy parameters.

The Pourbaix diagrams are named after the Russian chemist Marcel Pourbaix (1904-1998). He based his diagrams on Nernst equation which relates potential to pH under equilibrium conditions.



$$Eh = E^0 + \frac{0.0592}{n} \text{Log} \frac{[C]^c[D]^d}{[A]^a[B]^b}$$

Here E is the electrode potential, E^0 is the standard electrode potential, and n is the number of electrons transferred from a given chemical reaction where reactants A and B reacts to give products C and D. a, b, c and d are the concentrations of reactants A and B and products C and D respectively. [112]

The Kar-Liang diagrams on tantalum mimics the pH-potential phase detection graphs of Pourbaix but also considers the influence of mechanical energy in formation of unstable oxides. The experiments performed also tests the thermodynamic time-

dependent stability of the oxides formed. The experiments can be broadly classified into 4 groups as shown in chapter III in tables 3.4 and 3.5 (page 32) as follows:

1. Tantalum in DI water with KCl under electro-chemical mechanical energy.
2. The samples formed in condition 1 are tested after 48 hours.
3. Tantalum in DI water with KCl under mechano-chemical energy.
4. The samples formed in condition 2 are tested after 48 hours.

6.1 Analysis of tantalum under electro-chemical mechanical parameters

Tantalum was subjected to electro-chemical mechanical investigation in three different pH solutions. pH 1 representing highly acidic conditions (sample 6.1), pH 7 representing neutral conditions (sample 6.2) and pH 10 representing highly basic conditions (sample 6.3). The speed was kept at 0.5 cm/sec; the load was 1N and +2.4 V potential was applied. The same samples were tested after 48 hours to test the stability of the sub-oxides formed.

The figures 6.1 – 6.5 in the following pages show the XPS deconvolution of peaks obtained under different test conditions.

6.1.1 Analysis of sample 6.1 (pH 1, 0.5 cm/sec, 1 N, +2.4 V)

Table 6.1 gives a brief analysis of the XPS peaks found in pH 1.

Table 6.1: XPS analysis of sample 6.1 after subjecting it to ECMP process

	Ta $f_{5/2}$	Ta $f_{7/2}$	Oxidation state
Tantalum sample	26.2	24.4	+ 2
0.5 cm/sec; 1 N	25.6	23.7	+1
pH 1; +2.4	21.3	19.5	0

Figure 6.2 shows the existence of sub-oxides after ECMP.

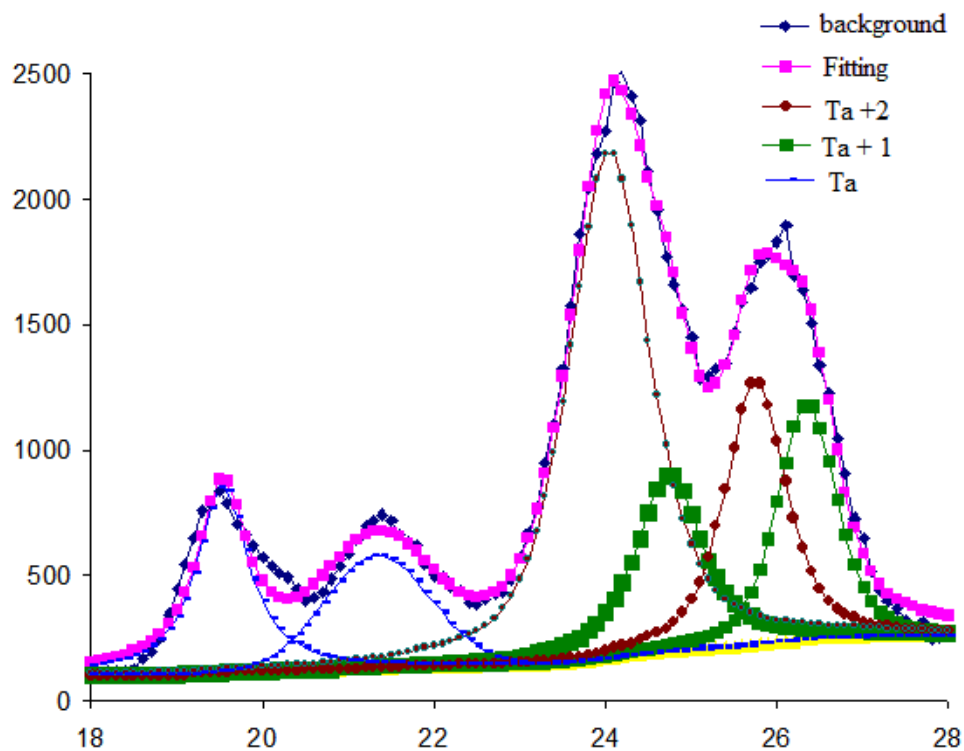


Figure 6.2: XPS analysis of tantalum sample in pH 1 after ECMP process.

6.1.2 Analysis of sample 6.1 (pH 1, 0.5 cm/sec, 1 N, +2.4 V potential, after 48 hrs)

Table 6.2 gives a brief analysis of the XPS peaks found in pH 1 after 48 hours.

Table 6.2: XPS analysis of sample 6.1 subjected to ECMP process after 48 hrs

Tantalum sample	Ta $f_{5/2}$	Ta $f_{7/2}$	Oxidation state
0.5 cm/sec; 1 N	27.9	26.3	+ 4
pH 1;48 hrs;	27.3	25.5	+3
+2.4 V	23.2	21.0	0

Figure 6.3 shows the existence of sub-oxides after ECMP when 48 hours have passed.

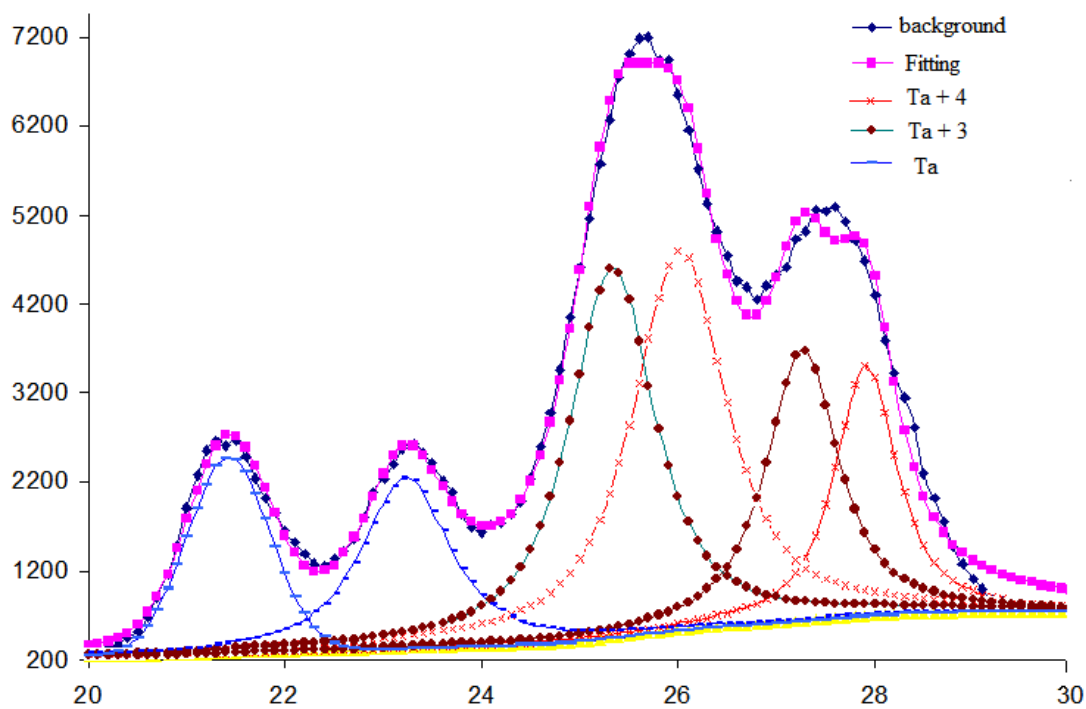


Figure 6.3: XPS analysis of tantalum sample in pH 1 after ECMP process after 48 hrs.

6.1.3 Analysis of sample 6.2 (pH 7, 0.5 cm/sec, 1 N, +2.4 V potential)

Table 6.3 gives a brief analysis of the XPS peaks found in pH 7.

Table 6.3: XPS analysis of sample 6.2 after subjecting it to ECMP process

Tantalum sample	Ta $f_{5/2}$	Ta $f_{7/2}$	Oxidation state
	26.78	25.27	+ 3
0.5 cm/sec; 1 N	26.16	24.41	+2
pH 7; +2.4 V	21.71	19.82	0

Figure 6.4 shows the existence of sub-oxides after ECMP under neutral conditions.

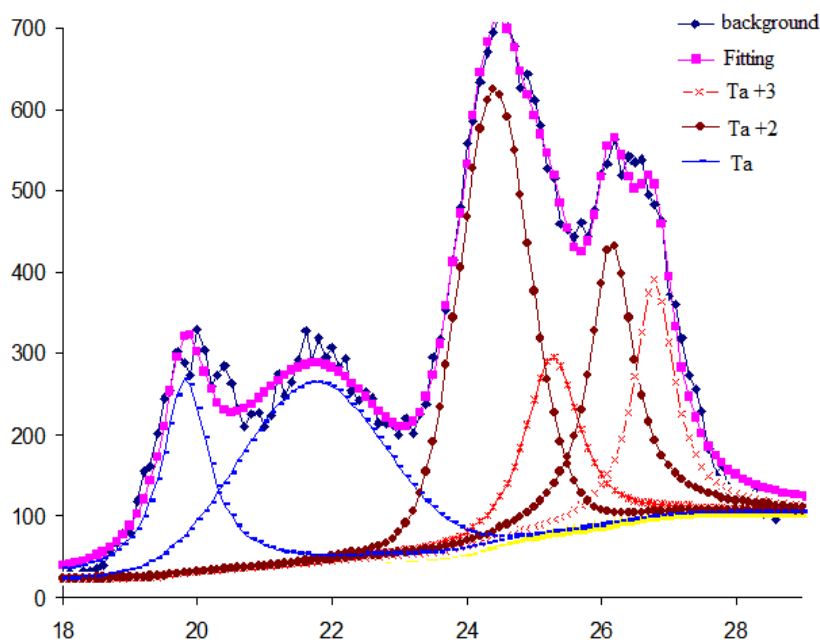


Figure 6.4: XPS analysis of tantalum sample in pH 7 after ECMP process.

6.1.4 Analysis of sample 6.2 (pH 7, 0.5 cm/sec, 1 N, +2.4 V potential, after 48 hours)

Table 6.4 gives a brief analysis of the XPS peaks found in pH 7.

Table 6.4: XPS analysis of sample 6.2 subjected to ECMP process after 48 hrs

Tantalum sample	Ta $f_{5/2}$	Ta $f_{7/2}$	Oxidation state
0.5 cm/sec; 1 N	28.85	26.45	+ 5
pH 7;48 hrs;	28.3	26.53	+4
+2.4 V	23.78	21.94	0

Figure 6.5 shows the existence of sub-oxides after ECMP when 48 hours have passed.

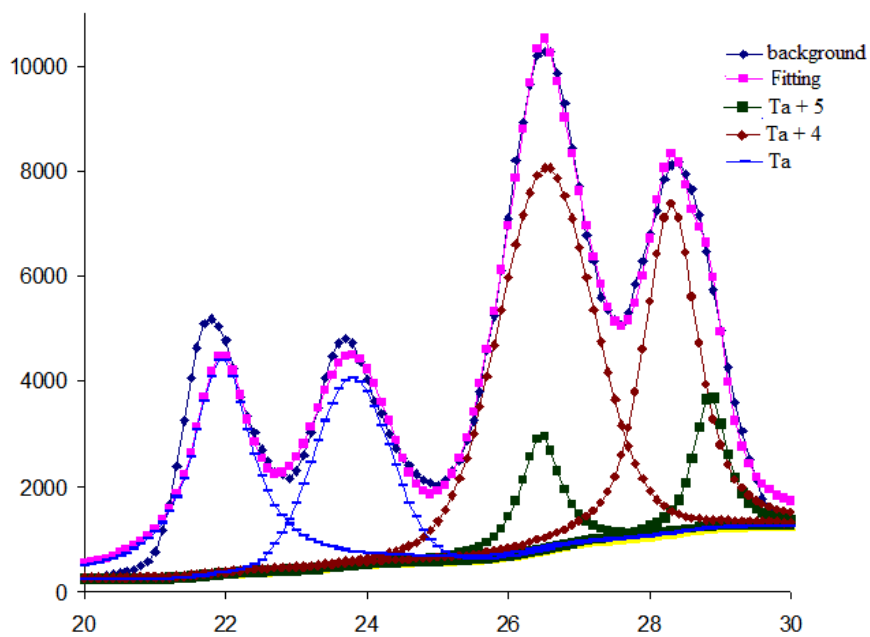


Figure 6.5: XPS analysis of tantalum sample in pH 7 after ECMP process after 48 hrs.

6.1.5 Analysis of sample 6.3 (pH 10, 0.5 cm/sec, 1 N, +2.4 V potential)

Table 6.5 gives a brief analysis of the XPS peaks found in pH 10.

Table 6.5: XPS analysis of sample 6.3 after subjecting it to ECMP process

	Ta $f_{5/2}$	Ta $f_{7/2}$	Oxidation state
Tantalum sample	27.99	25.89	+4
0.5 cm/sec; 1 N	26.54	24.17	+2
pH 10; +2.4 V	24.85	23.8	+1
	21.76	19.97	0

Figure 6.6 shows the existence of sub-oxides after ECMP in basic conditions.

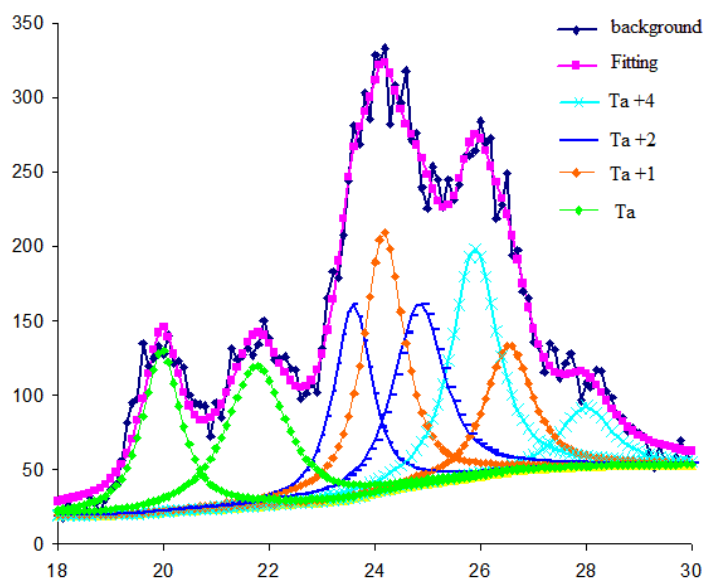


Figure 6.6: XPS analysis of tantalum sample in pH 10 after ECMP process.

6.1.6 Analysis of sample 6.3 (pH 10, 0.5 cm/sec, 1 N, +2.4 V, after 48 hours)

Table 6.6 gives a brief analysis of the XPS peaks found in pH 10.

Table 6.6: XPS analysis of sample 6.3 subjected to ECMP process after 48 hrs

	Ta $f_{5/2}$	Ta $f_{7/2}$	Oxidation state
Tantalum sample	28.85	26.96	+ 5
0.5 cm/sec; 1 N	27.7	25.47	+4
pH10;48 hrs;+2.4 V	22.9	21.15	0

Figure 6.7 shows the existence of sub-oxides after ECMP when 48 hours have passed.

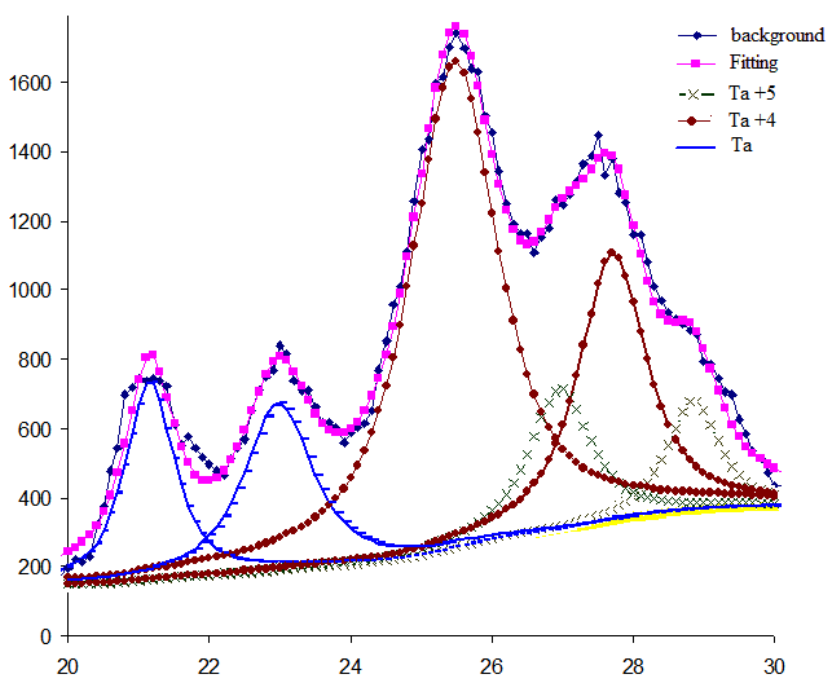


Figure 6.7: XPS analysis of tantalum sample in pH 10 after ECMP process after 48 hrs.

From the XPS analyses [90] as seen in figures 6.2 – 6.4 it is found that tantalum shows lower metastable oxidation states in acidic, neutral and basic conditions after ECMP process. In both acidic and basic conditions we find +1 oxidation state. In neutral condition +1 oxidation state is absent. +2 oxidation state is common in all the three processes with basic condition showing an addition of +4 oxidation state and the neutral condition +3 oxidation state. This can be explained as Ta towards basic conditions favors oxidation and hence presence of higher oxidation states. [60]

A time dependent experiment was also performed. The samples that had been subjected to ECMP process were analyzed after 48 hours. Interestingly in all the three pH conditions the tantalum samples reverted back to its energetically favorable +5/+4 states as seen in figures 6.5 – 6.7. This shows that the metastable oxidation states of tantalum formed in ECMP process is not thermodynamically stable over a longer period of time. Tantalum being oxyphyllic reverts back to its equilibrium state of +5 in 48 hours. The Kar-Liang diagram for non-equilibrium oxidation states of Ta in three pH solutions at +2.4 V is shown in the figure below.

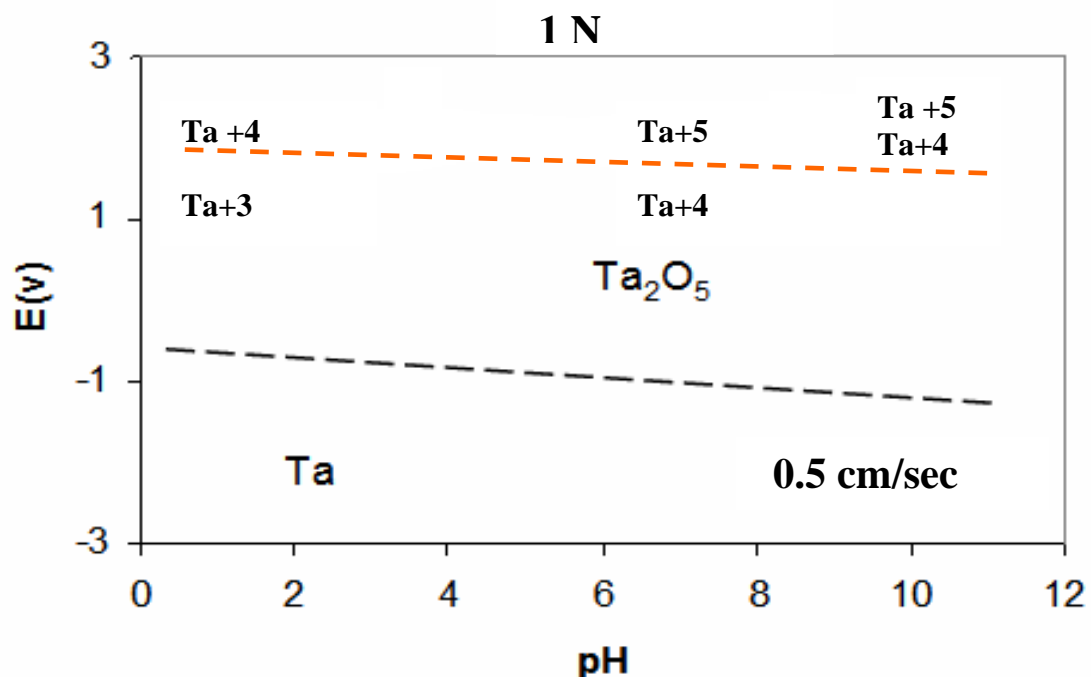


Figure 6.8: Illustration of pH-potential Kar-Liang diagram of Ta under ECMP. The load and speed parameters are put in the graph. The red dashed line showing the region where the sub-oxidation states of tantalum have been found. The potential is at +2.4 V.

6.2 Analysis of tantalum under mechano-chemical parameters

Tantalum was subjected to mechanical investigation in three different pH solutions. pH 1 representing highly acidic conditions (sample 6.4), pH 7 representing neutral conditions (sample 6.5) and pH 10 representing highly basic conditions (sample 6.6). The speed was kept at 0.5 cm/sec; the load was 1N and a potential of +2.4 was applied. After 48 hours the samples were again analyzed in XPS to account for the stability of the oxidation states of tantalum formed.

6.2.1 Analysis of sample 6.4 (pH 1, 0.5 cm/sec, 1 N, 0 V)

Table 6.7 gives a brief analysis of the XPS peaks found in pH 1.

Table 6.7: XPS analysis of sample 6.4 after subjecting it to CMP process

Tantalum sample	Ta $f_{5/2}$	Ta $f_{7/2}$	Oxidation state
0.5 cm/sec; 1 N	25.38	23.45	+ 1
pH 1;	24.59	22.81	0

Figure 6.9 shows the existence of sub-oxides after CMP process.

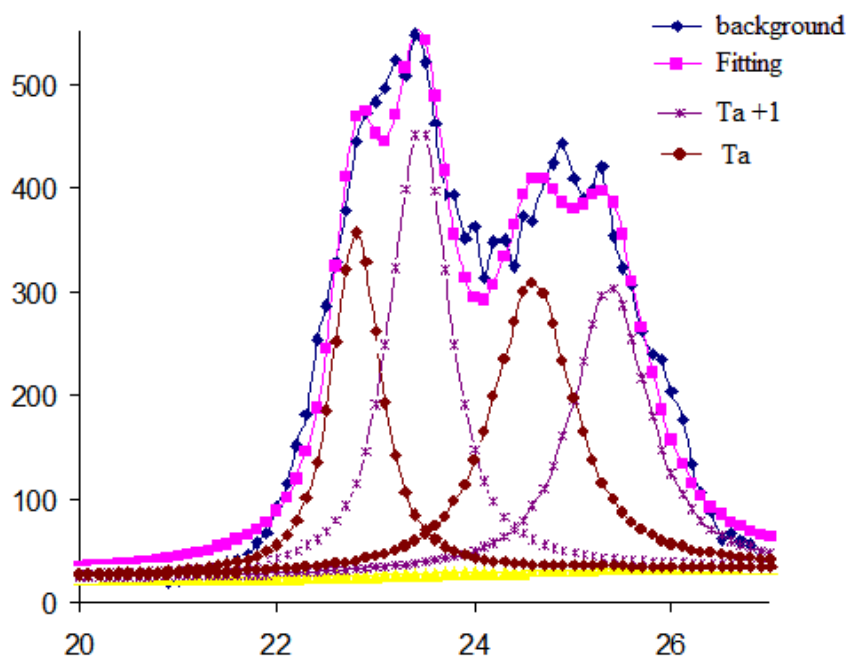


Figure 6.9: XPS analysis of tantalum sample in pH 1 after CMP process.

6.2.2 Analysis of sample 6.4 (pH 1, 0.5 cm/sec, 1 N, 0 V, after 48 hrs)

Table 6.8 gives a brief analysis of the XPS peaks found in pH 1.

Table 6.8: XPS analysis of sample 6.4 subjected to CMP process after 48 hrs

	Ta $f_{5/2}$	Ta $f_{7/2}$	Oxidation state
Tantalum sample	26.06	24.08	+ 2
0.5 cm/sec; 1 N			
pH 1;48 hrs; 0 V	25.5	23.8	+1

Figure 6.10 shows the existence of sub-oxides after CMP when 48 hours have passed.

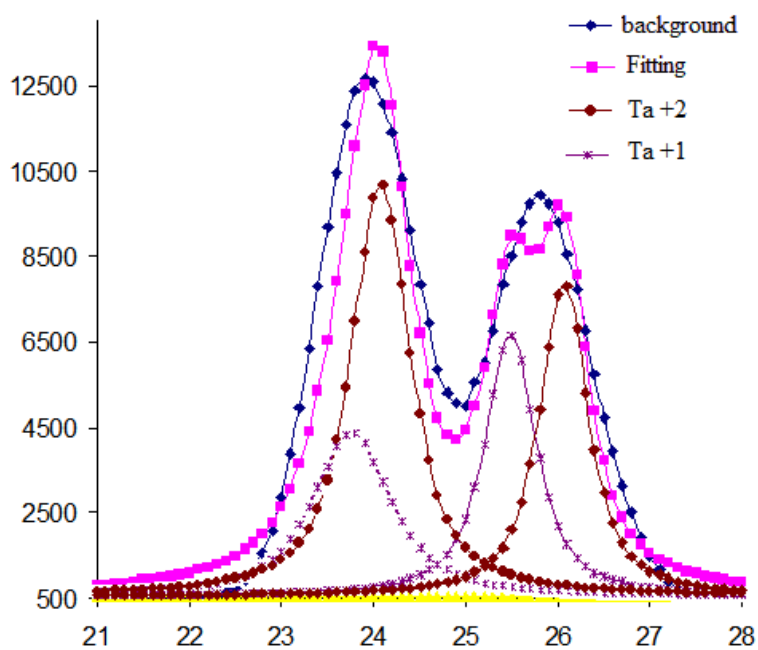


Figure 6.10 XPS analysis of tantalum sample in pH 1, 48 hrs after CMP process.

6.2.3 Analysis of sample 6.5 (pH 7, 0.5 cm/sec, 1 N, 0 V)

Table 6.9 gives a brief analysis of the XPS peaks found in pH 7.

Table 6.9: XPS analysis of sample 6.5 after subjecting it to CMP process

	Ta $f_{5/2}$	Ta $f_{7/2}$	Oxidation state
Tantalum sample	26.55	24.54	+ 2
0.5 cm/sec; 1 N pH 7	25.73	23.84	+ 1

Figure 6.11 shows the existence of sub-oxides after CMP in neutral conditions.

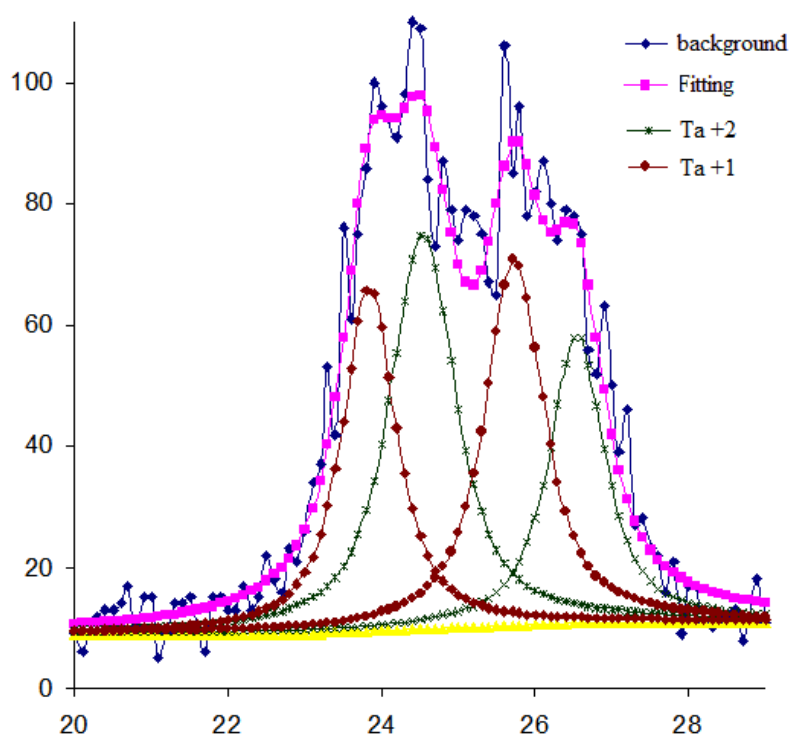


Figure 6.11: XPS analysis of tantalum sample in pH 7, after CMP process.

6.2.4 Analysis of sample 6.5 (pH 7, 0.5 cm/sec, 1 N, 0 V, after 48 hrs)

Table 6.10 gives a brief analysis of the XPS peaks found in pH 7.

Table 6.10: XPS analysis of sample 6.5 subjected to CMP process after 48 hrs

	Ta $f_{5/2}$	Ta $f_{7/2}$	Oxidation state
Tantalum sample	26.89	24.99	+ 3
0.5 cm/sec; 1 N pH 7;48 hrs; 0 V	26.08	24.33	+2

Figure 6.12 shows the existence of sub-oxides after CMP when 48 hours have passed.

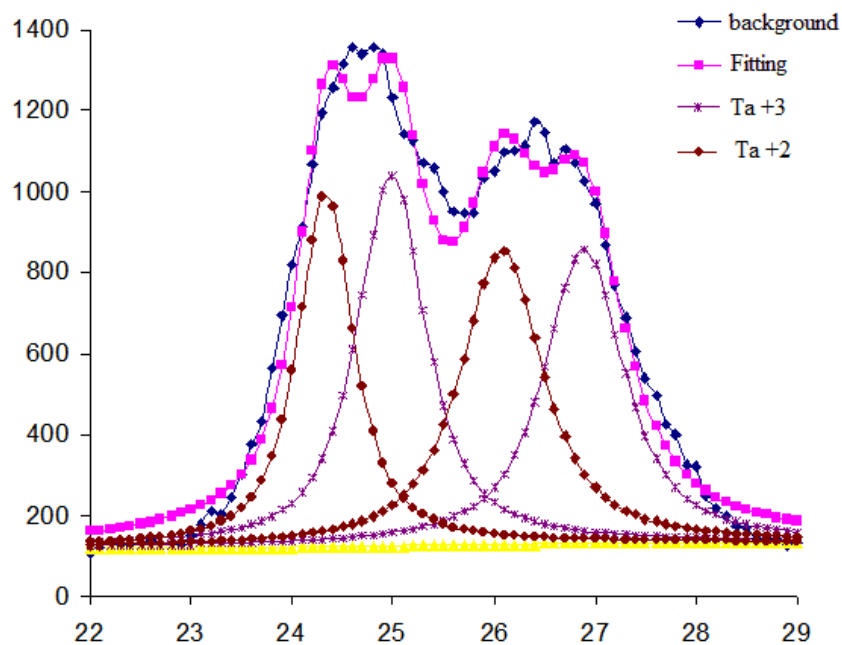


Figure 6.12: XPS analysis of tantalum sample in pH 7, 48 hrs after CMP process.

6.2.5 Analysis of sample 6.6 (pH 10, 0.5 cm/sec, 1 N, 0 V)

Table 6.11 gives a brief analysis of the XPS peaks found in pH 10.

Table 6.11: XPS analysis of sample 6.6 after subjecting it to CMP process

	Ta $f_{5/2}$	Ta $f_{7/2}$	Oxidation state
Tantalum sample	26.1	24.52	+ 2
0.5 cm/sec; 1 N			
pH 10	25.44	23.57	+ 1

Figure 6.13 shows the existence of sub-oxides after CMP in basic conditions.

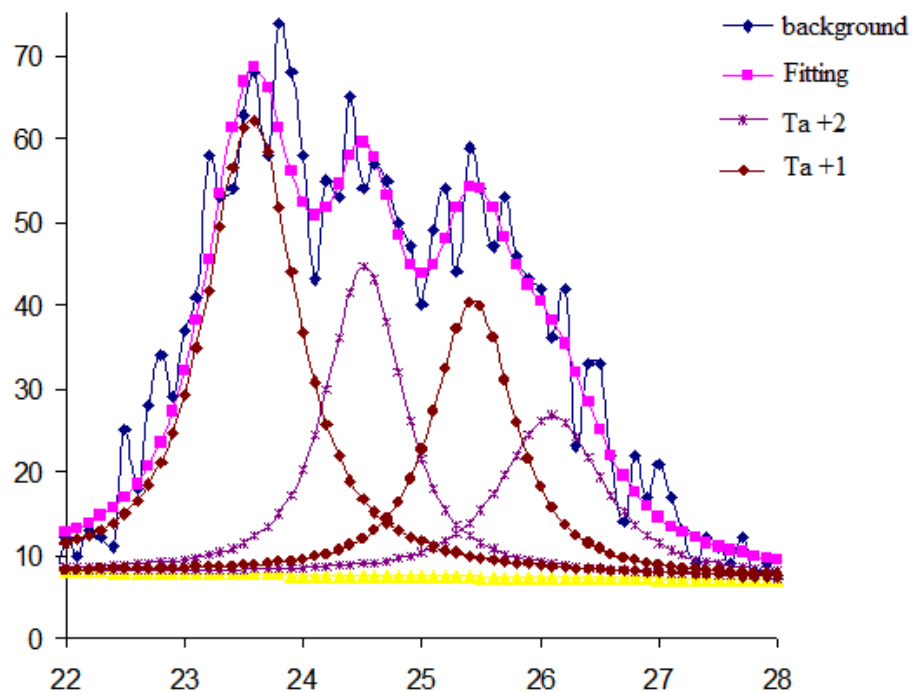


Figure 6.13: XPS analysis of tantalum sample in pH 10, after CMP process.

6.2.6 Analysis of sample 6.6 (pH 10, 0.5 cm/sec, 1 N, 0 V, after 48 hrs)

Table 6.12 gives a brief analysis of the XPS peaks found in pH 10.

Table 6.12: XPS analysis of sample 6.6 subjected to CMP process after 48 hrs

Tantalum sample	Ta $f_{5/2}$	Ta $f_{7/2}$	Oxidation state
0.5 cm/sec; 1 N	26.19	24.33	+ 2
pH 10;48 hrs; 0			
V	25.45	23.68	+1

Figure 6.14 shows the existence of sub-oxides after CMP when 48 hours have passed.

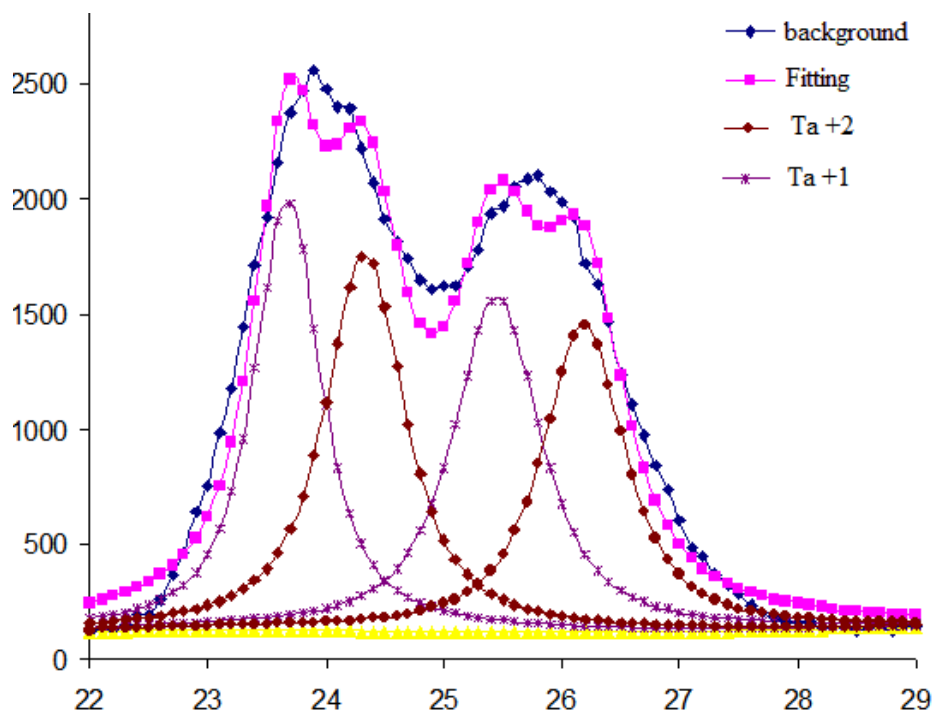


Figure 6.14: XPS analysis of tantalum sample in pH 10, 48 hrs after CMP process.

From the XPS analyses as seen in figures 6.9 – 6.11 [90] it is found that tantalum shows lower metastable oxidation states in acidic, neutral and basic conditions after CMP process. In acidic, neutral and basic conditions we find +1 oxidation state. In neutral condition as well as in basic condition we find +2 oxidation state as common. The acidic condition however exhibits metallic tantalum state. This can be explained as acetic acid is corrosive to oxide films in acidic solutions.[60]

A time dependent experiment was also performed. The samples that had been subjected to CMP process were analyzed in XPS after 48 hours. Interestingly unlike ECMP process, in CMP process in all the three pH conditions the tantalum samples did not revert back to its energetically favorable +5/+4 states. In pH 1 and pH 7 conditions we do find the next higher oxidation state of + 2 and +3 respectively suggesting the oxyphylic mechanism of tantalum as seen in figures 6.12 and 6.13. But the process is very slow as compared to the fast reversion process in ECMP. In case of pH 10, no reversion to the original oxidation state takes place as seen in figure 6.14.

This apparent contradiction in results between CMP and ECMP process can be explained from our previous results. In Chapter IV we found that the thickness of oxide film in mechanical process is higher than that of oxide films of tantalum formed in electro-mechanical chemical process (see figure 4.5). High friction rate due to evolution of gas in the surface and competing anodization and removal rate mechanisms give a thinner oxide film and a more mixed oxide film than in mechano-chemical processes. In mechanical polishing, no such evolution of gas occurs and friction is always lower when compared with ECMP process as evident from friction coefficient measurements done in

Chapters IV and V (see figures 4.1, 5.1 a, 5.1b). This leads to the formation of a thicker sub-oxide film as already shown in this dissertation (see figure 4.5). Thicker sub-oxide growth means more time required for the entire sub-oxide layer to get converted to the more stable oxidation states. However we do see the slow reversion process in pH 1 and pH 7 but no change is observed in pH 10. It is known that oxide formation is favored in alkaline conditions. Hence, it is proposed that a thicker oxide film is formed in pH 10 which leads to failure in XPS to detect the changes in the sub-oxide states of tantalum.

Based on the above findings the Kar-Liang diagram for non-equilibrium oxidation states of Ta in three pH solutions at 0 V is shown in the figure below.

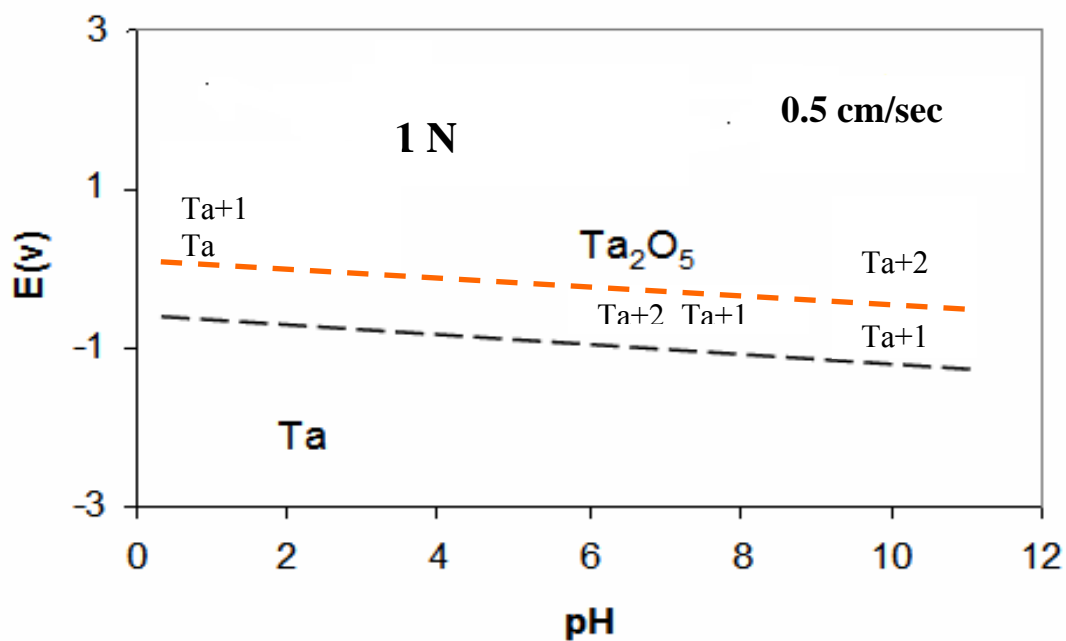


Figure 6.15: Illustration of pH-potential Kar-Liang diagram of Ta under non-equilibrium conditions showing the sub-oxides formed. The load and speed parameters are put in the graph. The compounds formed are at pH 1, pH 7 and pH 10 when no potential is applied. The red dashed lines show the region where the sub-oxidation states of Ta were found.

After 48 hours minor changes occur in the Kar-Liang diagram on the sub-oxidation states of tantalum. These changes are shown in the time dependent non-equilibrium Kar-Liang diagram. The samples are kept for 48 hours and then XPS data is taken. A slow reversion to the more stable oxidation state is found in the graph.as shown in page 107.

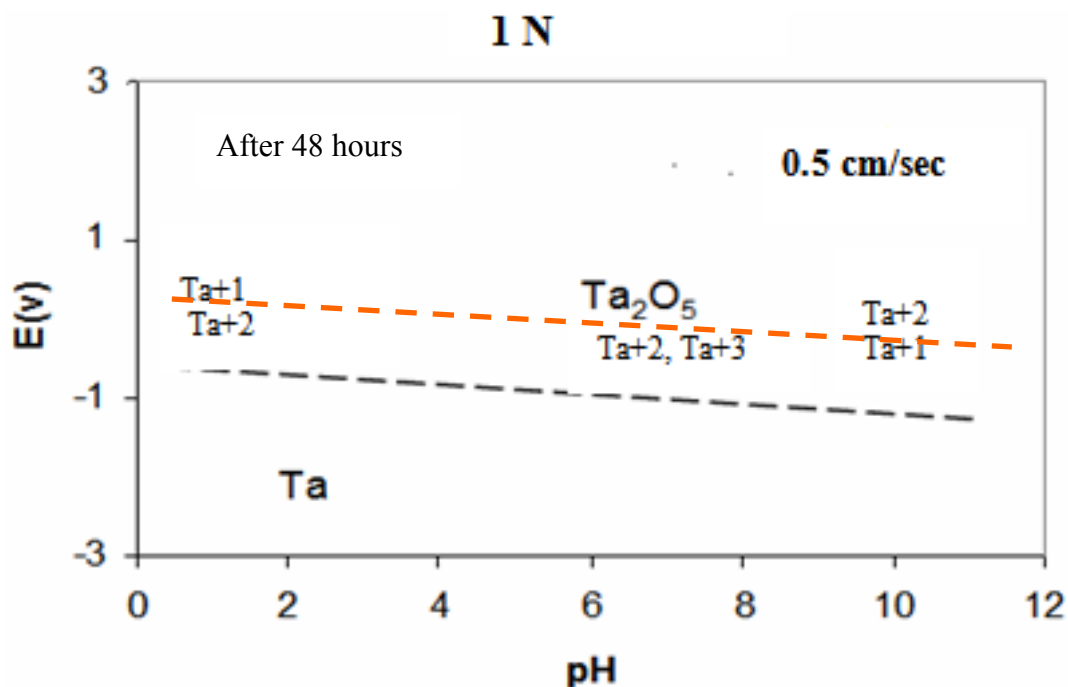


Figure 6.16: Illustration of pH-potential Kar-Liang diagram of Ta under non-equilibrium conditions showing the sub-oxides formed. The load and speed parameters are put in the graph. The compounds formed are at pH 1, pH 7 and pH 10 when no potential is applied. The XPS analysis was done 48 hours after the experiment was performed. The red dashed lines represent the region where the sub-oxides of Ta were found.

6.3 Summary

The chapter presents a series of unique Kar-Liang diagrams which makes it easier to understand the changes in the oxidation states of Ta under mechanical and electro-chemical-mechanical parameters. Time dependent parameters are also included in one of the graphs. The diagrams in future can be elaborated to make a more comprehensive chart taking every potential and every pH condition. This will help the semi-conductor industry tremendously to understand the chemistry of tantalum during the CMP process in an easier way.

CHAPTER VII

CONCLUSIONS AND FUTURE SUGGESTIONS

7.1 Conclusions

This research studied dynamics and kinetics of tantalum oxidation in a non-equilibrium process resulting non-equilibrium states of oxides. A unique approach was used through an experimental setup that enables in situ synergetic detection. Several major discoveries were found. The following highlights results and major impacts.

An *in situ* tribochemical set up was developed which can detect surface changes on application of potential through coefficient friction changes. It has been proved that under mechanical and electrochemical-mechanical forces tantalum does not remain in its equilibrium +5 oxidation state but changes to its sub-oxide states. The dissertation also proposed a Kar-Liang equation which considered the mechanical energy parameter which drives a non-spontaneous reaction to spontaneity. Also a series of non-equilibrium Kar-Liang diagrams were put forward which helps to easily understand the chemistry of tantalum under mechanical parameters. Time-dependent non-equilibrium Kar-Liang diagram was also put forward. These diagrams are unique and first of its kind and can be used as an easy guide of reference by CMP industry to understand the chemistry of tantalum in polishing working environment.

Tantalum was studied here as a model system. Other transition metals, vanadium, and niobium are expected to have similar behavior due to reasons of their similar electronic configuration belonging to sub-group IVb of the 1st transition metal series.

Niobium is especially important as it is used in oseeintegration.[113] As such the effects of mechanical behavior on oxidation states of tantalum can be extended to study of niobium.

This research has important impacts on several areas. Mechanochemistry is a new breach of chemistry. The Kar-Liang equation helps in understanding the parameter which drives a non-spontaneous reaction to a spontaneous reaction under mechanical energy. CMP industry also will benefit in better understanding the chemistry of tantalum. The non-equilibrium diagrams generated help to form an easy reference point for mechano-chemistry of tantalum.

7.2 Future suggestions

The band gap reduction theory put forward in the dissertation (Chapter IV) for the possible formation of tantalum sub-oxides can be further investigated. Computational study on the effects of reduction of band gaps on oxidation states of tantalum by application of stress would be a pioneering work and help to better understand the experimental processes reported in this dissertation.

Other metals such as niobium and vanadium can also be studied. The study can also be extended to non-transition metals like silicon as well as widely used transitional metals like iron.

Kar-Liang diagrams generated can be further worked upon and more comprehensive reference diagrams for CMP industry can be generated. This will prove beneficial for the semi-conductor industry. Such diagrams can be generated for other

transitional metals resulting in an immense benefit to scientific community and industries working under non-equilibrium conditions on day to day basis.

REFERENCES

- [1] B.N.J. Persson, Sliding Friction: Physical Principles and Applications, Springer, New York, (1998).
- [2] C. Hatchet, Philos. T. Roy. Soc. A (MDCCCIII- 1803) 43.
- [3] D. Dowson, History of Tribology, London and Bury St Edmunds, Professional Engineering Publishing Ltd, London, UK (1998).
- [4] F. P. Wickens, Fundamentals of Rail Vehicle Dynamics: Guidance and Stability, Taylor and Francis, London, UK (2003).
- [5] G. Amontons, On the Resistance Originating in Machines (in French), Mem. Acad. Roy. (1699), 206.
- [6] C.A.,Coulomb, The Theory of Simple Machines (in French), Mem. Math. Phys. Acad. Sci. 10, (1785) 161.
- [7] F.P. Bowden, D. Tabor, The Friction and Lubrication of Solids, Oxford Clarendon Press, Oxford, (1950).
- [8] J.Vizintin, M. Kalin, K. Dohda, S. Jahanmir, (Eds.), Tribology of Mechanical Systems: A guide to the present and future technologies, ASME Press, New York, (2004).
- [9] J. J. Gilman, Science, 274 (5284), (1996), 65.
- [10] E.M. Gutman, Mechanochemistry of Solid Surfaces, World Scientific, Hackensack, NJ, (1994).
- [11] J. K. Burdett, Chemical Bonding in Solids, Oxford University Press, New York (1995).

- [12] P. P. Edwards, T. V. Ramakrishnan, C. N. R. Rao, *Metal-Insulator Transitions Revisited*, Taylor & Francis, London, UK (1995).
- [13] J.B. Hudson, *Surface Science: An Introduction*, John Wiley & Sons Inc., New York (1998).
- [14] H. Over, A.P. Seitsonen, *Science*, 297 (5589) (2002) 2003.
- [15] R. H. Crabtree, *The Organometallic Chemistry of the Transition Metals*, John Wiley & Sons Inc., New York (2000).
- [16] A. N. Artsyukhovich, V. A. Ukraintsev, I. Harrison, *Surf. Sci.*, 347(3) (1996) 303.
- [17] B. Hallwell, J. M. C. Gutteridge, *J. Biochem.*, 219, (1984) 1.
- [18] H. J. H. Fenton, *J. Chem. Soc. Trans.*, 65, (1894) 899.
- [19] K. Andersson, *Structure, bonding and chemistry of water and hydroxyl on transition metal surfaces*, Ph.D Dissertation; Stockholm University, 18, (2006).
- [20] F. Vidal, B. Busson, C. Six, A. Tadjeddine, L. Dreesen, C. Humbert, A. Peremans, P. Thiry; *J. Electroanal. Chem.*, 563 (1) (2004) 9.
- [21] S. M. Hsu, *Tribol. Int.*, 37(7) (2004) 553.
- [22] J.A. Caram, C. Gutiérrez, *J. Electroanal. Chem.* 323, (1992) 213.
- [23] A. Cambiella, J.M. Benito, C. Pazos, J. Cooa, A. Hernández, J.E. Fernández, *J. Mater. Process. Tech.*, 184 (1-3) (2007) 139.
- [24] Edison, T., US Patent No. 158787 (1875).
- [25] V. Guruswamy, O. M. J. Bockris, *Comprehensive Treatise of Electrochemistry*, Vol. 4, Plenum Press, New York (1980).
- [26] S.S. Wang, S.C. Tung, *Tribol. T.*, 33, (1990) 563.

- [27] S.C. Tung, Tribol. T., 34, (1991) 479.
- [28] W. Zhai, Front. Mech. Eng. Chi., 2(4) (2007) 463.
- [29] N.P. Brandon, N. Bonanos, P.O. Fogarty, J. Appl. Electrochem., 23, (1993) 456.
- [30] Y. Naerheim, M. W. Kendig, Wear, 139, (1985) 104.
- [31] H.A. El-Kader, S.M. El-Raghy, Corros. Sci., 26(8) (1986) 647.
- [32] G.H. Kelsall, Y.Y. Zhu, H.A. Spikes, J. Chem. Soc., Farad. T., 89(2) (1993) 267.
- [33] B. R. Pearson, P.A. Brook, R. B. Waterhouse, Tribol. Int., 21(4) (1988) 191.
- [34] A. Iwabuchi, T. Sonoda, H. Yashiro, Wear, 225, (1999) 181.
- [35] A. Iwabuchi, T. Tsukamoto, Y. Tatsuyanagi, N. Kawahara, T. Nonaka, Wear, 156, (1992) 301.
- [36] Y. Y. Zhu, G. H. Kelsall, H. A. Spikes, Tribol. T., 37(4) (1994) 811.
- [37] Y. Zhu, S. Ogano, G. Kelsall, Tribol. T., 43(2) (2000) 175.
- [38] S. S. Wang, S.P. Maheswari, Y. M. Wang, ASLE T., 30, (1987) 394.
- [39] S.S. Wang, S. P. Maheswari, S.C. Tung, Tribol. T., 32, (1989) 91.
- [40] W. L. C. M. Heyboer, G. A. C. M Spierings, J. E. A. M. Van den Meerakker, J. Electrochem. Soc., 138(3) (1991) 774.
- [41] L. Zhou, V. Audurier, P. Pirouz, J. Electrochem. Soc., 144(6) (1997) L161.
- [42] G. H. Xu, H. Liang, J. Electron. Mater., 31(4) (2002) 272.
- [43] C. Li, I. B. Bhat, R. J. Wang, J. Electron. Mater., 33(5) (2004) 481.
- [44] T.E. Fischer, Ann. Rev. Mater. Sci., 18, (1988), 303.
- [45] S.R. Hah, C.B. Burk, T.E. Fischer, J. Electrochem. Soc., 146, (1999), 1505.
- [46] K. Chattopadhyay, V. Varghese, Mat. Sci. Eng. A-Struct., A375, (2004) 72.

- [47] D. A. Emel'yanov, K. G. Korolev, M. A. Mikhailenko, A. V. Knot'ko, N. N. Oleinikov, Yu. D. Tret'yakov, V. V. Boldyrev, *Inorg. Mater.* (Translation of *Neorgan. Mater.*), 40(6) (2004) 632.
- [48] T. Tojo, Q. Zhang, F. Saito, *J. Alloy. Compd.*, 427(1-2) (2007) 219.
- [49] A. Hayashi, K. Iio, H. Morimoto, T. Minami, M. Tatsumisago, *Solid State Ionics*, 175(1-4) (2004) 637.
- [50] N. Kosova, E. Devyatkina, *Solid State Ionics*, 172(1-4), (2004) 181.
- [51] L. Pardo, A. Castro, P. Millan, C. Alemany, R. Jimenez, B. Jimenez, *Acta Materialia*, 48(9) (2000) 2421.
- [52] C.T. Au, W.D. Zhang, H.L. Wan, *Catal. Lett.* (241) (1996) 37.
- [53] V. V. Zyryanov, N. F. Uvarov, V. A. Sadykov, G. M. Alikina, L. S. Ivashkevich, M. I. Ivanovskaya, S. Neophytides, *J. Struct. Chem.*, 45(Suppl.), (2004) S127.
- [54] B. H. Liu, J. Ding, Z. L. Dong, Z. Y. Zhong, J. Y. Lin, T. White, *Diffusion and Defect Data—Solid State Data, Pt. B: Solid State Phenomena*, 111, (2006) 183.
- [55] A. Molnar, M. Varga, G. Mulas, I. Bertoti, M. Mohai, *Prog. Cat. Res.*, 177 (2005)
- [56] P. P. Edwards, T. V. Ramakrishnan, C. N. R. Rao, *Metal-Insulator Transitions Revisited*, Taylor & Francis, London (1995).
- [57] J.J. Gilman, *Philosophical Magazine B*; 207, (1993) 67.
- [58] IUPAC Compendium of Chemical Terminology, 2nd Edition (1997) 43.
- [59] Cotton, F. Albert; Wilkinson, G; Murillo, C. A.; *Advanced Inorganic Chemistry* (6th Ed.), John Wiley & Sons Inc., New York, (1999).

- [60] S. C. Kuiry, S. Seal, W. Fei, J. Ramsdell, V. H. Desai, Y. Li, S. V. Babu, B. Wood, *J. Electrochem. Soc.*, 150 (1) (2003), C36.
- [61] K. Chen, G. R. Yang, M. Nielsen, T. M. Lu, E. J. Rymaszewski, *Appl. Phys. Lett.*, 70 (3) (1997) 399.
- [62] J. J. Randall, W. J. Bernard, R. R. Wilkinson, *Electrochem. Acta*, 10, (1965) 183.
- [63] J. Van Muylder, M. Pourbaix, *Atlas of Electrochemical Equilibria in Aqueous Solutions*, M. Pourbaix. Pergamon Press, Oxford, (1966).
- [64] A. J. Bard, R. Parsons, J. Jordan, *Standard Potentials in Aqueous Solution*, CRC Press, Florida (1985).
- [65] A. Serdar, L. Wang, F.M. Doyle, *J. of Electrochem. Soc.*, 150 (11) (2003).
- [66] M. Kulkarni, M. Baker, D. Greisen, D. Ng, R. Griffin, H. Liang, *Tribo. Lett.*, 25 (1) (2007) 33.
- [67] G. Binnig, *Phys. Rev. Lett.*, 9 (1986) 56.
- [68] Nano-R™ AFM User's Manual, Revision 1.1, Pacific Nanotechnology Incorporated, San Francisco, CA (2004).
- [69] P. Asthana, *Micro-and nano-scale experimental approach to surface engineer metals*, Master's Dissertation, Texas A&M University, College Station, (2006).
- [70] R.G. Steinhardt, *Anal. Chem.*, 25, (1953) 697.
- [71] C. Nordling, *Phys. Rev. Lett.*, 105, (1957) 1676.
- [72] K. Siegbahn, C. Nordling, E. Sokolowski, *Proceedings of Rehovoth Conference on Nuclear Structure North- Holland, Amsterdam, North Holland, (1957) 291.*

- [73] J. F. Moulder, Handbook of X-Ray Photoelectron Spectroscopy, Physical Electronics, Inc., Minneapolis (1995).
- [74] H. P. Bonzel, C. Klient, Prog. Surf. Sc. 49, (1995) 107.
- [75] G. Heinicke, Tribochemistry, Carl Hanser, Munchen, (1984).
- [76] J. M. Martin, Th. Le Mogne, C. Grossiord, Th. Palermo, Tribo. Lett., 3, (1997) 87.
- [77] J. M. Martin, Tribo. Lett., 6, (1999) 1.
- [78] K. Varlot, J. M. Martin, C. Grossiord, B. Vacher, K. Inoue, Tribo. Lett., in press
- [79] D. A. Rigney, J. E. Hammerberg, MRS Bulletin, 6 (32) (1998) 23.
- [80] J. T. Dickinson, N.-S Park, M- W. Kim, S.C. Langford, Tribo. Lett., 3, (1997) 69.
- [81] N. F. Mott, The Metallic and Nonmetallic States of Matter, Ed. P.P. Edwards & C.N.R. Rao, Taylor and Francis, London (1985).
- [82] R. P. Feynman, R. B. Leighton, M. Sands, The Feynman Lectures on Physics, II-1, (1964).
- [83] P. Jemmely, S. Mischler, D. Landolt, Tribo. Inter., 32, (1999) 295.
- [84] D. Landolt, S. Mischler, M. Stemp, Electrochem. Acta, 46, (2001) 3913.
- [85] H. Liang, J. M. Martin, R. Lee, IEEE & TMS, J. Elect. Mater. 30(4) (2001), 391.
- [86] M. Kulkarni, D. Ng, M. Baker, R. Her, H. Liang, Wear, accepted.
- [87] D. Ng, M. Kulkarni, J. Johnson, A. Zinovev, D. Yang, H. Liang, to appear in Wear.
- [88] H. Liang, J. M. Martin, Th. Le. Mogne., J. App. Phys., 97(4) (2005) 043525.
- [89] J. M. Martin, Liang, H., Mogne, T.L., Malroux, M., Trib. Lett., 14 (1) (2005) 15.
- [90] E. Atanassova, D. Spassov, A. Paskaleva, K. Kostov, App. Surf. Sci., 253, (2006) 2841.

- [91] D. J. Smith, I. Young, *Thin Solid Films*, 11, (1981) 101.
- [92] V. A. Macagno, J.W. Schultze, *J. of Electroanal. Chem.*, 180, (1984) 157.
- [93] V. A. Mathieu, D. Landolt, *Surf. Inter. Anal.*, 5, (1983) 77.
- [94] Y. Kim, J. Zhao, K. Uosaki, *J. App. Phys.*, 94 (12) (2003) 7733.
- [95] H. Hertz, *Verhandlungen des Vereins zur Beförderung des Gewerbefleisses*, Leipzig, Nov. (1882).
- [96] E.R. Kral, K. Komvopoulos, D.B. Bogy, *ASME Journal of Applied Mechanics*, 60, (1995) 829.
- [97] E. D. Minot, Y. Yaish, V. Sazonova, M. Brink, P. L. McEuen, *Phys. Rev. Lett.*, 90 (15) (2003) 156401.
- [98] G. D. Sanders, Y.-C. Chang, *Phys. Rev. B*, 32 (6) (1985) 4282.
- [99] S. Kim, V. Gopalan, *App. Phys. Lett.*, 78 (2001) 3015.
- [100] F. J. Himpsel, J. F. Morar, F. R. McFeely, R. A. Pollak, G. Hollinger, *Phys. Rev. B*, 30 (12) (1984) 7236.
- [101] W. Kern, *Semicond. Intern.*, 8, (1985) 122.
- [102] S. Wolf, R. N. Tauber, *Silicon Processing for the VLSI Era, Vol I*, Lattice Press, Sunset Beach, CA, 1986.
- [103] W. Kern, G. L. Schnable, *IEEE Trans. Elect. Dev.*, 26, (1979) 647.
- [104] A. Feingold, A. Katz, *Mat. Sci.Eng.*, R (13) (1994) 56.
- [105] H. O. Pierson, *Handbook of Chemical Vapor Deposition: Principles, Technology and Applications*, Noyes Publications, Berkshire (1992).

- [106] P. C. van Buskirk, S. M. Bilodeau, Roeder, P. S. Kirlin, *Jap. J. App. Phys.*, 35, (1996) 2520.
- [107] T. M. Graettinger, S. H. Rou, M. S. Ameen, O. Auciello, A. I. Kingon, *App. Phys. Lett.*, 58, (1991) 1964.
- [108] N. Taga, H. Odaka, Y. Shigesato, I. Yasui, T. E. Haynes, *J. App. Phys.*, 80, (1996) 978.
- [109] P. Kar, K. Wang, H. Liang, *Electrochem. Solid State Lett.*, 11(2) (2008).
- [110] E. Mahe, D. Devilliers, H. Groult, J. Poulleau, *Electrochem. Acta*, 44, (1999) 2307.
- [111] N. P. Bansal, *J. Mater. Sci.*, 29 (19) (1994) 5065.
- [112] D. A. Jones, *Principles and Prevention of Corrosion*, Prentice Hall, Upper Saddle River, NJ (1996).
- [113] R. Godley, D. Starosvetsky, I. Gotman, *J. Mat. Sci.*, 15 (10) (2004) 1073.

VITA

Name: Prasenjit Kar

Address: c/o Jayasri Kar, Lane no- 2, Vivekananda Road, Silchar – 788007,
Dist- Cachar, Assam, India

Email Address: rajkar@neo.tamu.edu

Education: B.Sc., Chemistry, Assam Central University, 1999
M.Sc., Chemistry, Assam Central University, 2001
Ph.D., Materials Science, Texas A&M University, 2008